DEVELOPING UNCONVENTIONAL HOLOGRAPHY AND IMAGING METHODS USING INTENSITY AND POLARIZATION CORRELATION: SPATIAL STATISTICAL OPTICS APPROACH

A Thesis submitted

in partial fulfilment for the Degree of

Doctor of Philosophy

by

DARSHIKA SINGH

Department of Physics
INDIAN INSTITUTE OF SPACE SCIENCE AND TECHNOLOGY
Thiruvanthapuram- 695547
July 2021

CERTIFICATE

This is to certify that the thesis entitled **Developing unconventional Holography and Imaging methods using Intensity and Polarization Correlation: Spatial Statistical Optics Approach**, submitted by **Darshika Singh**, to the Indian Institute of Space Science and Technology, Thiruvananthapuram, in partial fulfilment for the award of the degree of **Doctor of Philosophy**, is a *bona fide* record of research work carried out by her under my supervision. The contents of this thesis, in full or in parts, have not been submitted to any other Institution or University for the award of any degree or diploma.
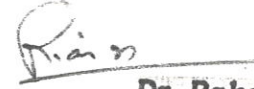
Dr. Rakesh Kumar Singh

Supervisor

Associate Professor

Department of Physics, IIST (Formerly)

Now at Indian Institute of Technology BHU

(Banaras Hindu University)

Dr. Rakesh Kumar Singh
Associate Professor
Department of Physics
Indian Institute of Technology
(Banaras Hindu University), Varanasi-221005

Thiruvananthapuram

July 2021

Counter signature of HOD with seal

डॉ. उमेश आर. कढणे/Dr. Umesh R. Kadhane
सह आचार्य एवं अध्यक्ष/Associate Professor & Head
भौतिकी विभाग/Department of Physics
भारतीय अंतरिक्ष विज्ञान एवं प्रौद्योगिकी संस्थान
Indian Institute of Space Science and Technology
अंतरिक्ष विभाग, भारत सरकार
Department of Space, Government of India
तिरुवनंतपुरम/Thiruvananthapuram-695 547

DECLARATION

I declare that this thesis entitled **Developing unconventional Holography and Imaging methods using Intensity and Polarization Correlation: Spatial Statistical Optics Approach** submitted in partial fulfilment of the degree of **Doctor of Philosophy** is a record of original work carried out by me under the supervision of **Dr. Rakesh Kumar Singh**, and has not formed the basis for the award of any other degree or diploma, in this or any other Institution or University. In keeping with the ethical practice in reporting scientific information, due acknowledgements have been made wherever the findings of others have been cited.

Darshika Singh

SC14D009

Thiruvananthapuram - 695 547

July 2021

ACKNOWLEDGMENT

I would like to thank all who have helped and encouraged me during my research at Indian Institute of Space Science and Technology.

First and foremost, I would like to express my sincere gratitude towards my supervisor Dr. Rakesh Kumar Singh for the continuous support towards my study & research and for his patience, motivation, enthusiasm, and immense knowledge. His guidance helped me a lot to complete this work with utmost satisfaction.

I would also like to thank Dr. V. K. Dadhwal, Director - IIST, Dr. Umesh Kadhane, HOD – Physics Department, IIST, Prof. C.S. Narayanamurthy, and my doctoral Committee members; Dr. S. Murugesh, Prof. P. Senthilkumaran, Dr. Nirmal K Viswanathan, and Dr. Deepak Mishra for timely evaluation and insightful discussions on my research topic. I extend my sincere thanks to the faculty members of Department of Physics for their support. On the finance side of things, I am highly grateful to IIST for its financial assistance towards my work.

I thank all my fellow scholars in IIST especially Mr. Pramod, Mr. Surya and Mr. Preetam, for their sincere help and support. I also thank my friends, Shashank, Shirish, Pragya who cheered me up during my tough days.

I also extend a warm thanks to my family. I am greatly indebted to my parents I B Singh and Savita Singh, my Sister Priyanka Singh and her family, and my brother Prashant Singh for their unconditional love, care and tolerance which made this thesis worthwhile. Without their support, I do not think that I could have overcome the difficulties during these years.

Darshika Singh

ABSTRACT

The random scattering of coherent and polarized light generates a complicated and spatially varying polarization states apart from the intensity and such random field is referred as polarization speckle. The speckle is a ubiquitous feature due to a complicated interference of the randomly scattered coherent light. Because the light is considered to be monochromatic and scattering medium is static, the scattered light is free from any temporal fluctuations and carries only spatial varying information. Investigations on such random light fields are important to understand physical properties of the speckles, and use physical parameters for applications such as lensless imaging and diagnosis etc.

This thesis covers investigations on the generation and analysis of the speckles using the spatial statistical optics. This is realized using the Hanbury Brown and Twiss (HBT) approach and polarization correlation. The HBT approach makes use of the two-point correlation of the random light fields. On the other hand, polarization is associated with the correlation between two orthogonal polarized components at a single point and described by the Stokes parameters. To characterize in-homogeneously polarized light, extension of the Stokes parameter to the two points known as generalized Stokes parameters and the HBT for polarized light are required.

New and significant features of this thesis are: The effects of different parameters of random source structures on two-point intensity correlation, in a two-dimensional and a three-dimensional propagation, are studied. A computational model is developed to analysis the 2D and 3D intensity correlations for comparison of the results with experiments. The effects of degree of spatial polarization on intensity correlation of the speckle are studied. An experimental technique is efficiently demonstrated to recover the polarimetric parameters of light field from a non-imaged laser speckle. To recover polarized objects hidden behind a scatter, a new approach, Lensless Stokes holography with Hanbury Brown Twiss interferometer is presented. The advantage of compressive sensing in correlation imaging is also presented.

TABLE OF CONTENTS

LIST OF FIGURES

LIST OF TABLES

ABBREVIATIONS

BS	Beam Splitter
CCD	Charge Coupled Device
CP	Coherence-Polarization
GG	Ground Glass
GSP	Generalized Stoke Parameter
HBT	Hanbury Brown-Twiss
He-Ne	Helium - Neon
HWP	Half Wave Plate
L	Lens
LP	Linear Polarizer
M	Mirror
MO	Microscope Objective
PBS	Polarization Beam Splitter
QWP	Quarter Wave Plate
SF	Spatial Filter
SLM	Spatial Light Modulator
SPP	Spiral Phase Plate

NOTATIONS

The research scholar should explain the meaning of special symbols and nomenclature used in the thesis. Some examples are provided below.

$|x|$ - absolute value of x

μ - mean

$\log_n(x)$ - logarithm (x) to the base n

$|.|$ - Absolute value

θ - Angle of rotation

δ - Delta function

$\langle \cdot \rangle$ - Ensemble average

f - Focal length of lens

k - Propagation factor

ϕ - Random phase from scattering layer

η - Reconstruction efficiency

$\langle \cdot \rangle_s$ - Spatial average

r - Spatial co-ordinates in observation plane

$\hat{r}$ - Spatial co-ordinates in source plane

σ - Standard deviation

t - Time

Tr - Trace of the matrix

v - Visibility

λ - Wavelength of light source

CHAPTER 1
INTRODUCTION

Randomness in a light field is an unavoidable yet a common problem due to various practical reasons. It may arise as a result of either erratic fluctuations in the light source or propagation of light through an optically inhomogeneous media. Propagation of coherent laser light through random media distorts light wavefront and spatially scrambled the light information. It further aggravates coherent noise due to stochastic interference of randomly scattered waves, known as speckle (Dainty, 1984; Goodman, 2007; Sirohi, 1933). A coherent beam diffused by the disordered media produces this speckle pattern which is a typically granular pattern. However, these random fluctuations carry an important signature of light source and its propagating medium, and can therefore by exploited to develop several lasers speckle-based instruments and in the analysis of light source. Based on the nature of propagation of coherent light through disordered medium, two broad strategies can be adopted. First one which considers the speckle pattern is time-invariant and the speckle can be utilized to investigate diffuser properties. This case is widely used in the speckle metrology such as displacement ((Archbold et al., 1970; Freund and Berkovits, 1990; Burch and Tokarski, 1968; Wang et al., 2006), vibration and source (Bianchi, 2014; Zalevsky et al., 2009), and blood flow mapping in tissues (Briers et al., 2013), high resolution imaging (Mehta and Srivastava, 2012) etc. Second case is a situation wherein diffuser is static and speckle pattern is used to probe properties of the incident light. Some of the examples in this category are laser stabilization (Mazilu et al., 2014; Hanson et al., 2015; Metzger et al., 2017; Bruce et al., 2019; 2020; O'Donnell et al., 2020; Gupta et al., 2019), spectroscopy (Redding and Cao, 2012; Redding et al., 2013; Cao, 2017), mode characterization (Mazilu et al., 2012; Mourka et al., 2013), and imaging (Singh et al., 2014).

1

To analyze the statistical properties of light, it is expedient to have a deep understanding of mathematical correlations. For instance, correlation at two points known as a complex coherence function is a significant parameter to characterize random light with the Gaussian statistics (Goodman, 2000). Other examples of correlation include correlation at the single point, in both, time and space that gives polarization information of the light. The seminal work and foundations developed by Emil Wolf on the wave nature of coherence have led to the significant interest on the correlation optics and its related areas (Mandel and Wolf, 1995; Wolf, 2007). Some other interesting and central results of the correlation optics are the Van Cittert Zernike theorem and Hanbury brown Twiss experiment. Significant progress and developments in the correlation optics had led to the emergence of numerous fundamental and practical applications. Van Cittert Zernike theorem provides a relationship between the intensity distribution and degree of spatial coherence of monochromatic beam in the source and detector planes (Gori et al., 2000). On the other hand, the correlation function of the fourth order with respect to complex amplitude is used in the Hanbury Brown Twiss approach (Hanbury and Twiss, 1956).

Intensity correlation proposed by Hanbury Brown and Twiss (HBT) has become a preferred approach to analyze the random fields. The work of HBT about 60 years ago led to development of several ideas covering classical and quantum optics domain. HBT approach makes use of the relation between second order and fourth order Gaussian random fields and provides a simple and stable experimental method to characterize the correlation parameters. The approach offered a novel insight into statistical optics. It led to the invention of several applications in the fields of speckle contrast imaging, high energy physics, nuclear physics, and atomic physics (Hassinen et al., 2011; Bromberg et al., 2010; Kumar et al., 2012; Singh et al., 2014; Schultheiss et al., 2016; Wiedemann and Heinz, 1997; Baym, 1997). Most of the investigations on HBT approach are limited to

temporal fluctuations and scalar optics (without polarization). Laser speckles are complex random pattern arising due to interference of randomly scattered light and at a particular time (frozen time) randomly scattered light in the speckle is completely coherent. This is the reason why a coherent speckle pattern is characterized as spatial fluctuation rather than temporal. Recently, Takeda and co-workers in a review article discussed the concept of spatial statistical optics and use this approach to explain some of the fundamental features of the laser speckle (Takeda, 2013; Takeda et al., 2014). Further, based on the concept they have established a well-known nonconventional holographic technique such as coherence holography and photon correlation holography.

Traditionally, the coherence has been associated (attributed only to) with interference fringe visibility of scalar light field. However, recent attempts have been made to incorporate both visibility and polarization in a common framework. Polarization has been associated with the correlation between two orthogonal polarized components at a single point observation. The state of polarization at a single point is described by Stokes parameters. These parameters are graphically presented by a point on Poincare sphere. In recent years, significant efforts have been made to generalize Stokes parameters at two different points (Singh et al., 2011; 2012). This enabled describing statistical properties of vectorial random fields in an inhomogeneously polarized field. Multiple scattering of coherent light in a random media and propagation of structured polarized light through an anisotropic media are few such examples of generating inhomogeneously polarized field. In contrast to the scalar speckle, these inhomogeneously polarized fields arise due to complex polarization interference, for instance, a monochromatic polarized light strongly scattered through a static rough surface which involves multiple scattering.

Presence of coherent noise in both scalar and vectorial domain affects the performance of a laser-based imaging and communication system. For instance, intensity correlation has been applied to image 3D object from a speckle pattern

3

using the two-point intensity correlation (Soni et al., 2016; Katz et al., 2014; Singh et al., 2014; 2016; Somkumar et al., 2017; Tripathi et al., 2014; Aguiar et al., 2014). However, emergence of polarization fluctuations in speckle field, i.e., in speckle polarization, intensity correlation parameter is significantly affected by polarization fluctuations and has its affect in 3D imaging reconstruction from the speckle. In another direction, random fields and their intensity correlation have been significantly utilized to develop to several unconventional imaging techniques such as correlation holography, ghost imaging, ghost diffraction, single pixel imaging etc. However, majority of these works are either limited to scalar and simple binary objects except some recent investigations. In a generic case, coherent beam interacts remotely with the object, and scattered light is characterized to recover information about the object. Roughness of the object and refractive index inhomogeneity in propagation medium creates speckle with/or without polarization fluctuations.

In context of the polarization speckle, random fluctuation is introduced into Stokes parameters. For a monochromatic and a static scattering surface, the scattered polarized field shows only spatial fluctuations rather than temporal. Attempts have been made to characterize polarization speckle in terms of complex degree of mutual polarization and two-point stokes correlation (Singh et al., 2011; 2012; 2014). In many applications, it is required to image a scalar or vectorial object obscured by scattering medium. When the object is hidden behind the random scattering media, it is difficult to apply usual conventional imaging methods. Correlation parameters can be used to develop a novel imaging technique by exploiting statistical features of random fields without restoring to any wavefront correction schemes. The invention of HBT can be combined with the holography to develop several new and innovation methods to overcome the challenges of imaging from random generic light such as polarization speckle. Such strategy provides opportunity to use tool and techniques of the coherent optics and export it to the coherence waves or issue of developing optics with

4

random light fields. Some attempts have been made in this direction. However, majority of these works are limited to speckle field with only intensity fluctuations and recovery of the scalar objects except some limited works. To overcome and examine the existing challenges in correlation optics particularly on polarization speckle and on the imaging of polarized objects, detailed investigations are carried out and reported in this thesis.

1.2   Background and Context

When a coherent polarized light travel through a static diffuser which involves multiple scatterings, random fluctuations are introduced into the spatial distribution of the state of polarization (SOP). Such a random field is referred to as polarization speckle. The polarization fluctuation of the light can be engineered using the random source parameters such as amplitude, phase and polarization etc. One simple representation of the light synthesis is shown in Fig. 1, where source is used to synthesize the correlation property of the light.
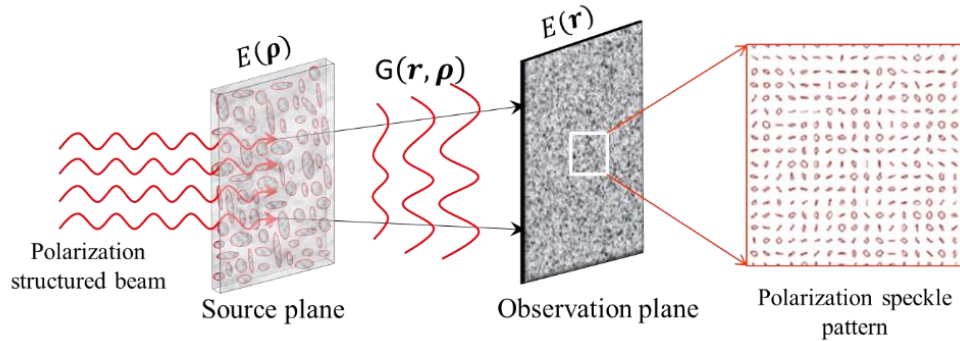
Figure 1-1 Geometry of source structure, propagation system and observation plane.

Propagation of a structured polarized light from scattering plane to any arbitrary observation plane can be represented by a proper propagation kernel for each polarization components as follows

$$E_i(\boldsymbol{r}) = \int G(\boldsymbol{r},\boldsymbol{\rho}) \, E_i(\boldsymbol{\rho}) \, d\boldsymbol{\rho}$$

$$\text{(1.1)}$$

where $E_i(\boldsymbol{\rho})$ and $E_i(\boldsymbol{r})$ with $i = x, y$ is polarization information of the object at diffuser and observation plane respectively and $G(\boldsymbol{r},\boldsymbol{\rho})$ is a propagation kernel. Transverse position vectors at the source and observation planes are denoted by $\boldsymbol{\rho}$ and r respectively. Synthesis of coherence and polarization properties of the randomly fluctuating electromagnetic field and consequently speckle grain size in two and three dimensions can be controlled by incident light structure at the source plane. For an instance, circular aperture of specific size and/or by introducing vortex of different topological charges which shapes the spatial degree of coherence and polarization at the observation plane. The intensity at the observation plane is related with the intensity correlation and cross-covariance of the intensity for Gaussian random field. The cross-covariance of the intensity is given as

$$\Gamma(r_1, r_2) = \langle \Delta I(r_1) \Delta I(r_2) \rangle = \sum_{i,j} \left| W_{ij}(r_1, r_2) \right|^2$$

$$\text{(1.2)}$$

where, $\langle \cdot \rangle$ stands for the ensemble average, $W_{ij}(r_1, r_2)$ is an element of 2X2 coherence polarization matrix. The coherence-polarization matrix for a monochromatic random light field is defined as

$$W(r_1, r_2) = \begin{pmatrix} W_{xx}(r_1, r_2) & W_{xy}(r_1, r_2) \\ W_{yx}(r_1, r_2) & W_{yy}(r_1, r_2) \end{pmatrix}$$

$$\text{(1.3)}$$

Under the condition of spatial ergodicity of the scattered field, elements of the CP matrix of the scattered field are obtained by space averaging (rather than temporal averaging). Non-separable experimental schemes designed to synthesize the spatial polarization fluctuations in the random fields.

The correlation method based on HBT approach has brought many results in the fundamental and applied statistical optics. Since intensity

interferometers are far stable and reluctant to the environmental fluctuations, they are preferred over field-based interferometers. HBT has led us to the development of new metrological tools for performing optical diagnostics of light-scattering objects and media. It provides opportunities to analyze the correlation property of optical fields. Coherence and polarization in randomly fluctuating electromagnetic field has inspired researchers to investigate vectorial coherence theory, and in the same context, HBT phenomenon has also begun to attract interest. Use of HBT is mostly limited to the exotic beams like electromagnetic Gaussian Schell model, Schell model etc. with some recent works on polarized light. HBT approach is also used to examine partially coherent electromagnetic beam by examining the different source parameters on correlation of intensity fluctuation (HBT effect) at two points of a random electromagnetic field. However, most of these investigations are either theoretical or limited to experiments dealing with scalar light. In this thesis, detailed investigation is carried out on extending concept of the HBT approach for the polarized random fields particularly on the polarization speckles. After establishing a link between the polarizations speckle with the HBT approach, such methods are used to develop new imaging methods by combining HBT approach with the holography.

1.3   Objectives

The primary objective of the thesis is to theoretically and experimentally investigate the properties of randomly fluctuating field in scalar and vectorial domain using HBT and to formulate it in imaging applications. The specific objectives of this work are summarized below.

- Investigation on the statistical properties of speckle field using second order intensity correlation technique.
- Impact of different parameters of random source structures on two-point intensity correlation in two-dimensional and three-dimensional space.

- Development of computational model to analysis 2D and 3D intensity correlations and comparing these results with experiments.
- Effect of degree of spatial polarization on intensity correlation of the speckle.
- Recovery of polarimetric parameters from non-imaged laser speckles.
- Experimental demonstration of Stokes holography with Hanbury Brown Twiss interferometer and its implementation in 3D imaging.
- Practical implementation of Compressive Sensing application in optical imaging.

1.4   Overview of Thesis

The thesis is split into 7 chapters. In chapter 2, a brief review of related literature is presented. In chapter 3-4 we describe the different experimental techniques developed for light synthesis and analysis of polarization speckles based on intensity interferometer. Chapter 5 presents the novel holographic technique to use intensity interferometer, i.e., HBT type for Stokes holography. Chapter 6 highlights the potential of compressed sensing in the imaging through a random scattering medium. In chapter 7 we conclude by summarizing the key points and looking into the future scope of a research work.

Chapter 2 is intended to provide preliminaries, giving a brief description of polarization, propagation, laser speckle pattern, polarization speckle, and analysis of speckle patterns. The significance of correlation of light field in optical characterization and its importance in optical imaging. Also discuss the concept of HBT approach that has opened a new field of holographic technique to use intensity correlation.

In chapter 3, we aim to study intensity correlation of the spatially fluctuating polarized random fields at different distances under the paraxial propagation. Quantitative analysis of the random field is carried out by following relation between the degree of coherence of the electromagnetic fields, spatial degree of polarization and the intensity correlation for the Gaussian random fields. An experimental scheme is designed to generate and analyze the random

fields with different polarization fluctuations and results are presented. The polarization fluctuation in the random field is synthesized by introducing different vortex modes into orthogonal polarization components of the light prior to the random scattering from a diffuser. Our purpose is to use the vortex beams to generate spatial polarization inhomogeneity in the laser speckle and analyze the speckles at the focal plane and at different transverse plane using the intensity correlation and spatial optics.

In chapter 4, we propose and experimentally demonstrate a new technique to recover the polarimetric parameters of the light field observed by a static non-birefringent diffuser. We recover the PPs from non-imaged laser speckle patterns. Propagation of coherent and polarized light through a static diffuser may generate polarization fluctuation in the random scattered field depending on the nature of incident polarized light. To analyze the polarization speckle, we apply idea of coherence wave interference for the vectorial light field. This is realized by using 2X2 coherence-polarization matrix elements and their interference. Moreover, this approach is free from any artifacts associated with imaging/or Fourier transforming lens and its possible impact on the spatial stationarity of the random field.

In chapter 5, we propose a new method to use intensity interferometer, i.e., HBT type for Stokes holography. The HBT approach permits to remove a Fourier transforming lens as required in the field-based interferometer for the Stokes holography. Making use of this feature, we design and develop a new lensless Fourier transform holography setup for the GSPs. This helps to achieve spatial stationarity of the random fields at an arbitrary distance z from the scattering plane and replaces the ensemble averaging by the space averaging of the random field. We further make use of the lensless Fourier transform holograms of the GSPs to recover the desired GSPs for depth recovery of the objects encoded into the Stokes fringes. This is implemented by digital propagation of the GSPs (rather than mechanical scanning of the detector). To the best of our knowledge, this is first such attempt to exploit the interference of

the GSPs to realize lensless Fourier transform hologram for the Stokes vector waves and apply the HBT type interferometer for 3D imaging of the polarized objects.

Chapter 6 highlights the potential of compressed sensing in the imaging through a random scattering medium. This method can reduce the noise level in recovered signal and super-resolved images can be obtained using the CS-based technique compared to the usual FT. The demonstrated technique is well efficient in retrieving the information by reconstructing objects from limited sized FTH. Quantitative analysis has been carried out to compare the quality of reconstruction using inverse Fourier transform (IFT) and CS techniques. The finding highlights that the CS reconstruction is better than that of IFT reconstruction.

In concluding chapter 7, we summarize the research work by pointing out key research outcomes and look on to the future scope of the work. Followed by this chapter bibliography, appendices and the list of publications are provided.

CHAPTER 2
COHERENCE: SCALAR AND VECTORIAL DOMAIN

2.1 Introduction

Light fields are inherently of a statistical in nature and correlations of the light play very important role in describing the fundamental features such as diffraction and interference. In particular, the cross-correlations at two points either in space/ time or both, known as the complex coherence, has been widely explore for large range of fundamental and practical interests. Theoretical bases and foundations of the optical coherence permit to deal with generalized light ranging from fully coherent to the incoherent. For an instance, the fully coherent light is a special case of the light where the correlation between two points is significant. Another case is light with correlation between two spatially/or temporally separated point becomes zero and this situation is referred as the incoherent light. Seminal work of Emil Wolf on the wave nature of the coherence function has provided a strong theoretical basis to the coherence optics and since then significant progress has been achieved in this area. Learning from analogy between the optical fields and complex coherence functions, various fundamental and practical aspects of the coherence optics have been explored and some of these are coherence current, conservation law (wang, 2006). In the context of experimental optics, the Young's interference approach has played a crucial role in characterization of the correlations features of the light field. Lately, the intensity interferometer approach proposed by the Hanbury Brown and twiss (HBT) has also been widely used in the characterization of the random light fields and correlation structures [HBT]. However, majority of these studies are mainly limited to the scalar light field ignoring polarization features of the light.

It has been noticed that a combined effect of the polarization and

coherence plays critical role in the wide range of applications such as diffraction, light matter interactions etc. For instance, propagation of spatially non-uniform polarized light has opened new fundamental questions on the interpretation of the interference effects for the vectorial light (Roy Chowdhury and Wolf, 2005; Gori et al., 2006; Wolf, 2003; Tervo et al., 2003; Setela et al., 2004; Luis, 2007; Korotkova and Wolf, 2005). In recent years, significant efforts are being made to address these questions and interpret the interference effects for polarized light using both fringe visibility and polarization characteristics. In contrast to two-point correlation for coherence, polarization of the light can be explained using the single point correlation between two orthogonal polarization components. The state of polarization (SOP) at a point is usually described by the Stokes parameters (SPs). Attempts are also being made to generalize concept of the degree of polarization and SPs to cover the inhomogeneous random fields. It has been highlighted that conventional SPs provide time averaged (as ensemble average replaced by the time average) evaluation and hence not suitable to access the instantaneous SOP. Observation of instantaneous SOP of a natural light source is practically challenging due to slow response of the detectors compared to the fast fluctuations of natural light. Nevertheless, a slowly fluctuating random light source can be designed in the laboratory by a controlled rotating ground glass with a monochromatic laser source illumination. Freezing rotation of the ground glass will lead to generation of random complex field known as laser speckle.

Propagation of the laser light in thick scattering mediums is one of the interesting examples of generating the inhomogeneously polarized light. Such random pattern arises from a complex interference effect and produces speckle pattern. Under consideration of a monochromatic light and static scattering, scattered field is free from temporal fluctuations and remains to be fully polarized with well-defined SOPs at each and every point is the random pattern according to traditional definition based on the temporal averaging. Such random field with

spatial varying SOP is refereed as a polarization speckle. The random field such as this remains to be fully polarized according to traditional definition, can be also regarded as partially or totally depolarized according to alternate definition relying on the spatial average as a replacement of the ensemble average (Takeda et al., 2014). The spatial degree of polarization, based on the spatial average, is analogous to the idea of degree of macroscopic magnetization of magnetic materials due to ordered or disordered orientations of microscopic atomic dipoles, and polarization speckles show resemblance to magnetic domains in their geometrical structures (Kittel, 1976). Existence of the polarization spackle is very common in the area of coherent light propagation through random scattering medium and such patterns are practically relevant in applications such as diffraction and imaging.

Based on the emerging interests in the analysis and applications of the coherence-polarization of the light, this chapter cover mathematical basis of the coherence optics ranging from scalar to the vector domains. Generation and analysis of light source with inhomogeneous polarization distributions are discussed in the context of existing literature and recent progress in this area. Different methods based on the field and intensity interferometers to measure coherence-polarization of the light are discussed and practical aspects are examined. In contrast to the usual practice to describe and discuss correlations properties of the light with time averaging as replacement of the ensemble average, we make special emphasis on the spatial averaging with some examples and applications in the imaging.

2.2 Coherence and Polarization of light

Consider a two-dimensional transverse quasi-monochromatic light field at the source plane $\tilde{A}$ with orthogonal polarization components $E_x(r,t)$ and $E_y(r,t)$ at transverse spatial position $r \equiv (x,y)$ at the source plane and

instantaneous time t. Here, subscripts x and y denotes direction on the polarization vector components. Propagation direction is represented by the longitudinal coordinate z.
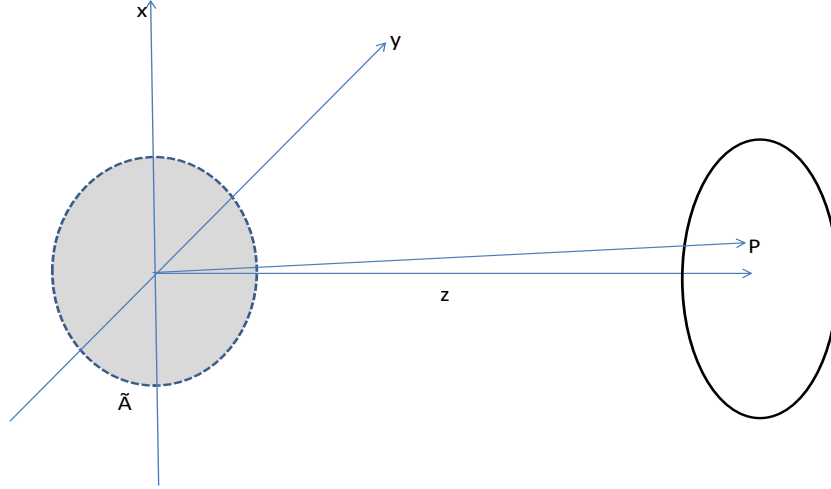
Figure 2-1 A representation of propagation of light from source plane $\tilde{A}$ to the observation point P in the coordinate system (x, y, z)

The polarization vector at the source plane is represented as

$$E(r,t) = \begin{pmatrix} E_x(r,t) \\ E_y(r,t) \end{pmatrix} \tag{2.1}$$

2.2.1 Coherence –Polarization matrix

Our main interests in this chapter to deal with the monochromatic light and spatial coherence and hence mathematical foundations are discussed in the context of only spatial coherence. The second-order spatial correlation properties of the field at a pairs of spatial position points r_1 and r_2 can be described by the coherence-polarization matrix (or cross-spectral density matrix) as

$$W(r_1, r_2) = \begin{pmatrix} \langle E_x^*(r_1)E_x(r_2) \rangle & \langle E_x^*(r_1)E_y(r_2) \rangle \\ \langle E_y^*(r_1)E_x(r_2) \rangle & \langle E_y^*(r_1)E_y(r_2) \rangle \end{pmatrix} \qquad (2.1.1a)$$

where $\langle \cdot \cdot \rangle$ stands for ensemble average and usually replaced by the temporal averaging and asterisk * denotes complex conjugate. Element of the 2x2 coherence polarization matrix is represented as $W_{mn}(r_1, r_2) = \langle E_m^*(r_1)E_n(r_2) \rangle$ where $m, n = x, y$ represents orthogonal polarization components.

Estimation of the CP matrix elements provides direct access of the degree of coherence and degree of polarization of the light field. Following definition proposed by Tervo et. al. (Tervo et al., 2003), the degree of coherence of the stochastic electromagnetic field is

$$\gamma^2(r_1, r_2) = \frac{\sum_{mn}|W_{mn}(r_1, r_2)|^2}{\sum_{mn} W_{mm}(r_1, r_1)W_{nn}(r_2, r_2)} \qquad (2.1.1b)$$

$$P(r) = \sqrt{2\gamma^2(r) - 1} \qquad (2.1.1c)$$

$$P(r) = \left(1 - \frac{4 \det W(r,r)}{|Tr\, W(r,r)|^2}\right)^{1/2} \qquad (2.1.1d)$$

where γ and P are degree of coherence and degree of polarization of the light. Definition of the degree of coherence of the electromagnetic field is different from the definition proposed by Emil Wolf (Wolf, 2007). Degree of polarization unity states that all four elements of the CP matrix at single point are equal and non-zero. Equations Eq. 2.1.1b and 2.1.1c highlights that light will be fully polarized when all four components are correlated. The degree of polarization will be unity for $\gamma(r, r) = 1$ and zero for $\gamma(r, r) = \sqrt{1/2}$. Therefore, light will be un-polarized when the single point correlation of the orthogonal polarization components vanishes, i.e., non-diagonal elements of CP matrix at the single point becomes zero. This can also be explained using Eq. 2.1.1d and the polarization

matrix. The single point correlation of the CP matrix is also known as polarization matrix J and defined as

$$J(r,r) = \begin{pmatrix} \left\langle E_x^*(r)E_x(r) \right\rangle & \left\langle E_x^*(r)E_y(r) \right\rangle \\ \left\langle E_y^*(r)E_x(r) \right\rangle & \left\langle E_y^*(r)E_y(r) \right\rangle \end{pmatrix} \qquad (2.1.1e)$$

Uniformly polarized light field or scalar case can be considered as a special case such as

An x polarized light source:

$$W(r_1, r_2) = \begin{pmatrix} \left\langle E_x^*(r_1)E_x(r_2) \right\rangle & 0 \\ 0 & 0 \end{pmatrix}$$

Light will be always fully polarized in this case.

Light with equal orthogonal polarization components but no correlations between them

$$W(r_1, r_2) = \begin{pmatrix} \left\langle E^*(r_1)E(r_2) \right\rangle & 0 \\ 0 & \left\langle E^*(r_1)E(r_2) \right\rangle \end{pmatrix}$$

Light will be un-polarized in this case and un-polarization of such light source is possible by attenuating strength of one of the orthogonal polarization components.

2.2.2 Propagation of elements of the coherence-polarization matrix

Consider that the beam propagates in free space from source at plane z=0 into the half space z>0. If $\{E(r,t)\}$ represents the ensemble of the electric field at the source plane and $\{E(\rho,t)\}$ denotes the ensemble of the propagated electric field at the observation point P (ρ,z) as shown in Fig.2.1. Then the field at the observation point can be connected with source under a paraxial

16

approximation as follows

$$E_m(\rho, t) = \int E_m(r, t) \, G(\rho, r) dr \tag{2.1.2a}$$

Eq.2.1.2a is a two dimensional integral due to source coordinate $r \equiv (x, y)$ and the propagation kernel $G(\rho, r)$ is given as

$$G(\rho, r) \approx \frac{\exp(ikz)}{i\lambda z} \, exp\left(ik \frac{|\rho|^2 - 2\rho.r + |r|^2}{2z}\right)$$

where λ and $k = \frac{2\pi}{\lambda}$ are, respectively, the wavelength and wave number of light. The observation distance z is considered to be larger than the transverse spatial extent of the source and observation point.

Under consideration of stochastic source at the plane z=0 and non-stochastic propagation kernel, elements of the CP matrix are given as

$$\langle E_m(\rho_1) E_n^*(\rho_2) \rangle = \iint \langle E_m^*(r_1) E_n(r_2) \rangle \, G^*(\rho_1, r_1) G(\rho_2, r_2) dr_1 \, dr_2 \tag{2.1.2b}$$

Eq. 2.1.2 b shows that elements of the CP matrix can be easily propagated from one plane to another and such relation helps to examine propagation induced coherence-polarization change of the light. Some special cases relevant to our thesis works are:

(i) **Incoherent light source**: $\langle E_m^*(r_1) E_n(r_2) \rangle = I_{mn}(r)\delta(r_1 - r_2)$

We would like to emphasize here that $I_{mn}(r)$ is nothing but polarization matrix represented by Eq. 2.1.1e and this term may be complex for $m \neq n$. For incoherent but polarized light, elements of the CP matrix elements at the observation plane are given as

$$W(\rho_1, \rho_2) = \iint J(r) \, G^*(\rho_1, r_1) \, G(\rho_2, r_2) \, dr$$

(ii) **Incoherent light and propagation kernel as Fourier transform**

Let us consider propagation kernel $G(\rho, r) = \exp\left(i\frac{k}{2z}\rho.r\right)$. Therefore, the complex coherence at the observation plane which is located at the far field is given as

$$W(\rho_1, \rho_2) = \iint J(r) \exp\left[-i\frac{k}{2z}(\rho_2 - \rho_1).r\right] dr$$

This relation is also referred as the van Cittert-Zernike theorem for the incoherent polarized light source.

2.2.3 Generalized Stokes parameters

It is possible to extend single point Stokes parameters (SPs) to the two points and develop formation similar to the coherence-polarization matrix. The generalization of the SPs from one-point to two-point, known as generalized Stokes parameter, helps to characterize stochastic electromagnetic fields and in the propagation of light. The Stokes parameter at a point r on the source plane can be explained using complex field from Eq. 2.1 and given as

$$S_0(r) = \langle E_x^*(r)E_x(r)\rangle + \langle E_y^*(r)E_y(r)\rangle \tag{2.1.3 a}$$

$$S_1(r) = \langle E_x^*(r)E_x(r)\rangle - \langle E_y^*(r)E_y(r)\rangle \tag{2.1.3b}$$

$$S_2(r) = \langle E_x^*(r)E_y(r)\rangle + \langle E_y^*(r)E_x(r)\rangle \tag{2.1.3c}$$

$$S_3(r) = i\left[\langle E_y^*(r)E_x(r)\rangle - \langle E_x^*(r)E_y(r)\rangle\right] \tag{2.1.3d}$$

It is very important to highlight close connection between Equations (2.1.1a-2.1.1d) and the polarization matrix given by Eq. 2.1.1e. The SPs elements can also be explained using the polarization matrix. In contrast to elements of the CP matrix, the polarization matrix elements and hence the SPs are real quantities and not suitable for propagation (Korotkova and Wolf, 2005). The generalized Stokes parameters (GSPs) are defined as

$$S_0(r_1, r_2) = \langle E_x^*(r_1)E_x(r_2)\rangle + \langle E_y^*(r_1)E_y(r_2)\rangle \qquad\qquad (2.1.3\ e)$$

$$S_1(r_1, r_2) = \langle E_x^*(r_1)E_x(r_2)\rangle - \langle E_y^*(r_1)E_y(r_2)\rangle \qquad\qquad (2.1.3f)$$

$$S_2(r_1, r_2) = \langle E_x^*(r_1)E_y(r_2)\rangle + \langle E_y^*(r_1)E_x(r_2)\rangle \qquad\qquad (2.1.3g)$$

$$S_3(r_1, r_2) = i\big[\langle E_y^*(r_1)E_x(r_2)\rangle - \langle E_x^*(r_1)E_y(r_2)\rangle\big] \qquad\qquad (2.1.3h)$$

The GSPs elements can also be explained using the CP matrix elements as follows

$$S_0(r_1, r_2) = W_{xx}(r_1, r_2) + W_{yy}(r_1, r_2) \qquad\qquad (2.1.3i)$$

$$S_1(r_1, r_2) = W_{xx}(r_1, r_2) - W_{yy}(r_1, r_2) \qquad\qquad (2.1.3j)$$

$$S_2(r_1, r_2) = W_{xy}(r_1, r_2) + W_{yx}(r_1, r_2) \qquad\qquad (2.1.3k)$$

$$S_3(r_1, r_2) = i\big[W_{yx}(r_1, r_2) + W_{xy}(r_1, r_2)\big] \qquad\qquad (2.1.3\ l)$$

Following propagation kernel described earlier, we can also connect the GSPs elements between the source z=0 and at the observation plane and relation is given as

$$S_l(\rho_1, \rho_2) = \iint S_l(r_1, r_2)G^*(\rho_1, r_1)G(\rho_2, r_2)dr_1\, dr_2 \qquad\qquad (2.1.3m)$$

where $i = 0 - 3$. Relation 2.1.3m permits to propagate the GSPs from one plane to another and helps to evaluate the propagation induced coherence-polarization change. Under consideration of incoherent -polarized light, the GSPs at the far field can be written as

$$S_l(\rho_1, \rho_2) = \iint S_l(r) \exp\left[-i\frac{k}{2z}(\rho_2 - \rho_1).r\right] dr \qquad\qquad (2.1.3n)$$

Term $S_l(r)$ represents the Stokes parameters at the incoherent source and this relation is interpretation of the van Cittert-Zernike theorem in terms of the SPs

19

and GSPs. Relation 2.1.3n can be utilized to design and develop polarization holography techniques and the Stokes holography (Singh et al., 2012).

2.3. Field interferometer

Consider a stationary polarized light illuminates two pinholes Q_1 and Q_2 in an opaque screen as shown in Fig. 2.2. Under this condition, relation of random electromagnetic field at a point ρ on the screen is given as

$$E(\rho) = K_1 \, E(Q_1) \frac{\exp\,(ikR_1)}{R_1} + K_2 \, E(Q_2) \frac{\exp\,(ikR_2)}{R_2} \qquad (2.2a)$$

where $E(Q_t), t = (1,2)$ represents complex fields in the pinhole, and R_t is the distance from source to the observation plane. The quantities $K_{1,2}$ are pure imaginary numbers that depends on the pinhole area at $Q_{1,2}$ (Setälä et al., 2006).
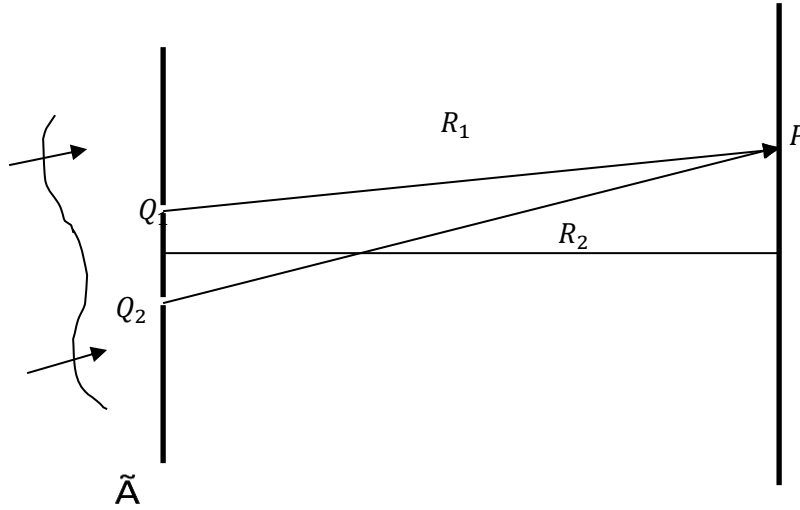
Figure 2-2 A representation of the young's interference with monochromatic polarized light

As discussed earlier, intensity and polarization state of the light at the observation point can be obtained from the polarization matrix elements $J_{mn}(\rho) =$

$\langle E_m^*(\rho)E_n(\rho)\rangle$. Substitution of the polarization matrix elements into Eq. 2.2a leads to relation as (Setälä et al., 2006)

$$J_{mn}(\rho) = J_{mn}^1(\rho) + J_{mn}^2(\rho) + \sqrt{trJ^1(\rho)}\sqrt{trJ^2(\rho)}\{\eta_{mn}(Q_1,Q_2)exp(-ik(R_1-R_2)+$$
$$\eta_{mn}(Q_2,Q_1)exp(ik(R_1-R_2)\})$$

$$(2.2b)$$

Term $J_{mn}^t(\rho), t = (1,2)$ are the polarization matrix elements when only the pinhole at the Q_t is open. In connection with elements of the CP matrix, we have defined

$$\eta_{mn}(Q_1, Q_2) = \frac{W_{mn}(Q_1, Q_2)}{\sqrt{tr\, J(Q_1)tr\, J(Q_2)}}$$

Using connection between the GSPs and elements of the CP matrix, we can also give relation of the polarization interference in terms of the Stokes parameters and the generalized Stokes parameters as

$$S_l(\rho) = S_l^1(\rho) + S_l^2(\rho) + 2 \begin{Bmatrix} S_l(Q_1, Q_2) \exp(-ik(R_1 - R_2)) \\ +S_l(Q_2, Q_1) \exp(ik(R_1 - R_2)) \end{Bmatrix} \qquad (2.2c)$$

Eq. 2.2c states that polarization modulation takes place at the observation plane and contrast of the polarization fringes depend on the GSPs at the source plane. First modulation for $l = 0$ corresponds to the intensity modulation as usually represented in the scalar interference. Stokes or intensity fringes discussed in this section depends on the second order correlation parameters such as $W_{mn}(Q_1, Q_2)$ or $S_l(Q_1, Q_2)$.

2.3.1. Stokes holography to see the unseen information

The Stokes parameters are useful in characterizing and encoding vectorial nature of the light in terms of the polarization modulations as explained in Eq. 2.2c. While interference plays a significant role in recording and

reconstructing the wavefront of the light and hence information of the object like in holography, majority of these investigations mainly deal with the intensity modulation, i.e., modulation in $S_0(\rho)$, and reconstruct only complex field of the light leaving aside the polarization feature. Attempts have been made to use full Stokes parameters in recording and reconstruction of the complete wavefront, i.e., amplitude, phase and polarization (Singh et al., 2012). Basic principle of this technique, known as Stokes holography, is explained below with the help of Fig. 2.3. Stokes fringes records complete wavefront information as explained in the previous section. Mode of recording and reconstructing such fringes is another crucial factor for appealing application of the holography based on the Stokes fringes. In conventional digital holography, recording of the intensity fringes is done optically and the intensity hologram is captured by a detector. Such holograms are digitally reconstructed using various types of algorithms (Schnars and Werner, 2003).
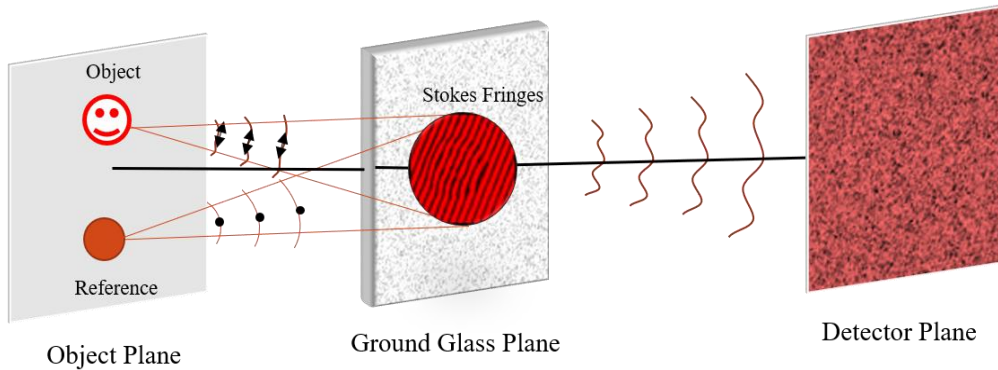
Figure 2-3 Schematic diagram for recording and reconstruction in the Stokes holography

Usually, SPs are recorded in multiple steps or using expensive commercial polarization camera. Formation and recording of the Stokes fringes is shown in the left side of Fig. 2.3. However, combination of polarization fringes with Eq. 2.1.3n provides an un-conventional way to reconstruct information in terms of the GSPs. This approach states that real time scattering of Stokes fringes through diffuser generated stochastic electromagnetic field in the reconstruction process in the right-hand side as shown in Fig. 2.2.1. This situation permits to exploit connection between the Stokes fringes and the generalized Stokes

22

parameters discussed earlier. Therefore, information encoded in the Stokes fringes is reconstructed as two or three dimensional distributions of the generalized Stokes parameters (GSPs). Measurement of the GSPs require specifically designed un-conventional detector as highlighted by a cartoon in the schematic sketch. In this chapter and thesis, we will discuss some experimental methods to measure the GSPs and hence reconstructs the Stokes fringes. Amplitude interferometers discussed in this section face several challenges, since such interferometers require coherence of the light detected at two different ports. For optical telescope and applications in the astronomical imaging, presence of atmospheric turbulence and the fact that light from the two different telescopes has to be brought together with same precision limits applications of such interferometers. Similar problems also come in the application of field interferometer in the issue of imaging through random scattering medium. Any external disturbance or vibrations during experiment affects quality of reconstruction (Chen et al., 2020).

2.3.2 Field interferometer: detection of instantaneous complex fields

To exploit advantage of the spatial averaging in evaluation of the coherence-polarization features of the stochastic electromagnetic fields, we present an experimental technique of a simultaneous complete polarization mapping of a field at a fixed time t and full data acquisition. This uses ensemble averaging of the spatially fluctuating random vector field with space averaging. Spatial distribution of the temporally frozen random electromagnetic field is detected using a specially designed field-based polarization interferometer (second order correlation). An experimental system to instantaneously detect ASPs. A linearly polarized beam from a coherent laser is oriented at 45 degrees by half wave plate (HWP1), spatially cleaned by combination of microscope objective O1, pinhole S, and a collimated lens L1. This collimated beam splits into two arms by a beam splitter BS1. A specially designed triangular Sagnac polarization interferometer in the first arm of the interferometer (shown by a blue

line) creates two mutually tilted orthogonally polarized reference beams with the help of a telescopes assembly formed by lens system L2 and L3. Linear polarized beam at 45 enters polarization beam splitter PBS1 and separates into two counter propagating beams in the Sagnac interferometer. These beams come out of the PBS1 as a pair of collimated orthogonally polarized reference beams. Mirror M3 and M4 together introduce desired amounts of tilts to the orthogonally polarized beams to make a spatial-frequency multiplexed fringes pattern suitable for Fourier fringe analysis.

The second arm of the interferometer (shown by a red line) created a spatial random field by illumination of the ground glass. Another triangular Sagnac interferometer along with imaging optics is placed in this arm to generate a secondary speckle with controlled statistics as explained in coming lines. A circular aperture, located at the entrance of the second arm, is imaged through the Sagnac interferometer by lens L4 on the ground glass in such a way that two counter propagating and orthogonally polarized beams (indicated by green and blue lines) together form duplicated images of the source at the diffuser plane as shown in Fig. 2.4. The separation between the two orthogonal polarization sources (twin images) at the diffuser is controlled by mirror M5 and M6 and hence this control instantaneous polarization modulation $I_{mn}(\hat{r})$ or $s^A(\hat{r})$. The degree of overlap of the orthogonally polarized source at the diffuser plane control the statistics of the random field at the observation plane according to the van Cittert-Zernike theorem established using the spatial optics. For instance, when the orthogonally polarized circular apertures fully overlap at the ground glass plane, the ground glass introduces a same random phase $\varphi(\hat{r})$ to the x-and y- field components, and hence polarization is uniform over the random field at the observation plane. This case will give spatial degree of polarization$P(0) = 1$. Similarly, partially overlapping replicas as the ground glass will introduce partial correlation between the x- and y- components at the observation plane and hence $0 < P(0) < 1$. The ratio of the orthogonal polarization components at the

ground glass can be controlled by rotation of the HWP2 and this will lead to increase in value of spatial degree of polarization, which is also known as en-polarization in literature. Another case is full separation between two copies of imaged source at the ground glass and this corresponds to complete loss of correlation between the x-and y- field components at the observation plane and hence generation of completely spatially depolarized (spatially random polarization) situation with $P(0) = 0$.
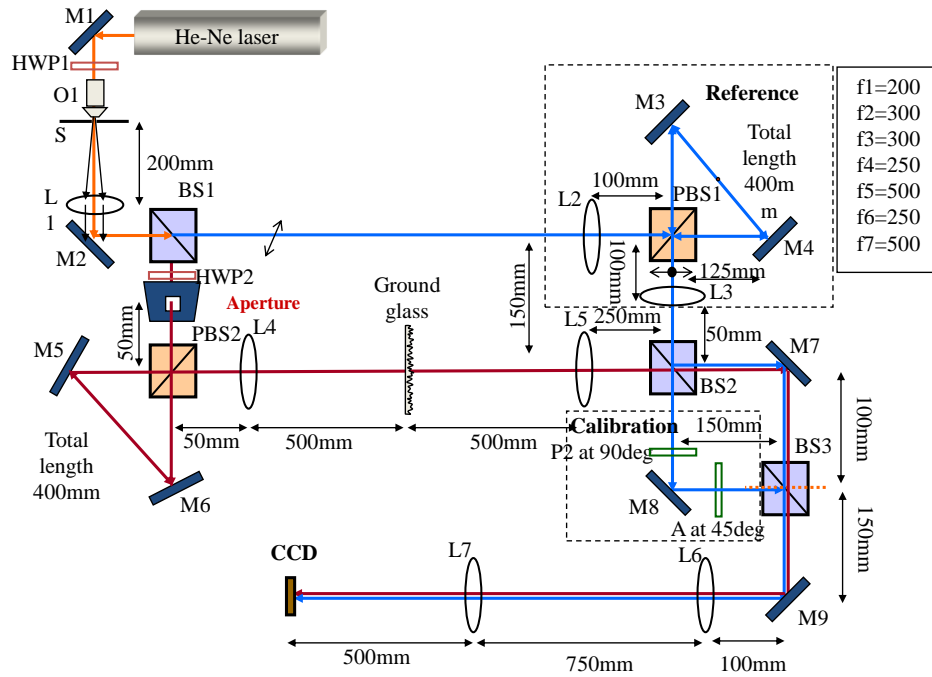
Figure 2-4 An experimental setup to detect ASP and orthogonal polarization components of random electromagnetic field from a single measurement at the CCD
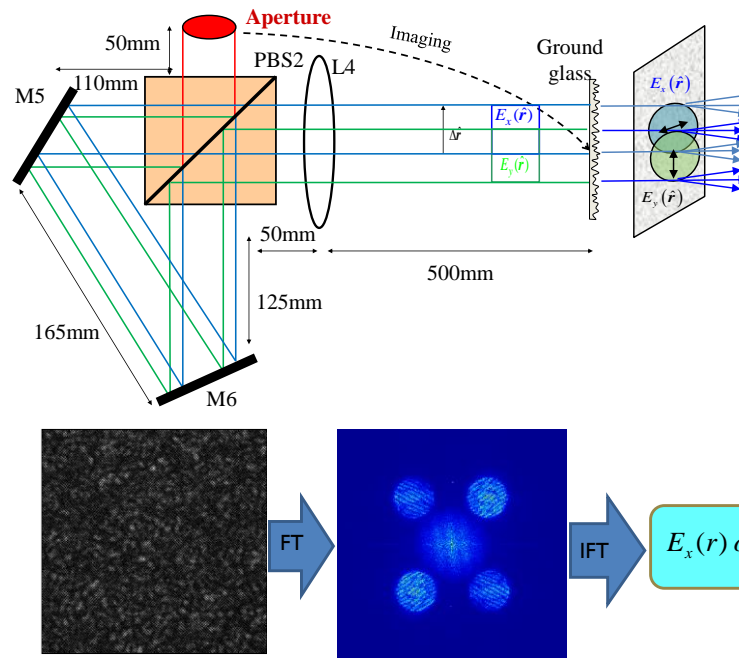
Figure 2-5 Triangular Sagnac interferometer to make two copies of the source

at the ground glass and control overlap of the orthogonal polarization components and second part shows recorded interferogram which is composed of two orthogonal polarization components with Fourier analysis process. FT and IFT stand for two dimensional Fourier and inverse Fourier transform

Scattering of polarization structured beam due to overlap of the two orthogonal polarization components through ground glass generated speckle pattern with the Gaussian statistics. The scattered fields polarization components encoded into interference fringes are recorded by the charged coupled device CCD with the help of magnifying lens combination L6 and L7. The fringe pattern is composed to the two sets of interference fringes with different periodicity for two orthogonal polarization components. Making use of the Fourier fringe analysis, the spectrum of each orthogonal polarization components is distinguishable in the Fourier space and the information about the amplitude and phase is retrieved in the signal domain. The complex amplitude of the x- and y-polarization components coming from the diffuser is calibrated with a standard

beam to erase errors introduced by optical system due to misalignment. Using the spatial averaging of these experimentally detected orthogonal polarization components at a fixed time, i.e., ASP, we can evaluate the GSPs and CP matrix of the random fields and detailed analysis in this direction can be found in Singh et al., 2014 and Singh et al., 2013). Stability challenge of the field-based polarization interferometer can be solved using the intensity interferometer and some of these techniques will be discussing in coming chapters.

2.4. The Hanbury Brown-Twiss (HBT) interferometer

A possible solution of challenges of the field interferometer is intensity interferometer which relies on not measuring light amplitudes at different positions but intensities, collecting photons in other words. In year 1956 Hanbury Brown and Twiss proposed to use the correlations of the intensities to determine diameter of the Sirius from the Jodrell Bank Experimental station of the University of Manchester as in Fig. 2.6. System was built with two mirrors focusing starlight on photo-multipliers, whose signals were amplified (Hanbury and Twiss, 1975).

Figure 2.6 The first Stellar intensity interferometer at Jodrell Bank (University of Manchester) in 1956. (Picture source: Davis, 2018)

After a series of laboratory experiments, which also generated considerable controversy and lead to birth of advance quantum optics, this group further explored intensity interferometry measurement with the Narrabri Stellar Intensity Interferometer as shown in Fig. 2.7. This circular rail has a diameter of 188 m and angular size up to(0.41 ∓ 0.03) mas were measured with this interferometer [23]. Advantage of an intensity interferometer is associated with the fact that this approach does not require measurement of the amplitude but number of photons. Hence, effect of turbulence which changes phase of the incoming wave does not influence the quality of measurement.
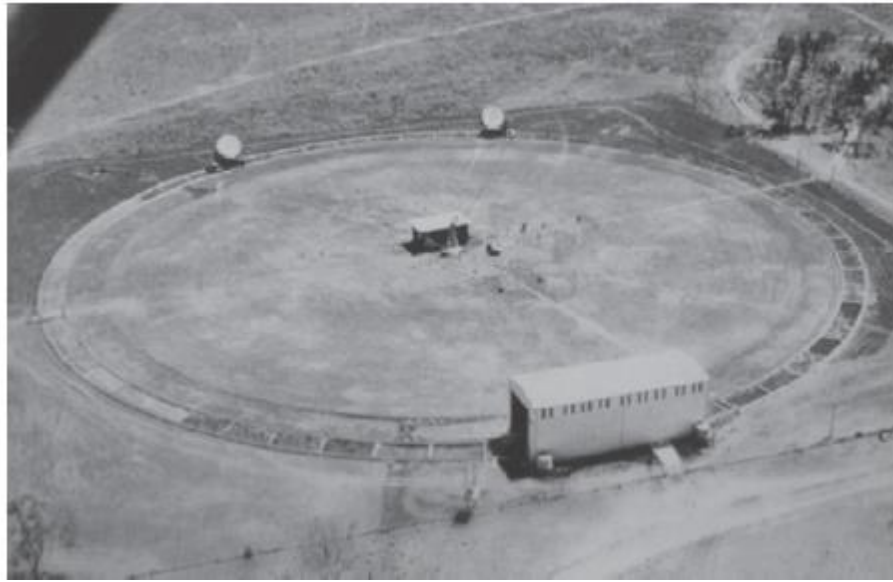
Figure 2.7 The intensity interferometer near Narrabri (Australia). The two telescopes placed on the circular track on move to vary the baseline and to change the angle of sight. (Picture source: Hanbury et al., 1974)

2.4.1 Physics of intensity interferometer

The normalized n[th] order correlation functions $g^{(n)}$ provides correlations at any arbitrary positions in space and time and such parameters are useful in characterizing light source and developing new applications as explained earlier. In this chapter and in line with theme of the thesis, we will consider only separation of points in space not in time, i.e., temporal correlation

28

part not considered. The first and second order correlation functions $g^{(1)}$ and $g^{(2)}$ are of special interests. The expression of the first order correlation function, also described earlier, is given as

$$g^{(1)}(Q_1, Q_2) = \frac{\langle E^*(Q_1,t)E(Q_2,t)\rangle}{\langle E^*(Q_1,t)E(Q_1,t)\rangle} \qquad (2.3.1a)$$

where Q_1 and Q_2 are two spatially separated points. The bracket $\langle \ \rangle$ denotes ensemble average and traditionally replaced by temporal averaging $\langle E(t)\rangle = \frac{1}{T}\int_0^T E(t)dt$ for recording time T. In the normalization, we assume that the average intensities at two-point sources are nearly same, therefore the choice of Q_1 and Q_2 does not influence result. The quantity given in Eq. 2.3.1a is also referred as the degree of coherence defined earlier by $\mu(Q_1, Q_2)$.

The second-order correlation can be described as

$$g^2(Q_1, Q_2) = \frac{\langle E^*(Q_1)\, E^*(Q_2)\cdot E(Q_1)\, E(Q_2)\rangle}{\langle E^*(Q_1)\, E^*(Q_1)\rangle\langle E^*(Q_2)\, E(Q_2)\rangle} \qquad (2.3.1b)$$

This equation can be further simplified by substituting intensities $I = E^*E$

$$g^2(Q_1, Q_2) = \frac{\langle I(Q_1)\cdot I(Q_2)\rangle}{\langle I(Q_1)\rangle\langle I(Q_2)\rangle} \qquad (2.3.1c)$$

The correlation (multiplication of the intensities as mentioned above) can be implemented either electronically or digitally. Using Siegart relation, the second order intensity correlation (or fourth order field correlation) can be explained in terms of the first order intensity (second order field) correlation (Goodman, 2000) as

$$\langle I(Q_1)I(Q_2)\rangle = \langle I(Q_1)\rangle\langle I(Q_2)\rangle + |E^*(Q_1)E(Q_2)|^2 \qquad (2.3.1d)$$

Therefore,

$$g^{(2)}(Q_1, Q_2) = 1 + \left|g^{(1)}(Q_1, Q_2)\right|^2$$

This highlights the insensitivity the intensity interferometers to the phase.

2.4.2 HBT for polarized light

Consider a stochastic polarized light field that propagates along the z direction in the coordinate system given in Fig. 2.1. The mean value of the optical intensity is given as

$$\langle I(r) \rangle = \langle |E_x(r)|^2 \rangle + \langle |E_y(r)|^2 \rangle = trW(r,r)$$

The electromagnetic degree of coherence of the vector light is given as

$$\gamma^2(r_1, r_2) = \frac{tr[W(r_1, r_2)W(r_2, r_1)]}{\langle I(r_1) \rangle \langle I(r_2) \rangle} \qquad (2.3.2a)$$

Fluctuations of the intensities from its mean value is given as

$$\langle \Delta I(r) \rangle = I(r) - \langle I(r) \rangle$$

Under consideration of Gaussian random process and applying the Siegart relation, correlation of the cross covariance at two points is given as

$$\langle \Delta I(r_1) \Delta I(r_2) \rangle = \sum_{m,n} |W_{mn}(r_1, r_2)|^2 = tr[W(r_1, r_2)W(r_2, r_1)] \qquad (2.3.2b)$$

The degree of coherence of the stochastic electromagnetic beam can also be expressed as second order intensity correlation as follows

$$\gamma^2(r_1, r_2) = \frac{\langle \Delta I(r_1) \Delta I(r_2) \rangle}{\langle I(r_1) \rangle \langle I(r_2) \rangle} \qquad (2.3.2c)$$

Hence, the correlation between intensity fluctuations, at a pair of points, depends on the mean intensities, and on the degree of electromagnetic coherence

(Hassinen et al., 2011). The normalized correlation of intensity fluctuations is equal to the square of the degree of coherence for electromagnetic fields.

2.5 Spatial statistical optics and its importance

Ranging from classical to quantum domains, the optical fields are intrinsically of statistical in nature. The statistical optics covers stochastic light which shows randomness in time and/or in space. To deal with the stochastic light fields, the ensemble average is usually replaced with the temporal average, considering that the statistical field is stationary and ergodic in time (Goodman, 2000). This approach is justifiable in majority cases of fundamental and practical interests, such as thermal light source, partially coherent beams etc. Such ideas of traditional statistical optics build on the foundation of temporal stationarity and temporal ergodicity is called 'temporal statistical optics' to clearly distinguish it from spatial statistical optics dealing with spatially fluctuating random light (Takeda et al., 2014).
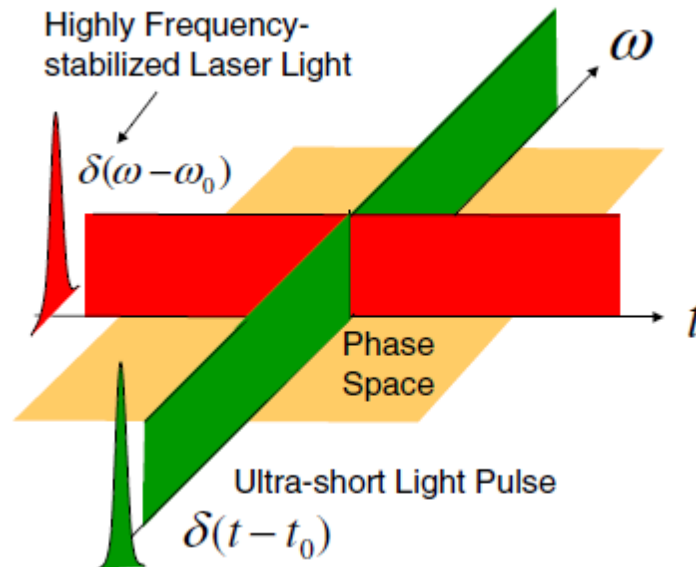
Figure 2.8 Schematic representation of light fields that are temporally and spectrally confined in phase space. (Picture source: Takeda 2014)

31

With development of the laser technology, applications have emerged on the basis of extreme optical fields that are strongly confined either on the time axis or on the optical frequency axis in the time-frequency phase space as shown in Fig. 2.6. For such situations, temporal statistical optics is not a useful tool. For instance, an ultra-short optical pulse strongly focused on the time axis, does not show temporal stationarity required for the temporal statistical optics. On the other hand, for ideally stabilized monochromatic laser light with the optical frequency confined on the optical frequency axis, time averaging is not useful because the light field is not fluctuating in time scale. Therefore, we have two set of example where different types of statistical optics are desired. Considering an example of the spatial variation of the light fields, we note that such light fields generate spatially fluctuating pattern when scattered by diffusing medium. An example of such spatially fluctuating light field is speckle pattern. The spatial statistics of the scattered field and replacement of the ensemble average by the space average provides signature of the object obscured by the diffuser using from a single random pattern (rather than several patterns as usually required in the temporal averaging). Such idea inspires to explore analysis of instantaneous or time frozen optical fields that cannot dealt with the temporal statistical optics. From the formal symmetry of space and time in the wave equation, this interchange between space and time appears to be a natural choice in the sense of analogy. A schematic representation of the polarized random field, known as polarization speckle, is shown in Fig. 2.3.2. Considering the orthogonal polarization components $E_x(r,t)$ and $E_y(r,t)$ as defined earlier. The GSPs terms of the time varying electric field are defined as

$$S_0(r_1, r_2; t_1, t_2) = \langle E_x^*(r_1, t_1) E_x(r_2, t_2) \rangle + \langle E_y^*(r_1, t_1) E_y^*(r_2, t_2) \rangle \qquad \text{(2.4 a)}$$

$$S_1(r_1, r_2; t_1, t_2) = \langle E_x^*(r_1, t_1) E_x(r_2, t_2) \rangle - \langle E_y^*(r_1, t_1) E_y(r_2, t_2) \rangle \qquad \text{(2.4b)}$$

$$S_2(r_1, r_2; t_1, t_2) = \langle E_x^*(r_1, t_1) E_y(r_2, t_2) \rangle + \langle E_y^x(r_1, t_1) E_x(r_2, t_2) \rangle \qquad \text{(2.4c)}$$

$$S_3(r_1, r_2; t_1, t_2) = i\left[\langle E_y^*(r_1, t_1)E_x(r_2, t_2)\rangle - \langle E_x^*(r_1, t_1)E_y(r_2, t_2)\rangle\right] \qquad (2.4\text{d})$$

where r_1, r_2 are two spatial coordinates and t_1, t_2 are two different instants of time. When $r_1 = r_2$ and $t_1 = t_2$, the GSPs transforms to conventional SPs. Considering stationarity and ergodicity in space, we replace ensemble average $\langle \cdot \rangle$ by the space average $\langle \cdot \rangle_R$. Since our interests in this thesis are on the spatial correlation, we put $t_1 = t_2 = t$ to evaluate GSPs as

$$S_0(\Delta r, t) = \langle E_x^*(r_1, t_1)E_x(r_2, t_2)\rangle_R + \langle E_y^*(r_1, t_1)E_y^*(r_2, t_2)\rangle_R \qquad (2.4\text{ e})$$

$$S_1(\Delta r, t) = \langle E_x^*(r_1, t_1)E_x(r_2, t_2)\rangle_R - \langle E_y^*(r_1, t_1)E_y^*(r_2, t_2)\rangle_R \qquad (2.4\text{ f})$$

$$S_2(\Delta r, t) = \langle E_x^*(r_1, t_1)E_y(r_2, t_2)\rangle_R + \langle E_y^*(r_1, t_1)E_x(r_2, t_2)\rangle_R \qquad (2.4\text{ g})$$

$$S_3(\Delta r, t) = i\left[\langle E_y^*(r_1, t_1)E_x(r_2, t_2)\rangle_R - \langle E_x^*(r_1, t_1)E_x(r_2, t_2)\rangle_R\right] \qquad (2.4\text{ h})$$

Here $\langle \cdot \rangle_R$ represents the space average as a replacement of the ensemble average and GSPs depend on the difference of spatial coordinates $\Delta r = r_2 - r_1$ The complex random field selected inside the $\langle \; \rangle$ represents a snap shot pattern at a particular instant of time as represented in Fig. 2.7. Polarization variation in the space (at a frozen time t) is shown in Fig. 2.7 using the Poincare sphere representation. In analogy to instantaneous intensity without time averaging, we can introduce at-the points (which means 'without space averaging') SPs (ASPs), which involve no averaging operation (neither in time nor in space) as

$$S_0^A(r) = E_x(r)E_x^*(r) + E_y(r)E_y^*(r) \qquad (2.4\text{ i})$$

$$S_1^A(r) = E_x(r)E_x^*(r) - E_y(r)E_y^*(r) \qquad (2.4\text{ j})$$

$$S_2^A(r) = E_x^*(r)E_y(r) + E_y^*(r)E_x(r) \qquad (2.4\text{ k})$$

$$S_3^A(r) = i\left[E_y^*(r)E_x(r) - E_x^*(r)E_y(r)\right] \qquad (2.4\text{ l})$$
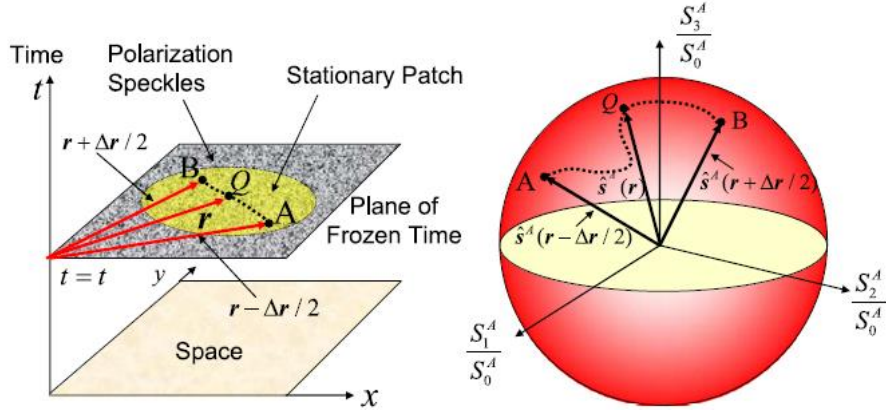
Figure 2.9 Space-time representation of stochastic electromagnetic field, and dynamics of polarization change in a single random pattern (at a frozen time t) is represented at the Poincare sphere. The SOPs in the random field is varying from point A to B. (Picture source: Singh et al., 2014)

The ASPs are real quantities and characterize instantaneous SOPS at the point in the space, which is well-defined at every spatial location in the randomly coherent field (Singh et al., 2014) and follows the relation

$$[S_1^A(r)]^2 + [S_2^A(r)]^2 + [S_3^A(r)]^2 = [S_0^A(r)]^2 \tag{2.4m}$$

The ASPs are geometrically represented by a Poincare vector as follows

$$S^A(r) = \big(S_1^A(r), \quad S_2^A(r), \quad S_3^A(r)\big) = \hat{s}^A S_0^A(r)$$

The length of the Poincare vector ss equal to the at-the point intensity $S_0^A(r)$, and $\hat{s}^A$ is a unit vector parallel to $S^A(r)$ that represents SOP at the spatial point r.

2.5.1 Vectorial van Cittert-Zernike theorem based on the spatial averaging

One of the important results of the coherence optics is the van Cittert Zernike theorem which connects a random source with the spatial coherence in the far field. In this section, we present a discussion on the derivation of the van

34

Cittert-Zernike theorem with the spatial averaging (rather than temporal averaging). To cover a more generalized situation, we deal with a polarized light and establish vectorial van Cittert-Zernike theorem. This generalized van Cittert-Zernike theorem will be on equal footing to the scalar case. This derivation is performed by considering ergodicity in space (rather than in time) and taking the space average over the observation plane (rather than over the source plane).

Van Cittert Zernike Theorem in scalar and vectorial domain: Spatial optics approach
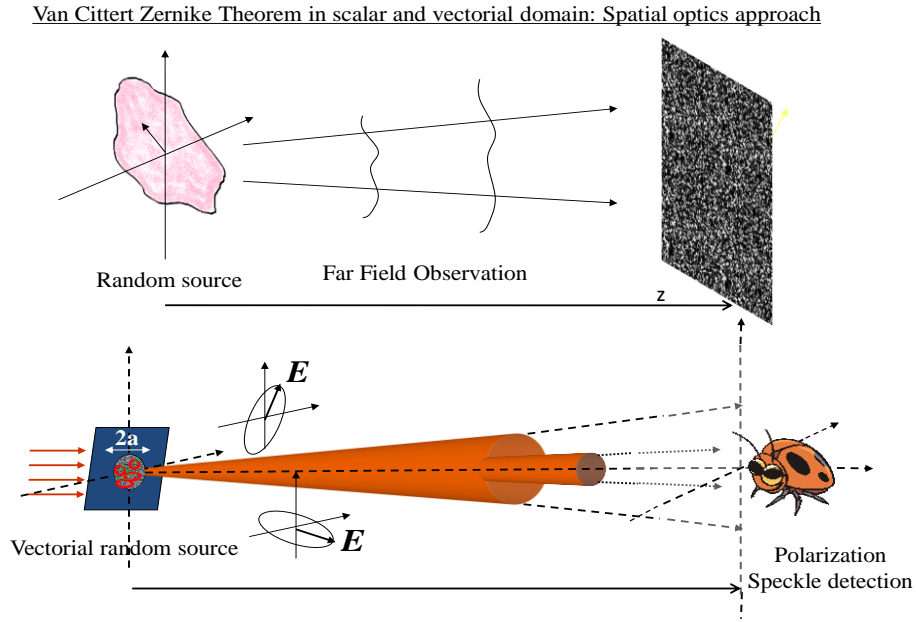
Figure 2.10 A sketch to represent scattering of the coherent light from a diffuser and generation of speckle pattern in the far field.

The scattered field at the observation plane locate in the far field, for a fixed time t, is given by

$$E_m(r) = \int E_m(\hat{r}) \exp(i\varphi_m(\hat{r})) \, exp\left(-i\frac{2\pi}{\lambda z} r \cdot \hat{r}\right) d\hat{r} \qquad (2.5.1a)$$

Here, $E_m(\hat{r})$ is the vector field component of the incident light at the diffuser plane as shown in Fig. 2.5.1, and $\hat{r}$ is the two-dimensional position vector at the diffuser (ground glass) plane, $\varphi_m(\widehat{r})$ is a random filed introduced by the diffuser. Elements of the CP matrix for the field are given (Singh et al., 2013) as

$$W_{mn}(r_1, r_2) = \langle E_m^*(r_1) E_n(r_2) \rangle_R = \langle E_m^*(r_1) E_n(r_1 + \Delta r) \rangle_R = W_{mn}(\Delta r) \propto$$

$$\int \left\{ \iint E_m^*(\hat{r}_1) E_n(\hat{r}_2) \times \exp\left[-i\frac{2\pi}{\lambda z}[(r_1 + \Delta r) \cdot \hat{r}_2 - r_1 \cdot \hat{r}_1] \right] d\hat{r}_1 d\widehat{r}_2 \right\} dr_1 \quad \propto$$

$$\int I_{mn}(\hat{r}) \exp\left(-i\frac{2\pi}{\lambda z}\Delta r \cdot \hat{r}\right) d\hat{r} \tag{2.5.1b}$$

Here, $\tilde{E}_m(\hat{r}) = E_m(\hat{r})\exp(i\varphi_m(\hat{r}))$ is the random field coming out of the diffuser and diffuser is considered to be non-birefringence, i.e., $\varphi_m(\hat{r}) = \varphi_n(\hat{r})$, and we have $r_2 = r_1 + \Delta r$. In equation (2.5.1b), the integration taken over the observation plane for spatial averaging results in a delta function $\int \exp\left(-i\frac{2\pi (\hat{r}_2 - \hat{r}_1) \cdot r_1}{\lambda z}\right) dr_1 \propto \delta(\hat{r}_2 - \hat{r}_1)$. In Eq. 2.5.1b, $I_{mn}(\hat{r}) = E_m^*(\hat{r})E_n(\hat{r})$, which can take a complex value for $m \neq n$. Eq. 2.5.1b is regarded as a spatial average version of the van Cittert-Zernike theorem for the CP matrix. Following definition of the degree of coherence for the stochastic electromagnetic field, we can characterize the spatial coherence-polarization matrix of the scattering field by

$$\gamma(\Delta r) = \left(\frac{tr[W^*(\Delta r)W(\Delta r)]}{tr\, W(0)tr\, W(0)} \right)^{1/2}$$

$$P(0) = \left(1 - \frac{4 \det W(0)}{|tr\, W(0)|^2} \right)^{1/2}$$

Here, $\gamma(\Delta r)$ and $P(0)$ are a spatial-average version of the degree of coherence and the spatial degree of polarization, respectively. The random field is fully spatially polarized for $\gamma(0) = 1$, i.e., no polarization fluctuation in space. On the basis of close relation between the GSPs and CP elements, we can also establish the vectorial van Cittert-Zernike theorem using the SPs and GSPs.

CHAPTER 3
DEGREE OF SPATIAL POLARIZATION AND INTENSITY CORRELATION IN 2D AND 3D

3.1 Introduction

Intensity correlation measurement, proposed by Hanbury Brown and Twiss (HBT), has become an important technique to analyze the correlations of the random fields (Hanbury and Twiss, 1956). The HBT technique was proposed to examine the angular size of the stars and has been studies in detail using both the classical and quantum theory of light (Hanbury and Twiss, 1957). The intensity correlations have been widely used in multidisciplinary applications. Some of these applications are in laser speckles, high energy physics, nuclear physics, and atomic physics etc. (Mandel and Wolf, 1995; Bromberg et al., 2010; Kumar et al., 2012; Singh et al., 2014; Schultheiss et al., 2016; Wiedemann and Heinz, 1997; Baym, 1997). Uniqueness of the HBT approach and the intensity-based interferometer lies with their ability to develop highly stabilized interferometer for light analysis in comparison to the field-based interferometers such as the Young's interferometer. Experimental measurement techniques to measure the field correlation of the light based on the Young's approach and second order correlation are highly sensitive to external disturbances such as vibration, noise etc. On the other hand, the intensity interferometers based on the HBT approach are highly stable and able to characterize the correlation structures of the light even in the non-stable conditions. Origin of the HBT approach can be traced back to the technological development in the astronomical imaging. Early works in the astronomical imaging were mainly confined to the direction detection of the optical field intensity with help of telescope. Later, the HBT experiment on the use of intensity correlation, i.e., fourth order correlation, brought a breakthrough in the astronomy.

Correlation methods, particularly the intensity correlation, has also brought major revolution in development of the un-conventional imaging techniques such as ghost imaging, ghost diffraction, single pixel correlation holography, intensity correlation holography etc. (Erkmen and Shapiro, 2010; Padgett and Boyd, 2017; Singh et al., 2017). The ghost imaging reconstructs the image from measurement of the intensity correlations between the two random fields. This measurement is realized by two photo detectors: a charged coupled device and a bucket detector. The ghost imaging was first detected with the correlation of quantum sources and later technique is also successfully implemented with the classical thermal light source. In recent years, new trends have also emerged to use intensity correlation of the spatially fluctuating random field such as laser speckle and develop new un-conventional imaging techniques such as correlation holography, ghost imaging etc.

However, majority of the investigations on the intensity correlations have been limited to the scalar wave treatment under notion of one polarization mode. With development of unified theory of coherence-polarization and emerging interests in the polarization inhomogeneous random fields, the correlation features of vector waves have drawn significant attention (Perrin et al., 2012; Wolf, 2007; Sahin et al., 2009; Xin et al., 2008; Korotkova, 2006; Kuebel, 2009). Tervo et al. (2011) discussed the intensity correlation effect with classical vector-valued fields in the space-time domain and showed that the electromagnetic degree of coherence of the stationary electromagnetic waves obeying Gaussian statistics can relate to the intensity correlation (Tervo et al., 2003). Such investigations have also been extended to the space-frequency domain and it is demonstrated that the spectral degree of electromagnetic coherence has an impact on the spectral HBT effect (Setälä et al., 2004). It has been shown that the correlation of intensity fluctuations between two detectors depends on the degree of cross polarization (Sirahi and wolf, 2007; Volkov et al., 2008; Al-Qasimi et al., 2010; Hassinen et. al., 2011). In a separate investigation, Hassinen et. al. (2011) has discussed the

effects of spatial correlations and the degree of polarization of the field on the correlations of the intensity fluctuations at pair of separate points, even when the degree of polarization varies with the position (Hassinen et. al., 2011). Wu and Visser, (2014) have recently derived expression to examine the effect of source parameters on the two-point intensity correlation in the same cross section of a random electromagnetic beam (Wu and Visser, 2014). Some experimental implementations of the intensity correlation for the vector light fields have been reported in recent years (Wu and Visser, 2014; Chen et al., 2014). Majority of these intensity correlation techniques are restricted to temporal ergodicity and applying temporal averaging as replacement of the ensemble averages except some recent works on the spatial ergodicity in the different context (Chen et al., 2016; Vinu and Singh, 2015).

The spatial ergodicity plays an important role in characterizing the spatially fluctuating random fields such as speckles. When a coherent polarized light travel through a static diffuser which involves multiple scatterings, random fluctuations are introduced into the spatial distribution of the state of polarization (SOP). Because the light is monochromatic and the diffuser is static, the random field is free from temporal fluctuation and remains to be fully polarized according to the conventional definition based on time averaging and has a well-defined SOP at each spatial point. Such a random field is referred to as polarization speckles (D Singh and Singh, 2018; Singh et al., 2014; Takeda et al., 2010; Reddy et al., 2017). An example of polarization fluctuation in the polarization speckle is represented on the Poincare sphere as shown in Fig. 3.1
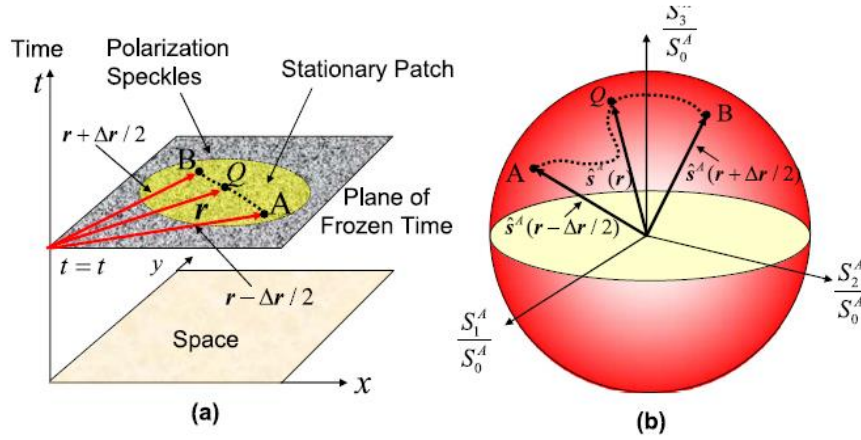
Figure 3.1. (a) Space-time distribution of polarization speckles. Point A and B are observation points in the area of a stationary patch within which statistics remains unchanged. (b) Trajectory of an at-the point Stokes vector $\hat{S}^A(r)$ on Poincare sphere as the observation point moves from A to B.

To analyze such random fields, definitions of the degree of coherence and spatial degree of polarization based on the spatial average can be introduced (Takeda et al., 2010). The spatial degree of polarization is conceptually analogous to the degree of macroscopic magnetization of magnetic materials induced by ordered or disordered orientations of many microscopic atomic dipoles, and the polarization speckles bear similarity to magnetic domains in their geometrical structures (Kittel, 1976). In a review article Takeda and coworkers have given a detailed discussion on spatial statistical optics that placed more emphasis on the spatial statistics of the optical field, rather than on their temporal statistics (Takeda et al., 2014). The intensity correlation with spatial averaging has been utilized in recent years for characterization of scalar and polarization speckles (Reddy et al., 2014; Vinu and Singh, 2015; Alves et al., 2015). However, these investigations are limited at a fixed transverse plane and with different objectives.

This chapter aims to study intensity correlation of the spatially fluctuating polarized random fields at different distances under the paraxial propagation. Quantitative analysis of the random field is carried out by following relation between the degree of coherence of the electromagnetic fields, spatial

degree of polarization and the intensity correlation for the Gaussian random fields. An experimental scheme is designed to generate and analyze the random fields with different polarization fluctuations and results are presented. The polarization fluctuation in the random field is synthesized by introducing different vortex modes into orthogonal polarization components of the light prior to the random scattering from a diffuser. Presence of the helical modes, i.e., vortex, in the one of the orthogonal polarization components of the incident light makes coupling between the spatial and polarization modes of the light and hence generates spatially varying polarization states. Our purpose is to use the vortex beams to generate spatial polarization inhomogeneity in the laser speckle and analyze the speckles at the focal plane and at different transverse plane using the intensity correlation and spatial optics. For quantitative comparison, experimental results are compared with the theory using digital propagation of the light.

3.2 Principle

Let's consider a monochromatic polarized light from a random source as shown in Fig. 3.2. The complex electric field at a fixed transverse plane is represented by the transverse polarization vectors as

$$E(\boldsymbol{r}) = \hat{x} E_x(\boldsymbol{r}) + \hat{y} E_y(\boldsymbol{r})$$

(3.1)

where $\hat{x}, \hat{y}$ are unit vectors along x and y direction and r is position vector in the transverse plane. The orthogonal polarization components of the light field are represented by $E_x(r)$ and $E_y(r)$. Following angular spectrum method, the complex field at an arbitrary transverse plane located at distance z from the source is given as

$$E(\boldsymbol{r}, z) = exp(ikz) \int E(\boldsymbol{u}) exp(ik_z(\boldsymbol{u})z) exp(i\boldsymbol{u} \cdot \boldsymbol{r}) d\boldsymbol{u}$$

(3.2)

where u is normalized optical coordinates at the source, λ wavelength of the light and $k = \frac{2\pi}{\lambda}$ wave number. Term $k_z(u) = \frac{|u|^2}{2k}$ under paraxial approximation. The intensity pattern of the light at a transverse plane z is given as

$$I(\boldsymbol{r}, z) = |E_x(\boldsymbol{r}, z)|^2 + |E_y(\boldsymbol{r}, z)|^2 \tag{3.3}$$

The correlation of intensity fluctuations at two points in the different transverse plane is defined as

$$c(\boldsymbol{r}_1, z_1; \boldsymbol{r}_2, z_2) = \langle \Delta I(\boldsymbol{r}_1, z_1) \Delta I(\boldsymbol{r}_2, z_2) \rangle \tag{3.4}$$

where $c(\boldsymbol{r}_1, z_1, \boldsymbol{r}_2, z_2)$ is cross-covariance of the intensity fluctuation and $\Delta I(\boldsymbol{r}, z) = I(\boldsymbol{r}, z) - \langle I(\boldsymbol{r}, z) \rangle$ is fluctuation of the intensity with respect to its mean value $\langle I(\boldsymbol{r}, z) \rangle$. Let us consider that the statistical properties of the random field are Gaussian. Therefore, the fourth order correlation, i.e., intensity correlation, can be expressed in terms of the second order field correlation. Substituting Eq. (3.2) into the intensity correlation relation, the cross covariance of the intensity at two different transverse planes is written as

$$\langle \Delta I(\boldsymbol{r}_1, z_1) \Delta I(\boldsymbol{r}_2, z_2) \rangle = \sum_{i,j} \left| \left\langle \int \int E_i^*(\boldsymbol{u}_1) E_j(\boldsymbol{u}_2) \, exp[i(k_z(\boldsymbol{u}_2) - \right. \right.$$
$$\left. \left. k_z(\boldsymbol{u}_1))] \, exp[i(\boldsymbol{u}_2 \cdot \boldsymbol{r}_2 - \boldsymbol{u}_1 \cdot \boldsymbol{r}_1)] \, d\boldsymbol{u}_1 d\boldsymbol{u}_2 \right\rangle \right|^2 \tag{3.5}$$

where $i, j = x, y$. Let us introduce spatial averages as replacement of the ensemble averages and considering $\boldsymbol{r}_1 = \boldsymbol{r}$, $\boldsymbol{r}_2 = \boldsymbol{r} + \Delta \boldsymbol{r}$, therefore the cross-covariance of the intensity is given as (D Singh and Singh, 2018)

$$\left\langle \Delta I(\boldsymbol{r}, z_1) \Delta I(\boldsymbol{r} + \Delta \boldsymbol{r}, z_2) \right\rangle_s =$$
$$\sum_{i,j} \left| \left\langle \int \int \int E_i^*(\boldsymbol{u}_1) E_j(\boldsymbol{u}_2) \exp\left[i\left(k_z(\boldsymbol{u}_2)z_2 - k_z(\boldsymbol{u}_1)z_1\right)\right] \exp\left[i(\boldsymbol{u}_2 \cdot \boldsymbol{r}_2 - \boldsymbol{u}_1 \cdot \boldsymbol{r}_1)\right] d\boldsymbol{u}_1 \, d\boldsymbol{u}_2 d\boldsymbol{r} \right\rangle \right|^2$$
$$= \sum_{i,j} \left| \int I_{ij}(\boldsymbol{u}) \exp\left[ik_z(\boldsymbol{u})(z_2 - z_1)\right] \exp\left[i\boldsymbol{u} \cdot \Delta \boldsymbol{r}\right] d\boldsymbol{u} \right|^2$$

$$\tag{3.6}$$

where $I_{ij}(\boldsymbol{u}) = |E_i(\boldsymbol{u})||E_j(\boldsymbol{u})|e^{i[\phi_j(\boldsymbol{u})-\phi_i(\boldsymbol{u})]}$is real for $i = j$and may take complex value for $i \neq j$. Eq. (3.6) is derived by making of using relation$\int exp[i(\boldsymbol{u}_2 - \boldsymbol{u}_1) \cdot r] \, dr = \delta(\boldsymbol{u}_2 - \boldsymbol{u}_1)$.

Therefore, polarization features of the random field are encoded into the intensity fluctuations as derived into Eq. (3.6). For the fields obeying Gaussian statistics, a connection exists between the intensity fluctuations and the degree of coherence (DOC). Following the definition of the degree of coherence of the electromagnetic fields proposed by Tervo et al. in the space-time domain, we define the DOC and the degree of polarization (DOP) of the spatially fluctuating fields as

$$\mu^2(\Delta\boldsymbol{r},\Delta z) = \frac{\langle \Delta I(\boldsymbol{r},z)\Delta I(\boldsymbol{r} + \Delta\boldsymbol{r}, z + \Delta z)\rangle_s}{\langle I(\boldsymbol{r},z)\rangle_s\langle I(\boldsymbol{r} + \Delta\boldsymbol{r}, z + \Delta z)\rangle_s}$$

$$P(0) = [2\mu^2(0) - 1]^{1/2} \tag{3.7}$$

Here $\mu(\Delta\boldsymbol{r}, \Delta z)$and $P(0)$ are spatial version of the DOC and DOP of the spatially fluctuating random fields. To examine the effect on polarization on the intensity fluctuations, we have experimentally measured intensity fluctuations of the random fields and these results are compared with the simulation based on right hand side of Eq. (3.6) based on the vectorial domain van Cittert-Zernike theorem (Singh et al., 2013).

3.3 Experiment Implementation

To study intensity correlation of the spatially fluctuating random fields at different distances following experimental set-up has been proposed as shown in Fig. 3.2. A monochromatic laser source of wavelength $\lambda = 632.8 nm$ (Melles Griot 25-LHP-928-230) is spatial filtered SF and collimated by a lens L1. A collimated beam propagates through a circular aperture of size 2.7mm diameter followed by the static ground glass and creates the speckle pattern. Subsequent speckle field is collected by a lens L2 of focal length 100mm and further propagates down to the camera plane. The intensity of the random speckle field is

captured using a CCD camera (PCO Pixel fly with 1040×1392 pixels and a pixel pitch of 6.45µm). A CCD is placed on a motorized z-scanner and hence, multiple speckle fields have been recorded at different longitudinal planes. Spatial averaging is performed on the scattered random fields to obtain cross-correlation of the speckles located at different longitudinal planes. Results are presented in the next section.
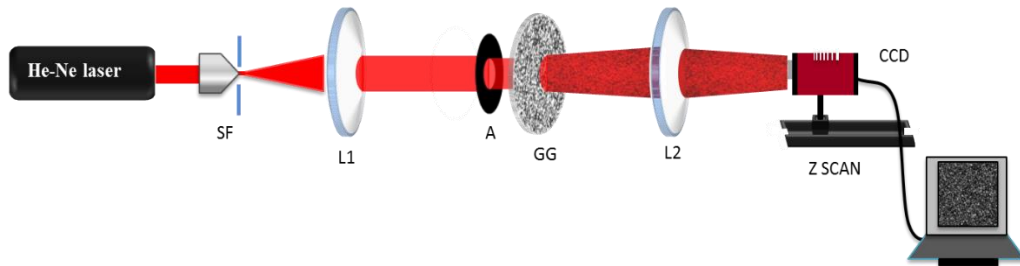
Figure 3.2. Experimental Set up to study degree of spatial polarization

In the second case, like the first experiment, a Spiral Phase Plate (SPP) is introduced in the set-up as shown in Fig. 3.4. The SPP as shown in Fig 3.3 is made by RPC photonics, USA. It can generate topological charges from 1 to 8. It is wavelength specific and is used for 633 nm only.
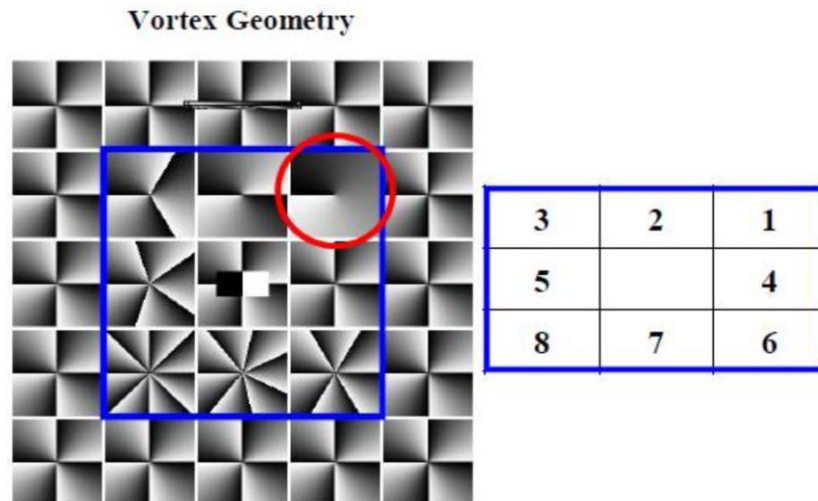
Figure 3.3 A schematic representation of the topological charge distribution in spiral phase plate (SPP).

Vortex generates spatial polarization inhomogeneity in the laser speckle. In this experiment, we have used vortices of different topological charges such as 0, 1 and 2 to record the speckle field at different longitudinal planes. The cross-correlation of the speckles has been measured by considering two speckles one with vortex beam and the other with non-vortex beam.
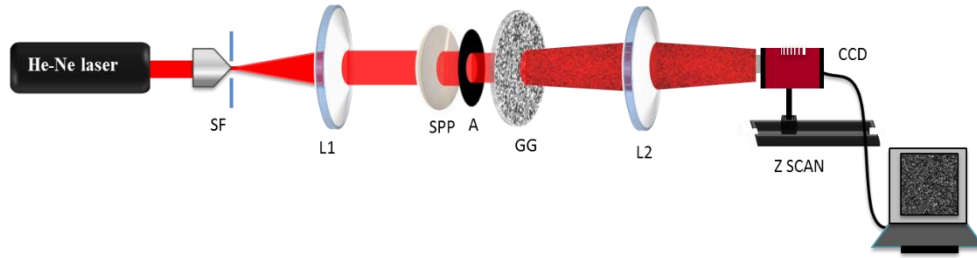
Figure 3.4. Experimental Set up to study degree of spatial polarization, with SPP.

In the third case as shown in Fig. 3.5, Mach-Zehnder type polarization interferometer is used which generates a complex interference pattern with spatial polarization variations known as polarization speckle. A linearly polarized laser light having 45˚orientation with respect to x-direction is spatially filtered SF and collimated by a Lens L1 respectively. Collimated beam splits into two orthogonal components using polarized beam splitter (PBS). In one of the components, a SPP is placed and it is combined with the other component of the beam by non-polarizing beam splitter BS. Combined beam propagates through a static ground glass and creates a speckle pattern. Further these polarized speckles fields are recorded by CCD camera at different longitudinal planes.
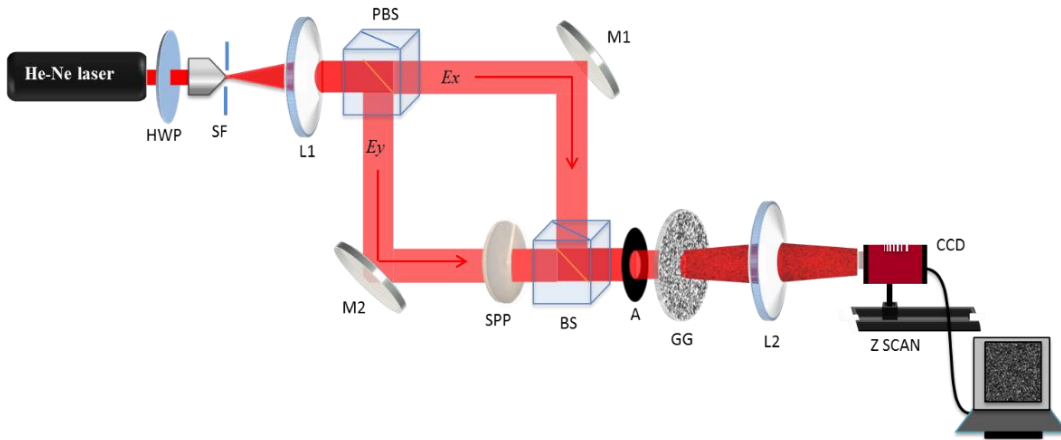
Figure 3.5. Mach-Zehnder type experimental Set up to study degree of spatial polarization

The effect of cross correlation of the intensity fluctuations in random fields has been studied at the focal plane and along the z-axis of a Fourier transforming lens using the spatial statistical optics approach and results are presented in the next section.

3.4 Results and discussions

Set of random fluctuating intensity patterns are recorded at different positions of CCD plane as shown in Fig. 3.6. By applying intensity correlation based on spatial averaging we have obtained correlation of intensity fluctuation of random fields at two different longitudinal planes using Eq. (3.4) -(3.6). The degree of coherence and degree of polarization have also been obtained using Eq. (3.7).
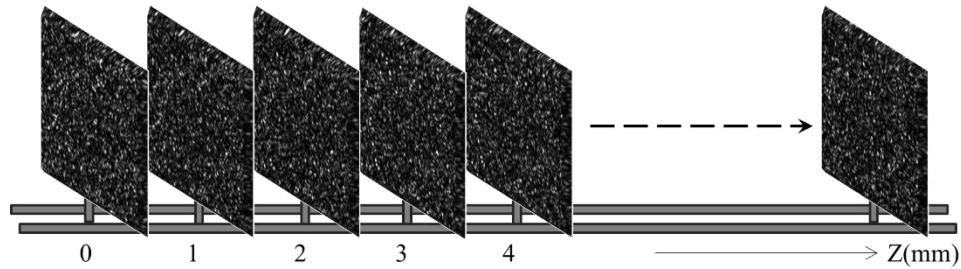
Figure 3.6. Set of random speckle patterns recorded at different CCD positions

These intensity patterns are utilized to estimate the cross-covariance of the intensity at two different longitudinal planes. Considering the first experimental case, we have obtained the cross-covariance function for a circular aperture of diameter 2.7mm propagated along the z-axis plane. Figure 3.7 shows the experimental and digitally simulated results of the cross- covariance function calculated for two different random fields.
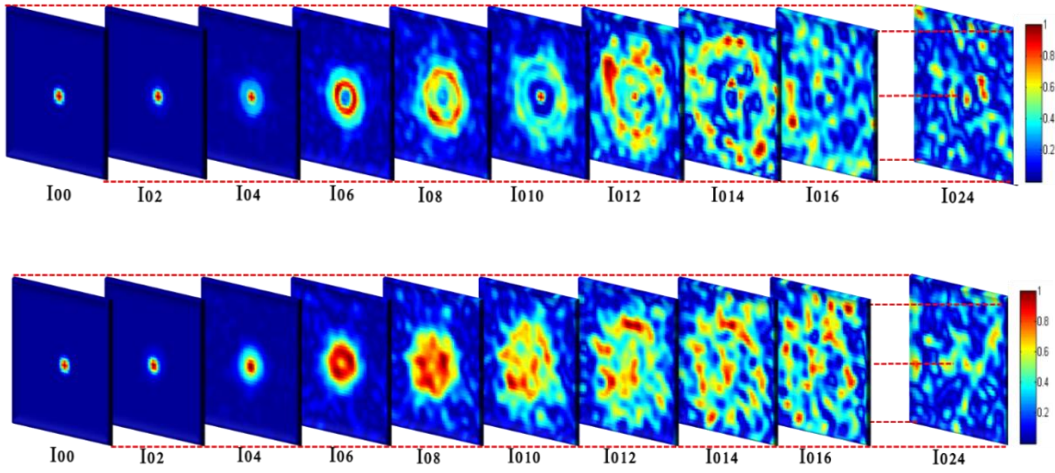
Figure 3.7. cross-covariance function for a circular aperture in scalar domain; top: experimental, bottom: simulation

The cross-covariance function is given by Iz1z2 where z1, z2 are the positions at z plane in mm units, where, z1, z2 = 0, 1, 2…. N, as shown in Fig. 3.7 for experimental and digitally simulated results respectively. I00 denotes the autocorrelation function of the intensity fluctuation at z = 0mm plane and cross-correlation has been calculated for two different intensity fluctuations recorded at z plane. For example, I02 is the cross-correlation function of two intensity fluctuations captured at 0mm and 2mm respectively. We can observe that as the field propagates in the longitudinal plane, the energy of the center lobe distributes to the side lobes and later it randomly spreads over an entire area. Since the DOC is proportional to the correlation, therefore DOC for the center pixel follows as same as correlation function. For a circular aperture in the scalar domain

maximum achieved DOC i.e., $\mu(\Delta r = 0, \Delta z = 0)$ is unity and confirms that the random light source is spatially fully polarized i.e., $P(0) = 1$. It can be observed that the amplitude of DOC is decaying as two farther points in the z plane are being correlated. It is shown in Fig. 3.8 how the correlation becomes weak and almost saturated after propagating to some distances.
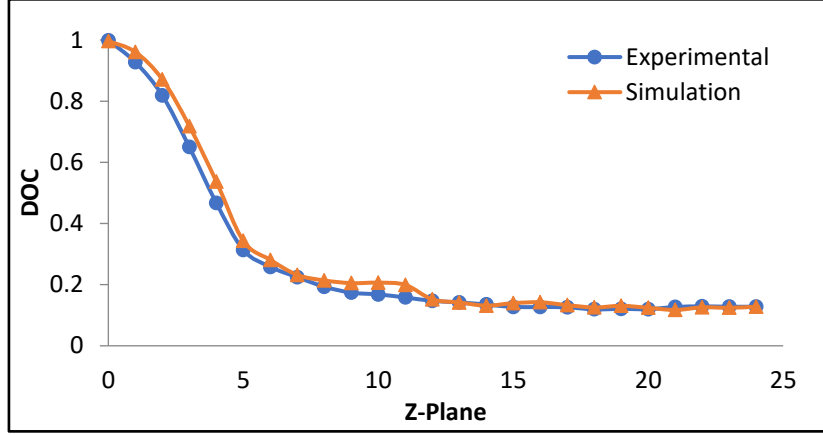
Figure 3.8. DOC for a circular aperture in scalar domain as described in Fig. 3.2

Considering the second case as described in Fig. 3.3, SPP with charge 1 has been introduced in the set-up and we have estimated cross-covariance function and DOC. It can be observed in Fig. 3.9, the maximum DOC is unity at z=0mm plane and later it decays while propagating to the further distances.
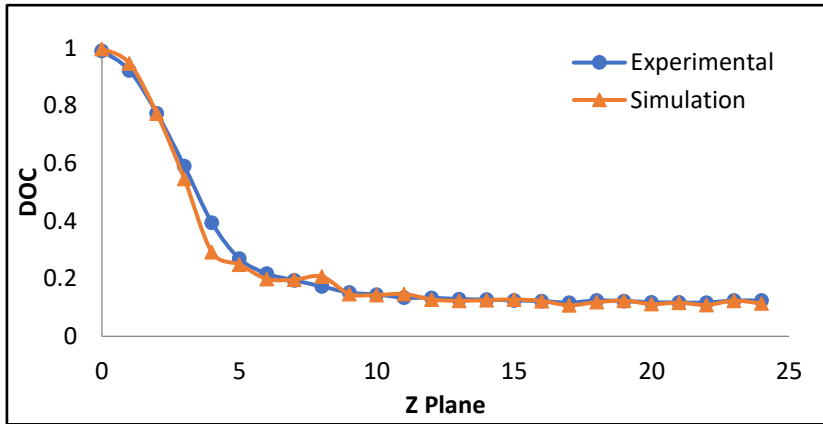
Figure 3.9. DOC for a SPP charge 1 in scalar domain as described in Fig. 3.3

A very interesting observation can be made from Figs. 3.8 and 3.9, that the coherence function of non-vortex and vortex source structures in scalar domain behaves exactly the same. For more confirmation we have compared both the experimental results of two different source structures in Fig. 3.10 where DOC has been plotted against the propagation distance.
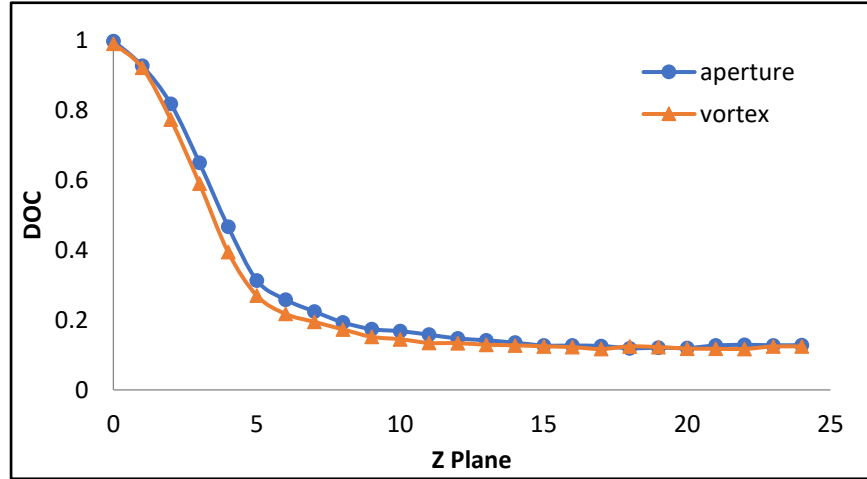
Figure 3.10. DOC behavior for vortex and non-vortex propagation

In the third case when vortex correlates with the non-vortex source structure, correlation turns out to be odd. In Fig. 3.11 SPP charge 1 is used and it is correlated with the non-vortex source structure and DOC drops to 0.5. Similarly, in Fig. 3.12 vortex beam having charge 2 is correlated with the non-vortex beam and the maximum DOC observed as 0.4.
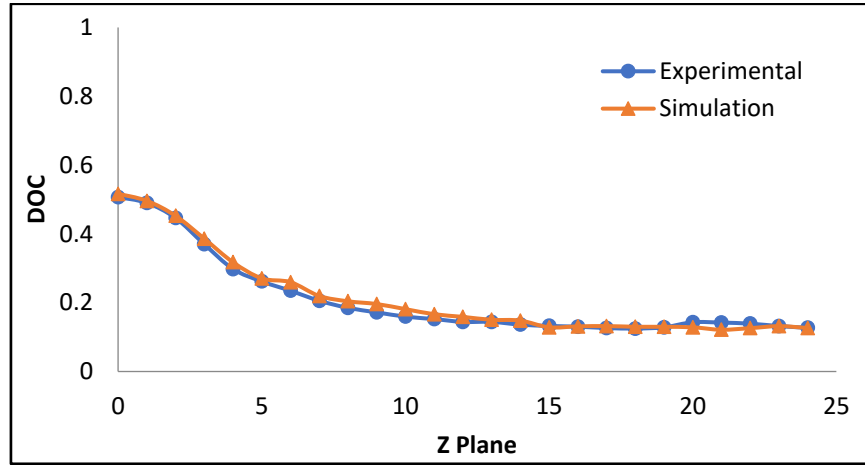
Figure 3.11. DOC for the vortex charge 1 correlated non-vortex structure
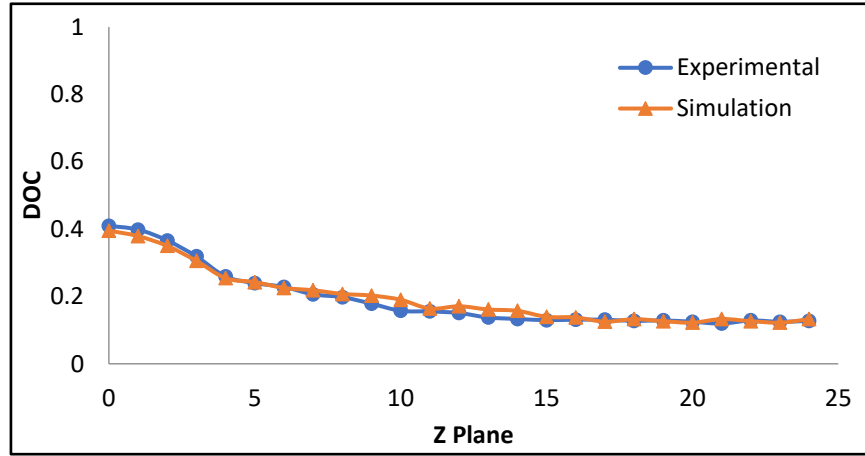
Figure 3.12. DOC for the vortex charge 2 correlated non-vortex structure

In the last case, a vortex has been introduced in the orthogonal states of the beam and allowed to pass through a static diffuser. DOC is obtained from the cross correlation of the intensity fluctuation of the random fields. Longitudinal profile of the DOC for the vector source is shown in the Fig. 3.13. Experimental and simulated results show the calculated DOC at z=0 plane is 0.7 and $P(0) = 0$. In case of Mach-Zehnder interferometry, the introduction of SPP (a vortex) in one of the orthogonal components of polarized light beam. A vortex changes the polarization of the beam and hence shows inhomogeneity in polarization when observed at Z=0 plane. Here, the degree of polarization is 0. Therefore, the

randomly scattered light field is spatially unpolarized.
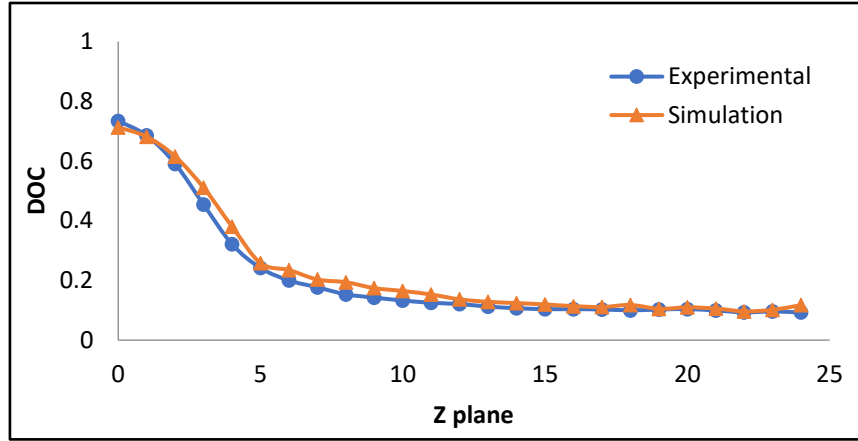
Figure 3.13. DOC distribution for a beam controlled by circular aperture and SPP introduced in one of the orthogonal components.

In summary, we have studied intensity correlation of the spatially fluctuating polarized random fields at different distances under the paraxial propagation. Quantitative analysis of the random field is carried out by following relation between the degree of coherence of the electromagnetic fields, spatial degree of polarization and the intensity correlation for the Gaussian random fields. For quantitative comparison, experimental results are compared with the theory using digital propagation of the light.

CHAPTER 4

RECOVERY OF POLARIMETRIC PARAMETERS FROM NON-IMAGED LASER-SPECKLE

4.1 Introduction

When a laser source propagates through an optically rough medium, light wavefront gets distorted and generates a coherent noise due to stochastic interference of randomly scattered waves, known as speckle. Presence of coherent noise makes measurement difficult and degrades the performance of a laser-based imaging system (Goodman, 1996; 2007). In a generic case, coherent beam interacts remotely with the object and scattered light is characterized to recover the information about the object. Roughness of the object and refractive index inhomogeneity in the propagation medium or both further aggravates the coherent noise challenge and creates speckle. Level of noise depends on optical length scale of the underlying processes creating random scattering. In spite of common occurrence of a speckle, a coherent laser is highly preferred source due to its high monochromaticity, brightness and color gamut. Therefore, significant efforts have been made to suppress the speckle using different means such as adaptive optics (Vorontsov and Kolosov, 2005), speckle averaging etc. (Goodman, 1976). The most common method to suppress the speckle is a moving diffuser to perform the temporal averaging. This conventional approach works on incoherent summation of several speckle patterns. Alternatively, significant reduction in the coherent noise is also achieved without mechanically moving the diffuser and by using diversity in parameters of the light beam such as frequency, angular, spatial, polarization and DOE (Schmitt et al., 1999; Mehta et al., 2012; Sorrentini et al., 2009; Zhao and Gao, 2015; Tran et al., 2016; Lapchuk et al., 2013).

It has been demonstrated that noise free images of coherently illuminated, diffuse object can be retrieved from measurement of backscattered laser-speckle

intensity using phase retrieval algorithm (Fienup, 1978; Idell et al., 1987; Das et al., 2017). This technique evaluates the autocorrelation function of the illuminated object's reflectance/transmittance from the average energy spectrum of laser-speckle intensity. The Fourier transform of the autocorrelation of the object transmittance/reflectance is related to the squared modulus of the Fourier transform; hence recovery of the object is possible by applying the phase retrieval algorithm. A problem of similar nature has been attempted by using higher order correlation and coherence optics (Bartelt et al., 1984; Singh et al. 2014; Akhlaghi and Dogariu, 2017). Recently, Akhlaghi and Dogariu have shown single-shot coherent noise suppression by spatial interferometric heterodyning. This technique separates the spectral components of the signal and noise and operates in very-low SNR conditions (Akhlaghi and Dogariu, 2017). Whereas such attempts on recovery of the polarized objects or PPs appear to be missing except some recent investigations in the context of ghost imaging (GI) (Kellock et al., 2014; Shi et al., 2014, Hannonen et al., 2016; 2017). It has been demonstrated that polarimetry can play an important role in distinguishing the object and its background having the same reflectivity or transmission in the classical GI (Shi et al., 2014). Recently a ghost ellipsometers operating with classical Gaussian statistics are also introduced to characterize the homogeneous and inhomogeneous samples (Hannonen et al., 2016; 2017). An ellipsometer is a device that gauges the change in the polarization state of light after interaction from an object and forms a picture of its ellipsometric information (Azzam, 2016). It has come to be recognized that a polarization fluctuation in the random field affects the degree of coherence and visibility of the intensity correlation (Shirai et al., 2011; Singh et al., 2014; Takeda et al., 2010).

Polarimetry is a method to measure the rotation of polarized light when it passes through an optical media. From the previous chapter, it has been well-known that a polarization fluctuation in the random field affects the degree of coherence and the correlation. To distinguish the object from its background

having same reflectivity and transmission, it is important to recover polarimetric parameters. In this chapter, we discuss and experimentally demonstrate our new technique to recover the polarimetric parameters of the light field observed by a static non-birefringent diffuser. We recover the polarization parameters (PPs) from non-imaged laser speckle patterns, i.e., without using any imaging lens. Propagation of coherent and polarized light through a static diffuser may generate polarization fluctuation in the random scattered field depending on the nature of incident polarized light. Because the incident light is monochromatic and the scattering surface is static, the scattered field is free from temporal fluctuation and remains to be fully a polarized according to the conventional definition based on time averaging and has a well-defined state of polarization at each point in space. Such a random field with spatially fluctuating polarization is referred to as polarization speckles and useful to provide signature of the incident polarized light (Singh et al., 2014; Takeda et al., 2010; Singh et al., 2013). To analyze the polarization speckle, we apply idea of coherence wave interference for the vectorial light field. This is realized by using 2X2 coherence-polarization matrix elements and their interference. Moreover, this approach is free from any artifacts associated with imaging/or Fourier transforming lens and its possible impact on the spatial stationarity of the random field. The detailed theoretical explanation and the corresponding experimental works are discussed below in detail.

4.2   Principle

Let us consider two-dimensional transverse electric field of the coherent light from the object. The orthogonal polarization components are represented by $E_x(\rho, t)$ and $E_y(\rho, t)$ at a position vector ρ and time t, where x and y denote direction of polarization components. Time t is fixed in our study and hence removed thereafter. Assuming that the object structure is located at the diffuser plane, therefore the orthogonal polarization components immediately after the diffuser is

$$E(\rho) = \begin{pmatrix} E_x(\rho)e^{i\varphi(\rho)} \\ E_y(\rho)e^{i\varphi(\rho)} \end{pmatrix} \qquad (4.1)$$

where $E_i(\boldsymbol{\rho})$ with $i = x, y$ is polarization information of the object and $\varphi(\rho)$ is a random phase introduced by the non-birefringent diffuser. Polarimetric parameter of the light field at the diffuser plane is given as

$$J(\rho) = \begin{pmatrix} |E_x(\rho)|^2 & E_x^*(\rho)E_y(\rho) \\ E_y^*(\rho)E_x(\rho) & |E_y(\rho)|^2 \end{pmatrix} \qquad (4.2)$$

Propagation of the orthogonal polarization components from the diffuser plane to an observation plane at a distance z is represented as

$$E_i(\boldsymbol{r}) = \int G(\boldsymbol{r},\boldsymbol{\rho}) \, E_i(\boldsymbol{\rho})d\boldsymbol{\rho} \qquad (4.3)$$

where $G(\boldsymbol{r},\boldsymbol{\rho})$ is propagation kernel. Equation (4.2) can be used to propagate the electric field vector represented by Eq. (4.1) as shown in Fig. 4.1. Let us consider propagation of the random field into the Fresnel domain as

$$G(\boldsymbol{r},\boldsymbol{\rho}) \approx \frac{\exp(ikz)}{i\lambda z}\exp\left(ik\frac{|\boldsymbol{r}|^2 - 2\boldsymbol{r}\cdot\boldsymbol{\rho}+|\boldsymbol{\rho}|^2}{2z} \right) \qquad (4.4)$$

where λ and $k = 2\pi/\lambda$ are, respectively, the wavelength and wave number of light. Consider that random field given in Eq. (4.2) is composed of two independent sources and represented as

$$\begin{aligned} E_i(\boldsymbol{r}) &= \int G(\boldsymbol{r},\boldsymbol{\rho})\left[E_i^1(\boldsymbol{\rho}) + E_i^2(\boldsymbol{\rho}) \right]d\boldsymbol{\rho} \\ &= \frac{\exp\ ikz}{i\lambda z}\exp\left(\frac{ik}{2z}|\boldsymbol{r}|^2 \right)\int \exp\left(\frac{ik}{2z}|\boldsymbol{\rho}|^2 \right)\exp\left(-ik\frac{\boldsymbol{r}\cdot\boldsymbol{\rho}}{z} \right)\left[E_i^1(\boldsymbol{\rho}) + E_i^2(\boldsymbol{\rho}) \right]d\boldsymbol{\rho} \end{aligned} \qquad (4.5)$$

where $E_i^1(\boldsymbol{\rho})$ and $E_i^2(\boldsymbol{\rho})$ are two independent (spatially separated) orthogonal polarized sources at the diffuser plane. The intensity at the observation plane is $I(\boldsymbol{r}) = |E_x(\boldsymbol{r})|^2 + |E_y(\boldsymbol{r})|^2$ which allows to measure the two point intensity correlation $\langle I(\boldsymbol{r_1})I(\boldsymbol{r_2})\rangle = \langle E^*(\boldsymbol{r_1})E(\boldsymbol{r_1})E^*(\boldsymbol{r_2})E(\boldsymbol{r_2})\rangle$ and the cross-covariance of the intensity as $\langle\Delta I(\boldsymbol{r_1})\Delta I(\boldsymbol{r_2})\rangle = |\langle E^*(\boldsymbol{r_1})E(\boldsymbol{r_2})\rangle|^2$ for the speckle field. Here $\langle.\rangle$ represents ensemble averaging and $\Delta I(\boldsymbol{r}) = I(\boldsymbol{r}) - \langle I(\boldsymbol{r})\rangle$ is the intensity fluctuation with respect to its mean value. The cross-covariance of the intensity is given as (Tervo et al., 2003)

$$\Gamma(r_1, r_2) = \langle\Delta I(r_1)\Delta I(r_2)\rangle = \sum_{i,j}|W_{ij}(r_1, r_2)|^2 \qquad (4.6)$$

where $W_{ij}(r_1, r_2) = \langle E_i^*(r_1)E_j(r_2)\rangle$ is an element of 2X2 coherence-polarization (CP) matrix. Therefore, intensity correlation relation for the randomly polarized light involves all four components of CP matrix and moreover phase information of CP matrix elements is lost.
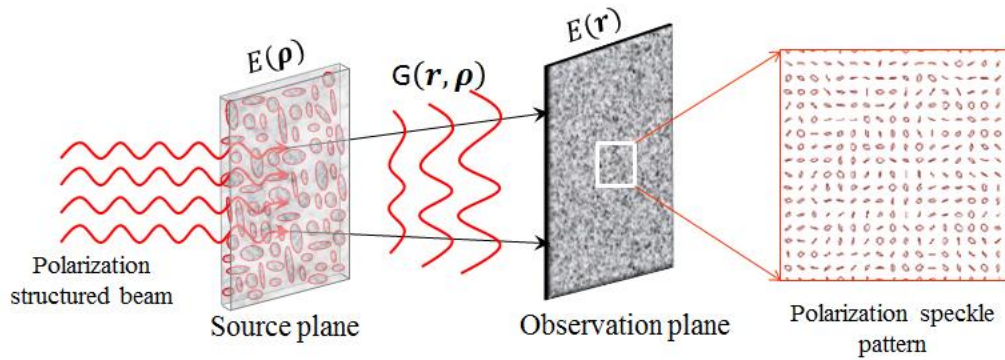
Figure 4.1 Geometry of source structure, propagation system and observation plane.

Let us consider that element of the CP matrix elements is in the form of $W_{ij}(\boldsymbol{r_1}, \boldsymbol{r_2}) = W_{ij}^1(\boldsymbol{r_1}, \boldsymbol{r_2}) + W_{ij}^2(\boldsymbol{r_1}, \boldsymbol{r_2})$, i.e., interference of the coherence waves. To describe the interference of polarized-coherence waves, let us start with Eq. (4.6) and write cross-covariance of the intensity as

$$\Gamma(r_1, r_2) = \sum_{i,j} \left| W_{ij}^1(r_1, r_2) + W_{ij}^2(r_1, r_2) \right|^2 \tag{4.7}$$

The terms $W_{ij}^n(\boldsymbol{r_1}, \boldsymbol{r_2})$, $n = 1,2$ represent the complex coherence function for the nth source. Since the two interfering speckles from polarized sources are statistically independent, therefore the CP matrix of the random field is given as

$$W(\boldsymbol{r_1}, \boldsymbol{r_2}) = \begin{pmatrix} W_{xx}^1(\boldsymbol{r_1}, \boldsymbol{r_2}) & W_{xy}^1(\boldsymbol{r_1}, \boldsymbol{r_2}) \\ W_{yx}^1(\boldsymbol{r_1}, \boldsymbol{r_2}) & W_{yy}^1(\boldsymbol{r_1}, \boldsymbol{r_2}) \end{pmatrix} + \begin{pmatrix} W_{xx}^2(\boldsymbol{r_1}, \boldsymbol{r_2}) & W_{xy}^2(\boldsymbol{r_1}, \boldsymbol{r_2}) \\ W_{yx}^2(\boldsymbol{r_1}, \boldsymbol{r_2}) & W_{yy}^2(\boldsymbol{r_1}, \boldsymbol{r_2}) \end{pmatrix} \tag{4.8}$$

The cross-covariance of intensity is expressed as interference of polarized coherence waves. This equation highlights that interference fringes can be generated in terms of the intensity correlation by considering one source, say $W^1(\boldsymbol{r_1}, \boldsymbol{r_2})$ and other polarized coherence waves $W^2(\boldsymbol{r_1}, \boldsymbol{r_2})$ as reference. A stationary source at a distance $Z > 0$ can be realized from a non-stationary source using a Fourier transforming lens (Takeda, 2013). It is also possible to realize a stationary field at any arbitrary plane $Z > 0$ from a non-stationary source using notion of coherence wave interference with intensity correlation (Singh et al., 2017). This helps to avoid the phase curvature $\exp\left(\frac{ik}{2z}|r|^2\right)$ outside the integration in Eq. (4.5), and hence avoids non-stationarity. However, in contrast to the scalar case, cross-covariance is composed of contributions of all four elements, in general, and needs to be separated for polarimetric applications. Therefore, the cross-covariance replaces the CP matrix elements in Eq. (4.8) with the following form

$$W_{ij}(r, r + \Delta r) =$$
$$\iiint E_i^*(\rho_1) E_j(\rho_2) \exp\left(-i\frac{k}{2z}|\rho_1|^2\right) \exp\left(i\frac{k}{2z}|\rho_2|^2\right) \exp\left[-i\frac{k}{z}\{r + \Delta r\} \cdot \rho_2 - r \cdot \rho_1\right] d\rho_1 d\rho_2 dr \tag{4.9}$$

By using relation $\int dr \left[\exp\left(-i\dfrac{k}{z}(\boldsymbol{\rho_2} - \boldsymbol{\rho_1}) \cdot r \right) \right] = \delta(\boldsymbol{\rho_2} - \boldsymbol{\rho_1})$, Eq. (4.9) can be expressed in terms of the Fourier transform of polarized random source (Takeda, 2013) as

$$W_{ij}(\boldsymbol{r_1}, \boldsymbol{r_2}) = \int I_{ij}(\boldsymbol{\rho}) \exp\left[-i\frac{k}{z}(\boldsymbol{r_2} - \boldsymbol{r_1}) \cdot \boldsymbol{\rho} \right] d\boldsymbol{\rho}$$

(4.10)

where $I_{ij}(\boldsymbol{\rho}) = E_i^*(\boldsymbol{\rho}) E_j(\boldsymbol{\rho})$ represents PPs at the random scattering plane as shown in Eq. (4.2). Term $I_{ij}(\boldsymbol{\rho})$ may be complex for $i \neq j$ but real for $i = j$. In what follows, Eq. (4.8) makes interference of four polarized-coherence waves. To record such patterns, we have selected two polarized sources at the scattering plane, and corresponding coherence functions are as follows

$$W_{ij}^1(\boldsymbol{r_1}, \boldsymbol{r_2}) = \int I_{ij}(\boldsymbol{\rho}) \exp\left(-i\frac{2\pi}{\lambda z}(\boldsymbol{r_2} - \boldsymbol{r_1}) \cdot \boldsymbol{\rho} \right) d\boldsymbol{\rho}$$

$$W_{ij}^2(\boldsymbol{r_1}, \boldsymbol{r_2}) = \int \delta(\boldsymbol{\rho} - \boldsymbol{\rho_g}) \exp\left(-i\frac{2\pi}{\lambda z}(\boldsymbol{r_2} - \boldsymbol{r_1}) \cdot \boldsymbol{\rho} \right) d\boldsymbol{\rho} = \exp\left[-i\alpha(\boldsymbol{r_2} - \boldsymbol{r_1}) \right]$$

(4.11)

where the spatial frequency α of the reference polarized coherence function $W_{ij}^2(\boldsymbol{r_1}, \boldsymbol{r_2})$ is given by $\alpha = \dfrac{2\pi \rho_g}{\lambda z}$. We consider a $45°$ linearly polarized point source as reference and therefore all elements of the polarization matrix of this reference source will be represented by a delta function. Therefore, the reference point source generates a uniform polarized coherence function covering the support of $W_{ij}^1(\boldsymbol{r_1}, \boldsymbol{r_2})$ to generate the lensless coherence wave holograms.

In order to recover the complex elements of the CP matrix, we invoke interference of the polarized coherence waves and insert a polarization device before detection of the intensity. The polarized device is composed by a quarter wave plate (QWP) followed by a linear polarizer (LP) in the light facing direction. The fast axis of QWP is oriented at θ angle with respect to x direction as shown in Fig. 4.2. The LP in the polarization device is directed along the x direction.

Figure 4.2. Geometry consists of QWP followed by linear polarizer to measure CP matrix elements.

The light field after the combination of polarization elements is given as (Vinu and Singh, 2015)

$$E(\boldsymbol{r},\theta) = \left[\cos^2\theta + i\sin^2\theta\right]E_x(\boldsymbol{r}) + \left[(1-i)\cos\theta\sin\theta\right]E_y(\boldsymbol{r})$$

(4.12)

Therefore, the cross-covariance of the intensity at the observation plane is given as

$$\Gamma(\boldsymbol{r}_1,\boldsymbol{r}_2,\theta) \propto \left| \begin{array}{l} (1+\cos^2 2\theta)W_{xx}(\boldsymbol{r}_1,\boldsymbol{r}_2) + (\dfrac{\sin 4\theta}{2} - i\sin 2\theta)W_{xy}(\boldsymbol{r}_1,\boldsymbol{r}_2) + \\[2mm] (\dfrac{\sin 4\theta}{2} + i\sin 2\theta)W_{yx}(\boldsymbol{r}_1,\boldsymbol{r}_2) + (1-\cos^2 2\theta)W_{yy}(\boldsymbol{r}_1,\boldsymbol{r}_2) \end{array} \right|^2$$

(4.13)

Considering orientations of the QWP at $\theta = 0°, 22.5°, 45°$ and $135°$, the cross-covariance for these angles is given as

$$\Gamma(\boldsymbol{r}_1,\boldsymbol{r}_2,0°) = \left|2W_{xx}(\boldsymbol{r}_1,\boldsymbol{r}_2)\right|^2$$

$$\Gamma(\boldsymbol{r}_1,\boldsymbol{r}_2,22.5°) = \left| \begin{array}{l} \dfrac{3}{2}W_{xx}(\boldsymbol{r}_1,\boldsymbol{r}_2) + \left(\dfrac{1}{2} - \dfrac{i}{\sqrt{2}}\right)W_{xy}(\boldsymbol{r}_1,\boldsymbol{r}_2) + \left(\dfrac{1}{2} + \dfrac{i}{\sqrt{2}}\right)W_{yx}(\boldsymbol{r}_1,\boldsymbol{r}_2) \\[2mm] + \dfrac{1}{2}W_{yy}(\boldsymbol{r}_1,\boldsymbol{r}_2) \end{array} \right|^2$$

$$\Gamma(\boldsymbol{r}_1,\boldsymbol{r}_2,45°) = \left| W_{xx}(\boldsymbol{r}_1,\boldsymbol{r}_2) - i\left(W_{xy}(\boldsymbol{r}_1,\boldsymbol{r}_2) - W_{yx}(\boldsymbol{r}_1,\boldsymbol{r}_2)\right) + W_{yy}(\boldsymbol{r}_1,\boldsymbol{r}_2) \right|^2$$

$$\Gamma(\boldsymbol{r}_1,\boldsymbol{r}_2,135°) = \left| W_{xx}(\boldsymbol{r}_1,\boldsymbol{r}_2) + i\left(W_{xy}(\boldsymbol{r}_1,\boldsymbol{r}_2) - W_{yx}(\boldsymbol{r}_1,\boldsymbol{r}_2)\right) + W_{yy}(\boldsymbol{r}_1,\boldsymbol{r}_2) \right|^2$$

(4.14)

These four cross-covariance structures are composed of different combinations of elements of the CP matrix. Fourier transform of these cross-covariance functions

generate spectra, its conjugate, and a dc term. The spectra is filtered and translated towards the origin of the frequency axis. The inverse transform of the centrally shifted spectra and its appropriate combinations will provide the CP matrix elements of the object's field as (Vinu and Singh, 2015)

$$W_{xx}^1(\Delta r) = 2\Gamma'(\Delta r, \theta_1)$$
$$W_{yy}^1(\Delta r) = 2\Gamma'(\Delta r, \theta_3) + 2\Gamma'(\Delta r, \theta_4) - 2\Gamma'(\Delta r, \theta_1)$$
$$W_{xy}^1(\Delta r) = 4\Gamma'(\Delta r, \theta_2) - 2\Gamma'(\Delta r, \theta_1) - (1 + \sqrt{2} - i)\Gamma'(\Delta r, \theta_3) - (1 - \sqrt{2} + i)\Gamma'(\Delta r, \theta_4)$$
$$W_{yx}^1(\Delta r) = 4\Gamma'(\Delta r, \theta_2) - 2\Gamma'(\Delta r, \theta_1) - (1 + \sqrt{2} + i)\Gamma'(\Delta r, \theta_3) - (1 - \sqrt{2} - i)\Gamma'(\Delta r, \theta_4)$$

(4.15)

where $\Delta r = r_2 - r_1$ and $\Gamma'(\Delta r, \theta_k)$ with $k = 1, 2, 3$ and 4 represents the inverse Fourier transform of the centrally shifted spectra. The PP at the diffuser plane can be obtained by suppressing the speckles using cross-covariance and applying the inverse Fourier transform to the recovered CP matrix of Eq. (4.15). We are able to retrieve the polarimetric information of the incident light from the non-imaged speckle patterns as

$$J_{ij}(\rho) = \int W_{ij}(\Delta r) \exp\left[i\frac{2\pi}{\lambda f}(\rho \cdot \Delta r) \right] d\Delta r$$

(4.16)

where i, j = x or y, represent the orthogonal polarization components of the source.

4.3   Experiment Implementation

Experimental realization of the proposed technique is shown in Fig. 4.3. A monochromatic laser beam of wavelength λ= 632.8nm (Melles Griot 25-LHP-928-230) is spatial filtered and collimated by spatial filter assembly (SF) and lens L1. This beam is converted into a $45°$ linearly polarized light by a half wave plate HWP1 and then enters into the beam splitter (BS1) and splits into two arms. The beam transmitted by BS1 folded by mirror M1 and then enters into an arbitrary polarization state generator (PSG) as shown by dotted lines. The PSG is an assembly of wave plate with an analyzer as shown in Fig. 4.2 and used to generate any arbitrary polarization state (Goldstein, 2010).
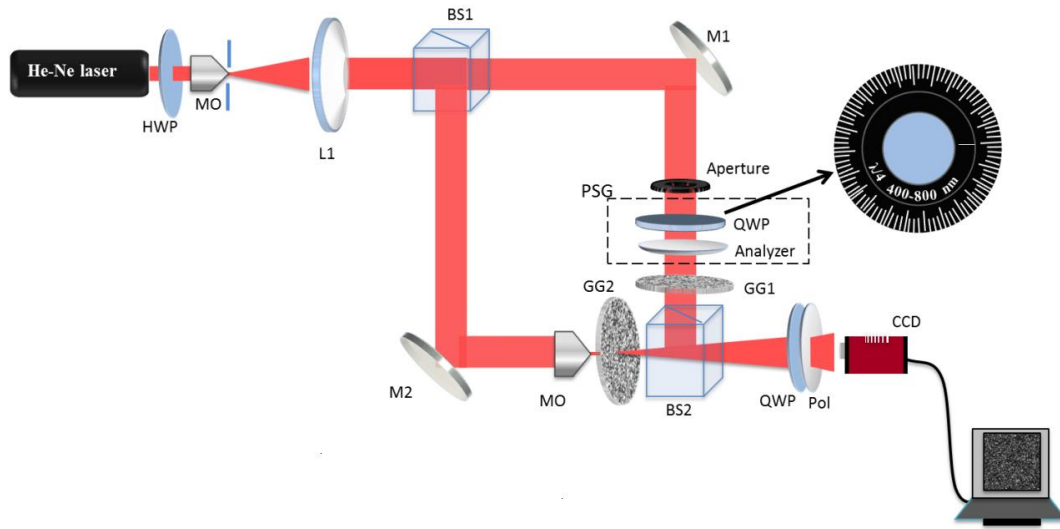
Figure 4.3. Experimental geometry for the proposed technique. HWP: half wave plate; MO: microscope objective; L: lens; BS: beam splitter; M: mirror; GG: ground glass; QWP: quarter wave plate; Pol: linear polarizer; CCD: charge coupled device.
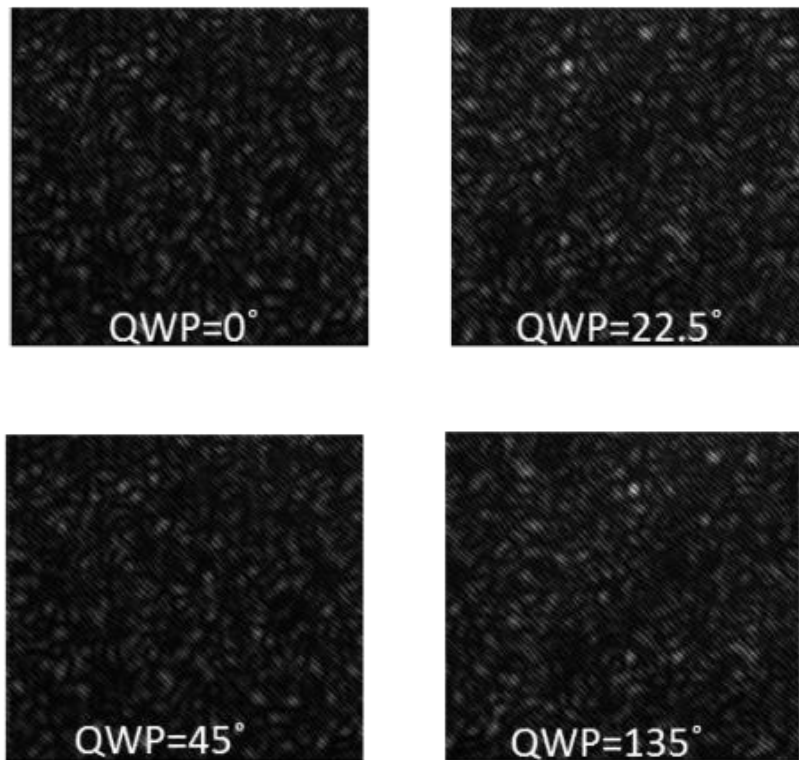
Figure 4.4. Four shots of speckle images captured by CCD.

The coherent light with an electric vector having arbitrary ellipticity and orientation passes through a non-birefringent ground glass (GG1). The ground glass GG1 generates the non-uniformly polarization speckle, known as the polarization speckle (Takeda et al., 2010), which further propagates and reaches the charge coupled device (CCD) plane. The beam reflected by the BS1 is titled by a mirror M2 and subsequently focused by a microscope objective (10X) at the off-axis location of another random scattering plane represented by ground glass GG2. Position of the off-axis point source is adjusted at the GG2 plane in order to give desired linear phase to the reference coherence wave as explained in Eq. (4.11). The random field coming out from the off-axis point source also propagates down to the charged couple device (CCD) plane. Both the random fields coming from GG1 and GG2 are fully coherent at a fixed time and recorded by a CCD at the distance z= 280mm from the source plane. The CCD camera is from Prosilica (model no GX 2750) with 14-bit dynamic range and 2750 X 2200 pixels and a pixel pitch of 4.54 micron.

4.4   Results and Discussions

A set of measurements were made through the scattering medium as shown in Fig. 4.4. Both linear and elliptical polarized incident states were investigated. The effect of scattering on the spatial distribution of polarization state scattered from the diffuser is quantitatively analyzed and is given by the polarization matrix using Eq. (4.16). The polarization matrix is the set of values which determines the polarization state of light field. Figs. 4.5 and 4.6 show the measured polarization state of an elliptically polarized source. This state of polarization is generated by modulating input polarization with the help of PSG placed just before the GG1. Figs. 4.5 and 4.6 describe the amplitude of all four elements of the polarization matrix i.e., $J_{xx}(\rho)$, $J_{xy}(\rho)$, $J_{yx}(\rho)$, and $J_{yy}(\rho)$ respectively and $\phi_{xy}(\rho)$ gives the polarimetric information. The calculated phase difference between the two orthogonal components is $\pi/2$. Hence it shows the

successful recovery of polarimetric parameters from the laser speckles. Working of the proposed approach is demonstrated by recovering the PPs from the diffused light. The theory and experimental results are compared, and good match is found between the two.

Figure 4.5. Polarization matrix for elliptical polarized beam at the ground glass plane. Experimental result shows the amplitude and phase of the polarization.

4.6. Polarization matrix for elliptical polarized beam at the ground glass plane. Theoretical results show the amplitude and phase of the polarization.

In order to study the effect of space averaging on intensity correlation, we performed detailed investigation on the effect of space averaging. From the given study we have obtained the ellipticity and orientation of the polarized source with different spatial averaging windows as shown in table 1 and table 2 respectively. The measurement of ellipticity and orientation for different averaging windows show the deviation from its expected value.

Table 1. Ellipticity for elliptically polarized beam

N	AVERAGING WINDOW	OBSERVED ELIPTICITY (x)	EXPECTED ELIPTICITY
1	1800 X 900	29.08	
2	1600 X 900	28.8	
3	1400 X 900	28.3	
4	1200 X 900	28.1	30
5	1000 X 900	26.9	
6	800 X 900	26.5	
7	600 X 900	26.4	

Table 2. Orientation for elliptically polarized beam

N	AVERAGING WINDOW	OBSERVED ORIENTATION (x)	EXPECTED ORIENTATION
1	1800 X 900	5.12	5
2	1600 X 900	6.13	
3	1400 X 900	7.8	
4	1200 X 900	10.3	
5	1000 X 900	12.8	
6	800 X 900	15	
7	600 X 900	15.8	

The above two tables show that the quality of recovered PPs depending on the ensemble averaging. The study shows the deviation in polarization parameters such as ellipticity and orientation of the beam with respect to the expected value for different spatial averaging window.

Noteworthy is the fact that the orientation of an elliptically polarized beam is only close to the expected value when the averaging window is of maximum size i.e., 1800 X 900. However, as we go lower in window size the error in observed orientation increases.
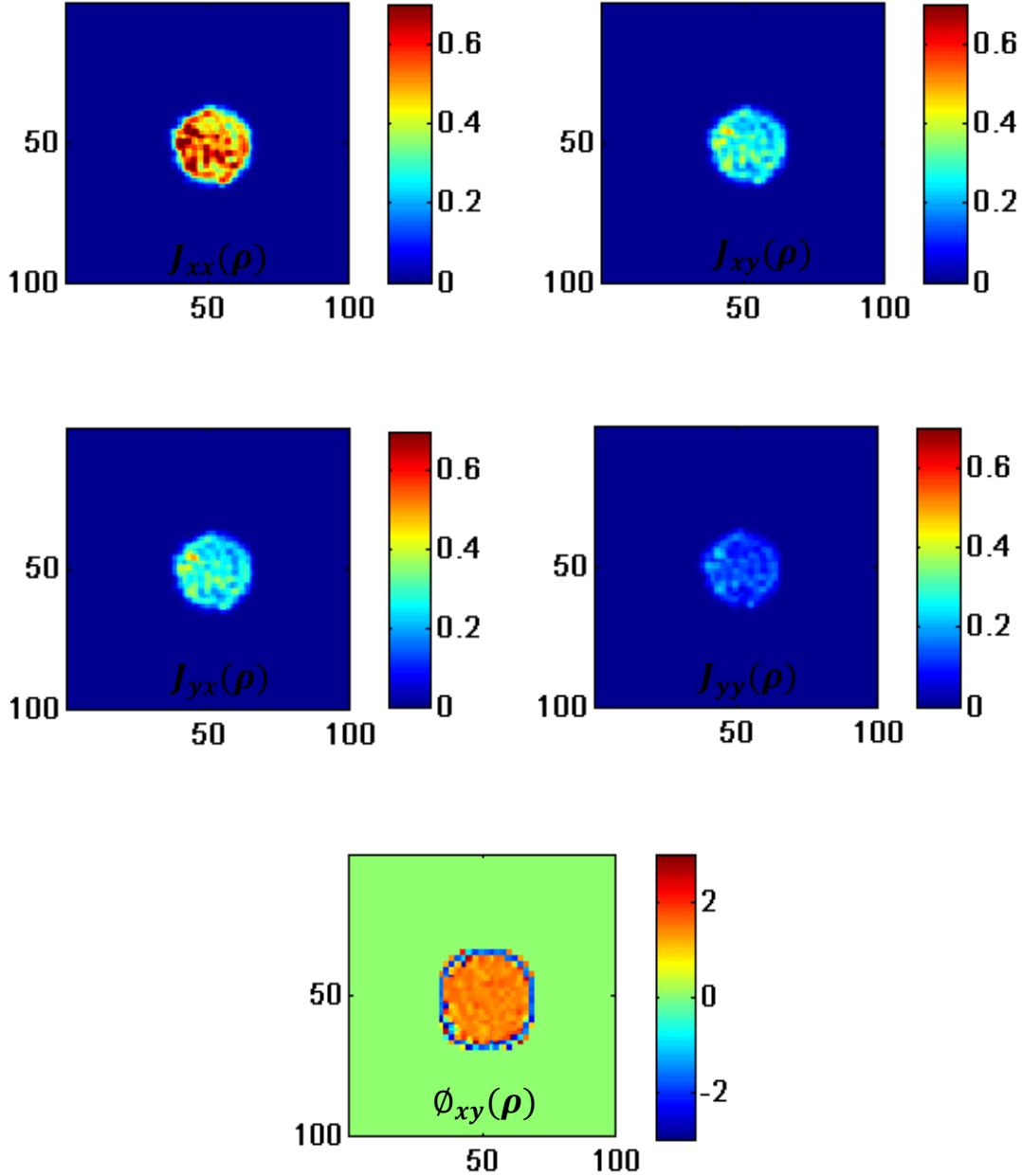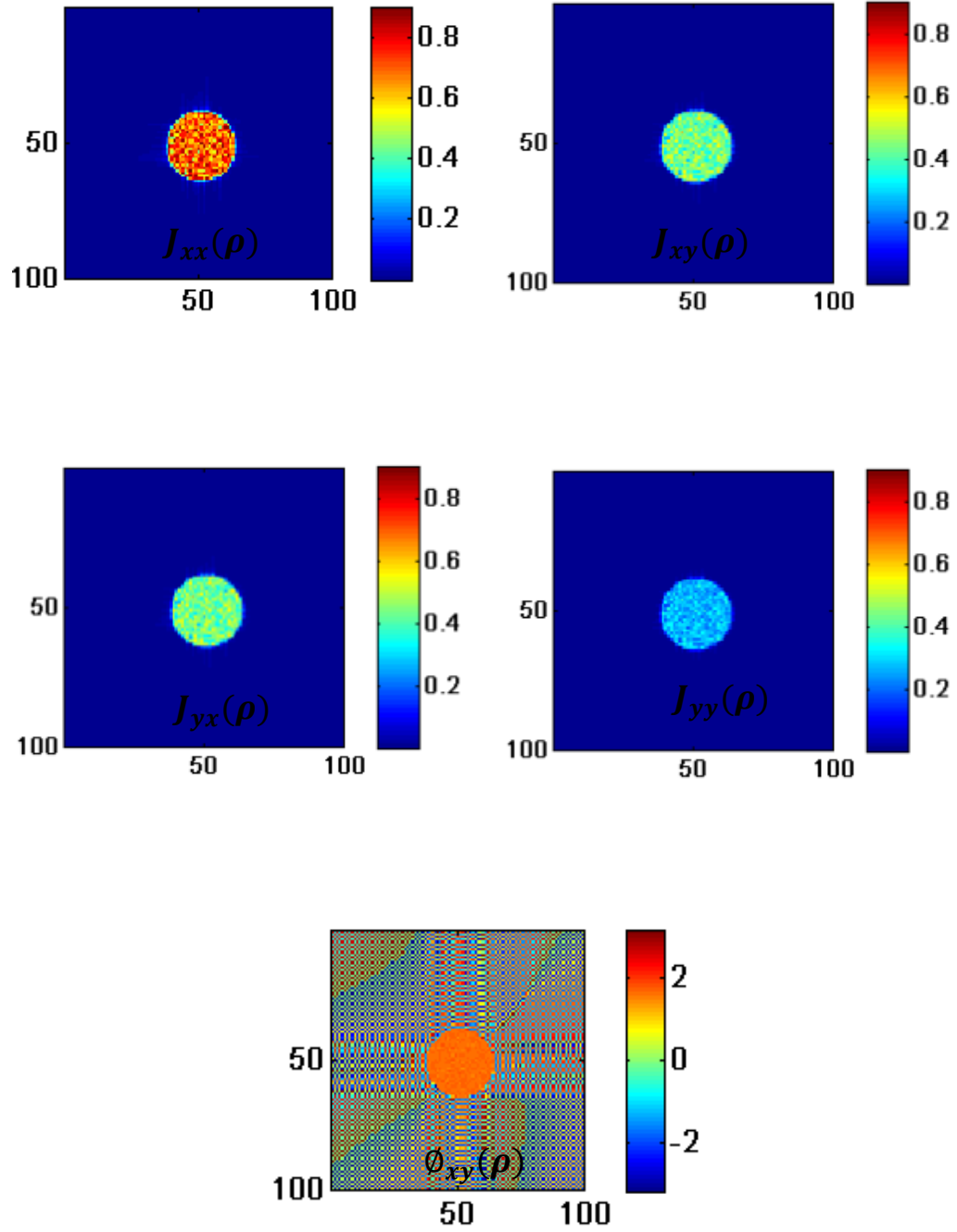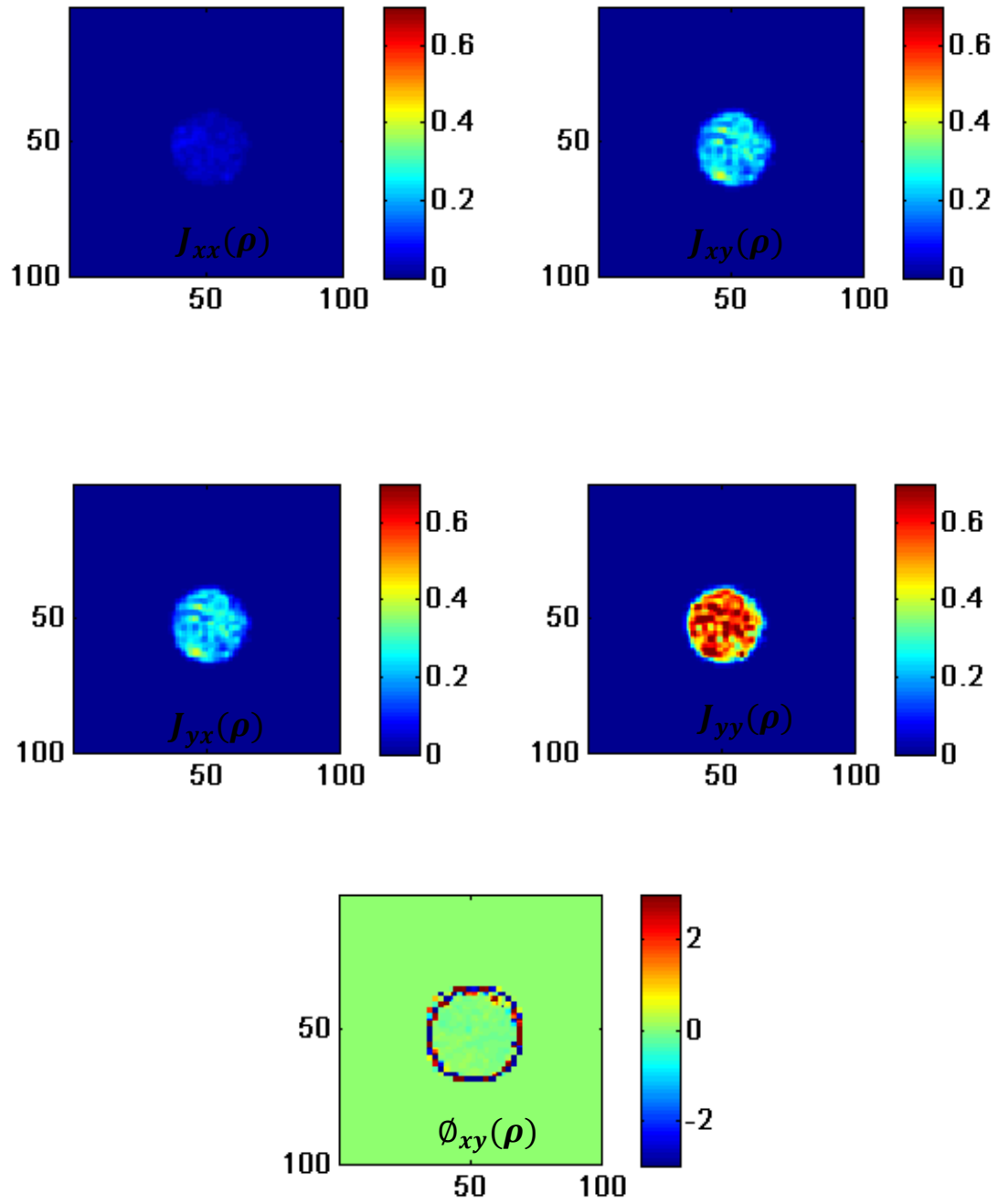
Figure 4.7. Polarization matrix for linear polarized beam at the ground glass plane. Experimental results show the amplitude and phase of the polarization.
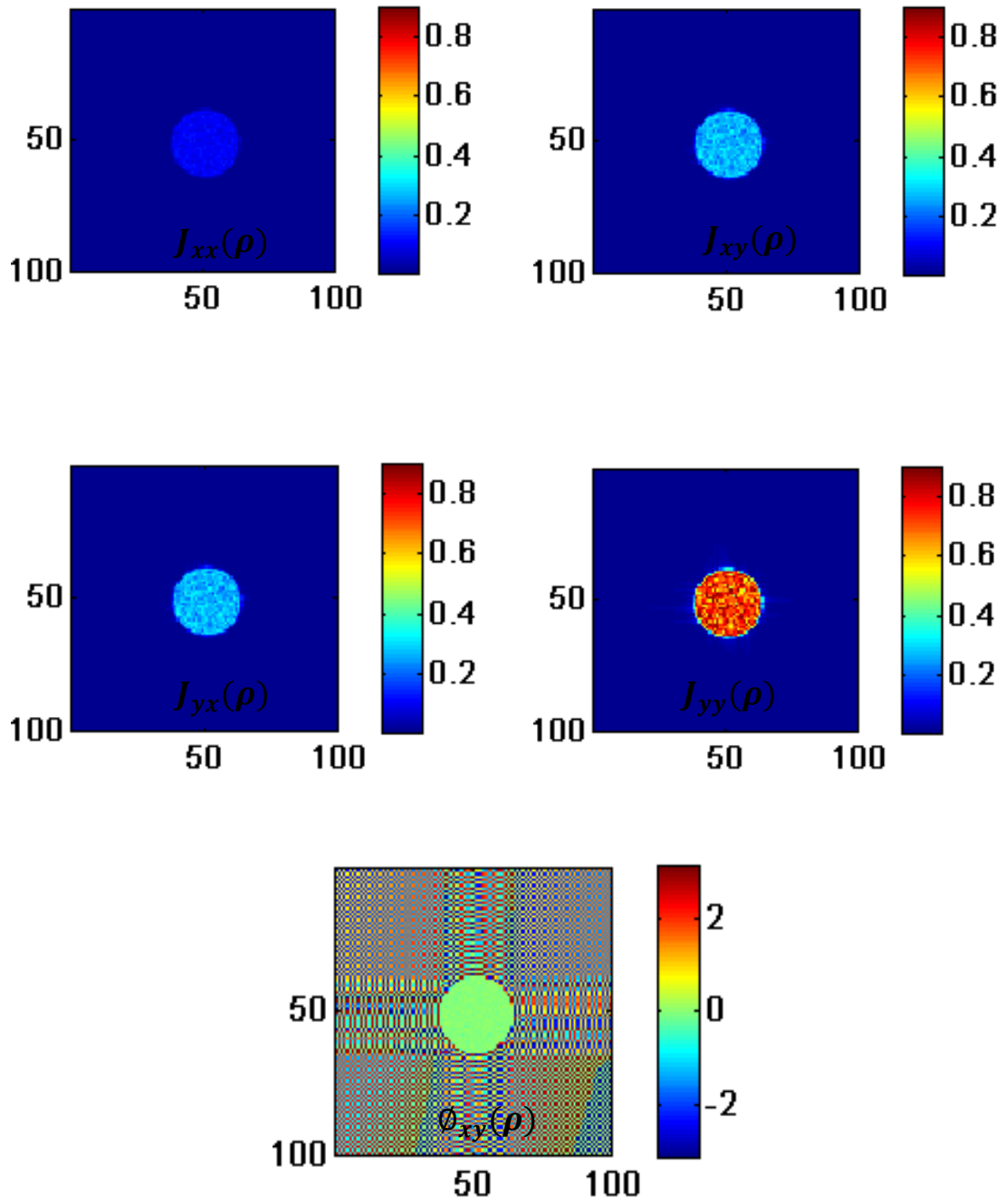
Figure 4.8. Polarization matrix for linear polarized beam at the ground glass plane. Theoretical results show the amplitude and phase of the polarization.

A similar case has also been studied when the input source is linear polarized. Figure 5describe the amplitude of all four elements of the polarization matrix i.e., $J_{xx}(\rho), J_{xy}(\rho), J_{yx}(\rho)$ and $J_{yy}(\rho)$ respectively and $\phi_{xy}(\rho)$ gives the polarimetric phase information of the source structure. The calculated phase difference between the two orthogonal components is 0. Working of the proposed approach is demonstrated by recovering the PPs from the diffused light. Proof of the principle is confirmed by experiment and compared with numerical results. Polarization parameters like ellipticity and orientation have been measured for different spatial averaging window and shown in the respective tables.

The quality of the recovered PPs depends on the ensemble averaging and the deviation from its expected value has been recorded, and same has shown in the table 3 and table 4 respectively.

Table 3. Ellipticity for linearly polarized beam

N	AVERAGING WINDOW	OBSERVED ELIPTICITY (x)	EXPECTED ELIPTICITY
1	1800 X 900	0.8	
2	1600 X 900	0.8	
3	1400 X 900	0.8	
4	1200 X 900	0.8	0
5	1000 X 900	0.9	
6	800 X 900	1	
7	600 X 900	1.1	

Table 4. Orientation for linearly polarized beam

N	AVERAGING WINDOW	OBSERVED ORIENTATION (x)	EXPECTED ORIENTATION
1	1800 X 900	20.3	
2	1600 X 900	20.7	
3	1400 X 900	21.2	
4	1200 X 900	22.2	20
5	1000 X 900	23.5	
6	800 X 900	25	
7	600 X 900	25.2	

In conclusion, we have shown recovery of the polarization vectors for different cases of the incident light by determining polarization matrix of the randomly polarized light. Results are presented to show the effect of spatial averaging of different window size on the coherent noise suppression and respective deviation on the recovered polarimetric parameters at the scattered plane. The results present here suggest that the higher spatial averaging is required to reduce the deviation of the polarization parameters from its actual values.

CHAPTER 5

LENSLESS STOKES HOLOGRAPHY WITH HBT APPROACH

5.1   Introduction

Holography records and reconstructs the wavefront of a light, finds its utility in a wide range of applications. Direct recording of a hologram by a detector and its numerical reconstruction is called Digital Holography (DH). It has brought about a big change in the concept of the holography which has proved to be a big step forward (Schnars and Jueptner, 2005). Advantages and uniqueness of the DH methods emerge from their ability in the non-destructive testing, quantitative three-dimensional imaging and digital propagation etc. In recent years, thee-dimensional (3-D) profiling and in-situ imaging of the microscale objects have been attractive significant attention in wide range of applications ranging from industry to the life sciences. For instance, quantitative evaluation of cancer cell morphology and shape variation in a 3-D condition provides signature of the biological characteristics for clinical need (Hong, 2014). One of the primary tools of the biologist is the light microcopy with staining agents for high visibility images. However, external staining agents are not desired in many conditions in order to preserves the inherent and pure structures of the target samples. Therefore, non-invasive optical means are gaining significant attention in recent years and some of the non-destructive techniques are digital holography microscopy and polarization microscopy.

Many geometries have been proposed for the digital holography imaging, in the past. The most significant among them are in-line, phase shifting, off-axis and the Fourier transform holography. It was demonstrated that a point-reference coherent source in the principal plane of the object generates a lensless Fourier-transform hologram which provides a high resolution in the wavefront-reconstruction imaging

(Stroke, 1965; Goodman, 1996). Lensless Fourier transform configuration is particularly useful at short, ultraviolet, x-ray wavelengths, imaging through diffusive medium and coherence waves (Lee et al., 2001; Gauthier et al., 2010; Zhang et al., 2013; Singh et al., 2017). A single Fourier transform operation is used to retrieve the information from the Fourier transform hologram and it plays an important role in real time applications. However, considering a complete wavefront, the amplitude, the phase and the polarization are important for a full field description of the light (Lohmann, 1965; Colomb et al., 2002; Nomura et al., 2007, Singh et al., 2011; 2012; Soni et al., 2016).

The polarization, a significant parameter to describe light matter interactions, have been very critical and significant in the contrast enhancement and highlighting specific cell structures which is otherwise missing in the conventional scalar imaging. Therefore, polarization imaging is considered to be a promising and futuristic tool, as it is capable to reveal order at a molecular scale that is usually hidden to the conventional microscopes (Tani et al., 1996; Cohen et al., 1968; Kuhn et al., 2001; Shribak et al., 2003). By showing the alignment of molecular bonds and submicroscopic shapes, polarized light offers a way to bridge the resolution gap between light and electron microscopy. In the early 1950, researchers demonstrated application of the polarization microscope and subsequently such techniques have been popularized for live cell imaging, chemistry, mineralogy, Biology, medical sciences etc. Moreover, the recovered polarization features of the light coming after light matter interaction can be quantitatively characterized using the Jones or Muller matrix approaches and physical parameters of the samples like dichroism, attenuation etc. can be quantified. Extension of digital holography to a vectorial domain is also possible by recording holograms of the orthogonal components of the light (Colomb et al., 2002). Idea and interests in the extension of the DH to the vectorial domain are based on our interests to keep advantages of the digital holography and also recover the polarization features of the light. In certain situations, however, interference effect does not manifest itself as intensity modulation. For instance, interference between an x-polarized object beam and a y-polarized reference beam generates only polarization modulation which can be

highlighted by measuring the Stokes Parameters (SPs). The SPs are important to characterize the light field and to describe the vectorial interference (Singh et al., 2012).

In many applications, it is required to image an object obscured by a scattering medium. When the object is hidden behind the random scattering media, it is difficult to apply the usual DH recording and reconstruction approach. Several techniques have been developed in order to image through scattering medium (Singh et al., 2011; 2012; Soni et al., 2016; Katz et al., 2014; Somkumar et al. 2017; Hilman et al., 2013; Tripathi et al., 2012; Aguiar et al., 2017). Random scattering scrambles the vectorial wavefront and makes it a spatially fluctuating polarized field. In this situation, correlation parameters such as coherence-polarization matrix and GSPs have been used to analyze the randomly polarized fields to recover the wavefronts (Singh et al., 2011; 2012; Takeda et al., 2014). These parameters can be used to develop a novel imaging technique by exploiting the statistical features of the random fields without resorting to any wavefront correction schemes. Recently, Stokes holography was developed to synthesize the GSPs structure in 3D space and the technique makes use of a Fourier transform relation between the Stokes fringes at the scattering plane and GSPs at the Fourier plane (Singh et al., 2012). Polarized objects hidden behind the random scattering medium is encoded into the Stokes fringes and reconstructed as distribution of the GSPs in 3D. This is realized by applying the field-based interferometer and evaluating the GPSs at the back focal plane of a Fourier transforming lens. In order to highlight significance of the presented polarization imaging method and its uniqueness, we present a following flow chart here and technical details of our technique is discussed in coming sections.
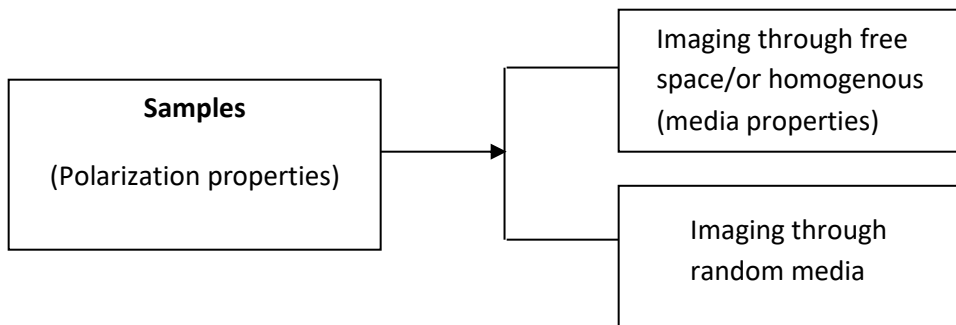
In this chapter, we propose a new method to use intensity interferometer, i.e., HBT type for Stokes holography. The HBT approach permits to offer a completely new approach for the digital holography with the polarization speckle and also helps to remove a Fourier transforming lens as required in the field-based interferometer for the Stokes holography (Singh et al., 2012). Making use of this feature, we design and develop a new lensless Fourier transform holography setup for the GSPs. This helps to achieve spatial stationarity of the random fields at an arbitrary distance z from the scattering plane and replaces the ensemble averaging by the space averaging of the random field. The GSPs also termed as Stokes vector wave follow the wave features in exact analogy to a coherent function of a scalar field (Takeda et al., 2010). We further make use of the lensless Fourier transform holograms of the GSPs to recover desired GSPs for depth recovery of the objects encoded into the Stokes fringes. This is implemented by digital propagation of the GSPs (rather than mechanical scanning of the detector). To the best of our knowledge, this is first such attempt to exploit the interference of the GSPs to realize lensless Fourier transform hologram for the Stokes vector waves and apply the HBT type interferometer for 3D imaging of the polarized objects. Moreover, combination of the HBT approach with the Stokes vector offers a new direction in the digital holography to analyze the randomly fluctuating electromagnetic fields and also offers new applications with coherence-polarization features of the light. The detailed theoretical basis, and experimental technique and results are discussed below.

5.2   Principle

Let us consider a polarized monochromatic light source at plane 1 as shown in Fig. 5.1. A coherent and polarized light passing through the scattering layer propagates down to the observation plane 2 located at a distance z from the source structure. The complex amplitude of the polarized field immediately after the scattering surface is represented as

$$E_p(\hat{\boldsymbol{r}}) = \left|E_p(\hat{\boldsymbol{r}})\right| \exp\left[i\left(\phi_p(\hat{\boldsymbol{r}}) + \varphi(\hat{\boldsymbol{r}})\right)\right]$$

(5.1)

where $\left|E_p(\hat{r})\right|$ and $\phi_p(\hat{r})$ are the amplitude and phase information of the polarized source at the scattering plane and $\varphi(\hat{r})$ is the random phase introduced by the non-birefringent scattering medium. The transverse spatial coordinate at the scattering medium plane is represented by $\hat{r}$ and $p = x, y$ represents two orthogonal polarization components.
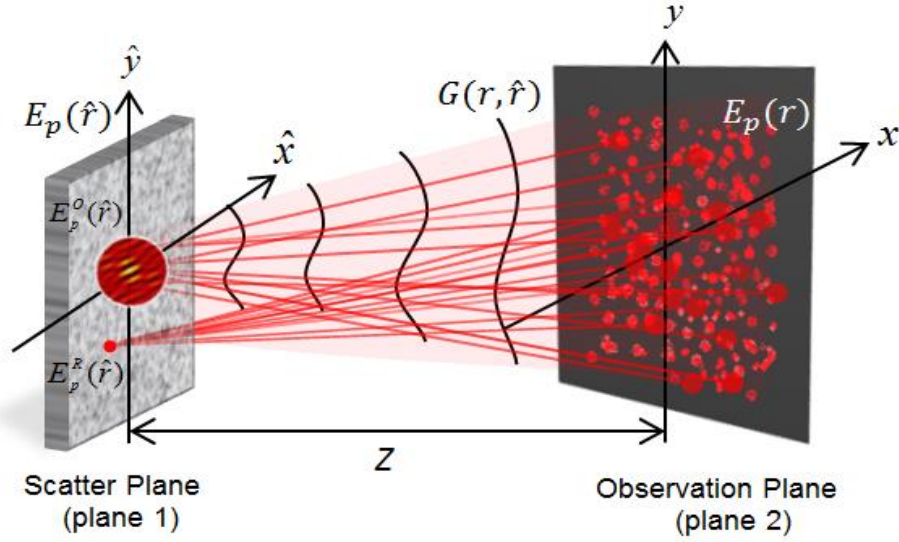
Fig. 5.1. Conceptual diagram shows the propagation of light from the scatter plane 1 to an observation plane 2. Here p stands for orthogonal polarization vector in x and y direction.

The scattered field at a distance z, is given as

$$E_p(\mathbf{r}, z) = \int E_p(\hat{r}) \exp\left(ik_z(\hat{r})z\right) \exp\left(-i\frac{2\pi}{\lambda f}\mathbf{r} \cdot \hat{r}\right)$$

(5.2)

where $k_z(\hat{r}) = k\sqrt{1 - \left(\left|\hat{r}\right|/f\right)^2}$, $k = \frac{2\pi}{\lambda}$ is wavenumber and λ is wavelength of the light and f is the Fourier transforming length. The correlation of the randomly scattered field is evaluated under the assumption of stationarity and ergodicity in space and is given (Singh et al., 2012) by

$$W_{pp'}(\boldsymbol{r}_1, z_1; \boldsymbol{r}_1 + \Delta\boldsymbol{r}, z_2) = \left\langle E_p^*(\boldsymbol{r}_1, z_1) E_{p'}(\boldsymbol{r}_1 + \Delta\boldsymbol{r}, z_2) \right\rangle_s$$

$$= \iiint E_p^*(\hat{\boldsymbol{r}}_1) E_{p'}(\hat{\boldsymbol{r}}_2) \exp\left(-ik_z(\hat{\boldsymbol{r}}_1)z_1\right) \exp\left(ik_z(\hat{\boldsymbol{r}}_2)z_2\right)$$

$$\times \exp\left(-i\frac{2\pi}{\lambda f}\left((\hat{\boldsymbol{r}}_2 - \hat{\boldsymbol{r}}_1)\cdot\boldsymbol{r}_1 + \hat{\boldsymbol{r}}_2\cdot\Delta\boldsymbol{r}\right)\right) d\hat{\boldsymbol{r}}_1 d\hat{\boldsymbol{r}}_2 d\boldsymbol{r}_1$$

$$= \int E_p^*(\hat{\boldsymbol{r}}) E_{p'}(\hat{\boldsymbol{r}}) \exp\left[ik_z(\hat{\boldsymbol{r}})\Delta z\right] \exp\left(-i\frac{2\pi}{\lambda f}\Delta\boldsymbol{r}\cdot\hat{\boldsymbol{r}}\right) d\hat{\boldsymbol{r}} \tag{5.3}$$

Here $W_{pp'}(\boldsymbol{r}_1, z_1; \boldsymbol{r}_1 + \Delta\boldsymbol{r}, z_2)$ represent two point correlation of the orthogonal polarization components p, p', $\Delta z = z_2 - z_1$, $\Delta\boldsymbol{r} = \boldsymbol{r}_2 - \boldsymbol{r}_1$ and $\langle\cdot\rangle_s$ represents spatial averaging and the relation $\int \exp\left[-i\frac{2\pi}{\lambda f}(\hat{\boldsymbol{r}}_2 - \hat{\boldsymbol{r}}_1)\cdot\boldsymbol{r}_1\right] d\boldsymbol{r}_1 = \delta(\hat{\boldsymbol{r}}_2 - \hat{\boldsymbol{r}}_1)$ is used in Eq. (5.3). It is important to mention here that a Fourier transforming lens is used to achieve spatial stationarity of the random field to replace ensemble average by spatial averaging in (Singh et al., 2011; 2012; Takeda et al., 2014). The random field at the observation plane can be characterized by the GSPs, given (Singh et al., 2011; Katz et al., 2014; Korotkova et al., 2005; Setala et al., 2006; Sahin, 2010; Singh et al., 2010) as

$$S_0(\boldsymbol{r}_1, \boldsymbol{r}_2) = \left\langle E_x^*(\boldsymbol{r}_1)E_x(\boldsymbol{r}_2)\right\rangle + \left\langle E_y^*(\boldsymbol{r}_1)E_y(\boldsymbol{r}_2)\right\rangle$$

$$S_1(\boldsymbol{r}_1, \boldsymbol{r}_2) = \left\langle E_x^*(\boldsymbol{r}_1)E_x(\boldsymbol{r}_2)\right\rangle - \left\langle E_y^*(\boldsymbol{r}_1)E_y(\boldsymbol{r}_2)\right\rangle$$

$$S_2(\boldsymbol{r}_1, \boldsymbol{r}_2) = \left\langle E_x^*(\boldsymbol{r}_1)E_y(\boldsymbol{r}_2)\right\rangle + \left\langle E_y^*(\boldsymbol{r}_1)E_x(\boldsymbol{r}_2)\right\rangle$$

$$S_3(\boldsymbol{r}_1, \boldsymbol{r}_2) = i\left[\left\langle E_y^*(\boldsymbol{r}_1)E_x(\boldsymbol{r}_2)\right\rangle - \left\langle E_x^*(\boldsymbol{r}_1)E_y(\boldsymbol{r}_2)\right\rangle\right] \tag{5.4}$$

where $\langle\cdot\rangle$ is ensemble average which can be replaced by spatial averaging (rather than time) for the spatial ergodic field (Takeda et al., 2014; Singh et al., 2010). The GSPs are transformed to the conventional SP for correlations at single point, i.e., $\boldsymbol{r}_1 = \boldsymbol{r}_2$.

The GSPs can be expressed in terms of the SPs at the scattering plane using Eqs. (5.3) and (5.4) and given (Singh et al., 2012) as

$$S_n(\Delta \boldsymbol{r}, \Delta z) = \int s_n(\hat{\boldsymbol{r}}) \exp\left[ik_z(\hat{\boldsymbol{r}})\Delta z\right] \exp\left[-i\frac{2\pi}{\lambda f}\hat{\boldsymbol{r}} \cdot \Delta \boldsymbol{r}\right] d\hat{\boldsymbol{r}}$$

(5.5)

Here $S_n(\Delta \boldsymbol{r}, \Delta z), (n = 0, 1, 2, 3)$ are 3D GSPs that show the reconstructed images from the random field while $s_n(\hat{\boldsymbol{r}})$ are the SPs of the source which may be in the form of polarization modulations, i.e., holographic or non-holographic. The polarization modulations $s_n(\hat{\boldsymbol{r}})$ carry signature of the object located at any arbitrary distance from the scatterer. Equation (5.5) is a basic relation of the Stokes holography and states that complex valued object encoded into the Stokes fringes can be reconstructed as 3D spatial structure of the GSPs of the random field.

To experimentally test the Stokes holography, a polarization interferometer is designed and developed in (Singh et al., 2012). This helps to simultaneously detect the orthogonal polarization components $E_p(\boldsymbol{r}, z)$ of the random fields and hence recover the GSPs. The field interferometer is successful in retrieving the complex field and evaluating the second order correlation but also sensitive to external disturbances. Here, we propose intensity correlation, i.e., HBT approach, for reconstruction of the GSPs in the Stokes holography. The HBT type interferometer is less susceptible to vibrations and evaluates the fourth order correlation of the random field. The fourth order correlation of the Gaussian random field is proportional to the modulus square of the second order field correlation (Mandel and Wolf, 1995; Hanbury and Twiss, 1956; Naik et al., 2011; Goodman, 1985; Shevchenko et al., 2008; Kumar et al., 2012; Singh et al., 2014). The HBT approach for the Stokes holography permits us to make use of the interference of the GSPs from two independent sources and realize a lensless Fourier transform geometry for the Stokes waves. The new recording and reconstruction approach for the lensless Stokes holography is as follows.

Let us consider that a coherent polarized light field at the observation plane is coming from two independent sources located in the Fresnel domain as shown in Fig. 5.1. The complex field at the plane 2 in the Fresnel region is given as

$$E_p(r) = \int E_p^1(\hat{r}) G(r, \hat{r}) d\hat{r} + \int E_p^2(\hat{r}) G(r, \hat{r}) d\hat{r}$$

(5.6)

Where $G(r, \hat{r})$ is a propagation kernel and given as

$$G(r, \hat{r}) \approx \frac{\exp(ikz)}{i\lambda z} \exp\left(ik \frac{|r|^2 - 2r \cdot \hat{r} + |\hat{r}|^2}{2z} \right)$$

(5.7)

The constant phase term $\exp(ikz)/(i\lambda z)$ is ignored from further consideration as we are interested in observations at a fixed z value. Using the above two relations along with the Fresnel kernel, the complex field is written as

$$E_p(r) = \exp\left(ik \frac{|r|^2}{2z} \right) \int E_p^1(\hat{r}) \exp\left(i \frac{k}{2z} |\hat{r}|^2 \right) \exp\left(-i \frac{k}{z} r \cdot \hat{r} \right) d\hat{r}$$

$$+ \exp\left(ik \frac{|r|^2}{2z} \right) \int E_p^2(\hat{r}) \exp\left(i \frac{k}{2z} |\hat{r}|^2 \right) \exp\left(-i \frac{k}{z} r \cdot \hat{r} \right) d\hat{r}$$

(5.8)

Intensity at the observation plane is given as $I(r) = |E_x(r)|^2 + |E_y(r)|^2$. The intensity correlation can be explained in terms of the second order field correlation for the Gaussian random field. Under consideration of the intensity correlation, as in the coming section, we have ignored the common phase factor outside the integration in Eq. (5.8). Removal of this phase factor is significant in the intensity correlation-based measurement for spatial stationarity (Takeda et al., 2014). Therefore, a GSP of the random field coming from two independent sources is represented as

$$S_0(r_1, r_2) = \int\int\int \left[\begin{array}{l} \left(E_x^1(\hat{r}_1) + E_x^2(\hat{r}_1) \right)\left(E_x^1(\hat{r}_2) + E_x^2(\hat{r}_2) \right) \times \\ \exp\left(i \frac{k}{2z} \left(|\hat{r}_2|^2 - |\hat{r}_1|^2 \right) \right) \exp\left(-i \frac{k}{z} \left(r_2 \cdot \hat{r}_2 - r_1 \cdot \hat{r}_1 \right) \right) \end{array} \right] d\hat{r}_1 d\hat{r}_2 dr_1 +$$

$$\int\int\int \left[\begin{array}{l} \left(E_y^1(\hat{r}_1) + E_y^2(\hat{r}_1) \right)\left(E_y^1(\hat{r}_2) + E_y^2(\hat{r}_2) \right) \times \\ \exp\left(i \frac{k}{2z} \left(|\hat{r}_2|^2 - |\hat{r}_1|^2 \right) \right) \exp\left(-i \frac{k}{z} \left(r_2 \cdot \hat{r}_2 - r_1 \cdot \hat{r}_1 \right) \right) \end{array} \right] d\hat{r}_1 d\hat{r}_2 dr_1$$

(5.9)

The common phase curvature term outside the integration in Eq. (5.8) is canceled out. Therefore, Eq. (5.9) justifies our approach to achieve a spatial stationary random pattern even from a non-stationary source at any observation plane in the Fresnel propagation domain. Under the assumption of two statistically independent sources $E_p^1(\hat{r})$ and $E_p^2(\hat{r})$, we are justified by taking the cross correlation of these two random fields $\left\langle E_p^{1*}(r)E_p^2(r+\Delta r)\right\rangle \approx 0$ and therefore the GSP in RHS of Eq. (5.9) is represented as

$$S_0(r_1,r_2) = \int\left[E_x^{1*}(\hat{r})E_x^1(\hat{r})+E_y^{1*}(\hat{r})E_y^1(\hat{r})\right]\exp\left(-i\frac{k}{z}(r_2-r_1)\cdot\hat{r}\right)d\hat{r} +$$
$$\int\left[E_x^{2*}(\hat{r})E_x^2(\hat{r})+E_y^{2*}(\hat{r})E_y^2(\hat{r})\right]\exp\left(-i\frac{k}{z}(r_2-r_1)\cdot\hat{r}\right)d\hat{r}$$

$$(5.10)$$

Equation (5.10) is derived by making use of the relation $\int\exp\left(-\frac{ik}{z}(\hat{r}_2-\hat{r}_1)\cdot r\right)dr = \delta(\hat{r}_2-\hat{r}_1)$ in Eq. (5.9). Similar relations can also be derived for the remaining GSPs by connecting GSPs with source SPs by a Fourier relation as

$$S_n(r_1,r_2) = \int s_n^1(\hat{r})\exp\left(-i\frac{k}{z}(r_2-r_1)\cdot\hat{r}\right)d\hat{r} + \int s_n^2(\hat{r})\exp\left(-i\frac{k}{z}(r_2-r_1)\cdot\hat{r}\right)d\hat{r}$$

$$(5.11)$$

where $S_n(r_1,r_2),(n=0,1,2,3)$ are the GSPs of the random fields while $s_n^1(\hat{r})$ and $s_n^2(\hat{r})$ are the SPs (instantaneous-non averaged for the source) at the scattering plane. The GSPs at the observation plane can be represented as interference of two Stokes waves as

$$S_n(r_1,r_2) = S_n^1(r_1,r_2) + S_n^2(r_1,r_2).$$

$$(5.12)$$

Equation (5.12) can be used to record the lensless Fourier transform hologram of the Stokes waves $|S_n(r_1,r_2)|^2 = |S_n^1(r_1,r_2)+S_n^2(r_1,r_2)|^2$. To record this hologram, we follow Eq. (5.5) and generate a reference Stokes wave as follows

$$S_n^2(r_1, r_2) = \int \delta(\hat{r}) \exp\left[-i\frac{2\pi}{\lambda z}\hat{r} \cdot (r_2 - r_1)\right] d\hat{r}.$$ Here, a point polarized source $\delta(\hat{r})$ is selected in order to generate a uniform reference Stokes wave covering the support of $S_n^1(r_1, r_2)$ to record the lensless Stokes wave hologram. This helps to recover the GSPs of the object's wave from a reference Stokes wave $S_n^2(r_1, r_2)$.

Let us turn to the generation of the Stokes waves hologram using the intensity measurements. Here, we introduce intensity correlation of the polarized speckle. The two-point intensity correlation of the Gaussian random field is directly related to the second order field correlation and given (Shevchenko et al., 2008; Singh et al., 2014) as

$$\Gamma(r_1, r_2) = \langle \Delta I(r_1)\Delta I(r_2)\rangle = \frac{1}{2}\sum_{n=0}^{3}\left|S_n(r_1, r_2)\right|^2 \tag{5.13}$$

where $\Delta I(r) = I(r) - \langle I(r)\rangle$ is an intensity fluctuation with respect to its mean value. Equation (5.13) emphasize that cross-covariance of the intensity is composed of contributions of modulus square of all four GSPs. Therefore, our objective is to retrieve the GSPs from the measured intensity correlation. We use Eq. (5.13) based on the HBT experiment to recover the GSPs from the intensity measurements.

In order to retrieve individual GSPs, we inserted an assembly of a quarter wave plate (QWP) with a linear polarizer (LP) before the observation plane 2. The QWP is oriented at angle θ with respect to the x-axis and a LP also oriented in the same direction as shown in Fig. 5.2. The complex field after the polarization elements is given as

$$E_\theta(r, z) = \left[\cos^2\theta + i\sin\theta\right]E_x(r, z) + \left[(1-i)\cos\theta\sin\theta\right]E_y(r, z) \tag{5.14}$$

with the appropriate trigonometric substitution, the intensity correlation at a fixed z plane can be expressed in terms of the GSPs and given as (Vinu and Singh, 2015)

$$\Gamma(r_1, r_2, \theta) = \left| S_0(r_1, r_2) + S_1(r_1, r_2)\cos^2 2\theta + S_2(r_1, r_2)\frac{\sin^2 4\theta}{2} + S_2(r_1, r_2)\sin 2\theta \right|$$

(5.15)

Therefore, the two-point intensity correlation is the direct function of the all four GSPs, which contains the Stokes wave, and interference of object and reference as described in Eq. (5.12). By selecting appropriate angles of QWP rotation (i.e., θ), such that $\theta_1 = 0°$ $\theta_2 = 22.5°$, $\theta_3 = 45°$ and $\theta_4 = 135°$ four intensity correlation patterns are recorded. They are combinations of the GSPs as

$$\Gamma(r_1, r_2, \theta_1) = \left| S_0(r_1, r_2) + S_1(r_1, r_2) \right|^2$$

$$\Gamma(r_1, r_2, \theta_2) = \left| S_0(r_1, r_2) + \frac{S_1(r_1, r_2)}{2} + \frac{S_2(r_1, r_2)}{2} + \frac{S_3(r_1, r_2)}{\sqrt{2}} \right|^2$$

$$\Gamma(r_1, r_2, \theta_3) = \left| S_0(r_1, r_2) + S_3(r_1, r_2) \right|^2$$

$$\Gamma(r_1, r_2, \theta_4) = \left| S_0(r_1, r_2) - S_3(r_1, r_2) \right|^2$$

(5.16)

Each of the intensity correlations resulting from a particular orientation of the QWP gives a hologram which comes from the interference of the different combinations of the Stokes waves in a lensless Fourier transform geometry. From these holograms, we recover the complex GSPs of the object field, i.e., $S_n^1(r_1, r_2)$ using the Fourier analysis technique (Vinu and Singh, 2015). Fourier transform of the intensity correlation hologram provides spectra, its conjugate and a dc term. The spectrum is filtered and translated to the origin of the frequency coordinate. The inverse Fourier transform of the centrally shifted spectra and its appropriate combinations provide all the desired GSPs of the object field. The recovered GSPs at the Fourier plane can be digitally propagated to retrieve the Stokes fringes at the scattering plane using Eq. (5.5), and also reconstruct the complex valued polarized objects as spatial distributions of the GSPs in the 3D space.

5.3   Experiment Implementation

In order to demonstrate a lensless Stokes holography for the Stokes waves and realize the spatial averaging, we design an experimental setup for the proof of principle experiment as shown in Fig. 5.2. This consists of a system to encode a polarized object into the Stokes modulations $S_n(\hat{r})$ behind the scattering medium as explained in section 2, and experimental arrangements to implement a lensless Fourier transform Stokes holography and reconstruction with the HBT approach. The experimental scheme is designed to apply spatial averaging as a replacement of the ensemble averaging at a particular observation plane z and uses the recovered GSPs for digital propagation as described in the Eq. (5.5). This gives an advantage in the context of recovering GSPs spatial structures and hence reconstructing the 3D object structures encoded into the hologram without any mechanical z scanning of the detector. Detailed description of Fig. 5.2 is as follows.
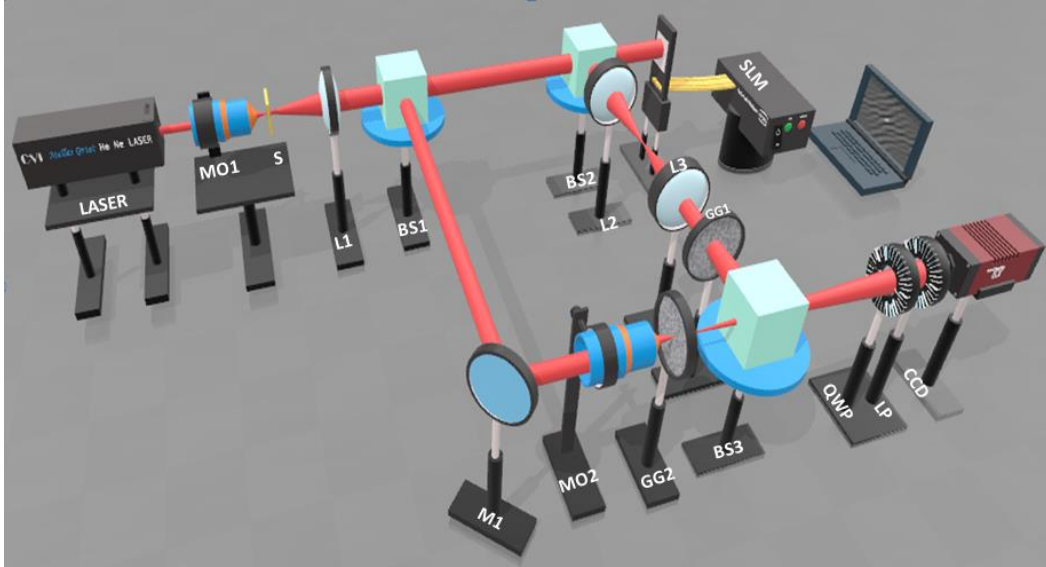
Fig. 5.2. Experimental set-up for the lensless Stokes holography. MO: microscope objective; S: pinhole; L: lens; BS: beam splitter; SLM: spatial light modulator; GG: ground glass; M: mirror; QWP: quarter wave plate; LP: linear polarizer; CCD: charge coupled device.

A linearly polarized beam from a He-Ne laser of wavelength 633nm (Melles Griot 25-LHP-928-230) is oriented at 45° with respect to x-direction, spatially filtered with

microscope objective O1 (20X, NA=0. 40) and pinhole S (10μm) and subsequently collimated by lens L1(f=150mm). The collimated beam splits into two arms by a non-polarizing beam splitter BS1. The transmitted beam illuminates the spatial light modulator SLM (Holoeye LC-R 720, reflective type; pitch pixel=20μm) which carries hologram of an object (H) and this hologram is projected at the scattering plane by a 4f imaging system with unit magnification. The digital hologram displayed on the SLM is a computer-generated hologram (CGH) of off-axis objects and numerically recorded in the Fourier geometry as shown in Fig. 5.3. Figure 5.3(a) shows the formation of Fourier transform hologram encoding the object information and Fig. 5.3(b) shows composition of two objects placed at different longitudinal planes and their digitally generated FTH.
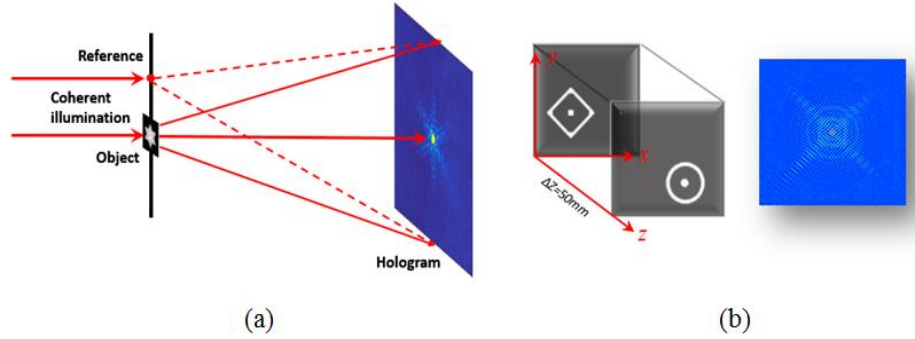
Fig. 5.3. (a) Formation of Fourier hologram. (b). Set of two objects with longitudinal distance of 50mm, and its Fourier transform hologram.

Light coming from the SLM have an arbitrary polarization and travels through the ground glass GG1 (DG20/120/MD, Thorlab, 3mm thickness) and gets randomly distorted and generates speckle pattern. The SLM (LC- R720) shows some crucial amplitude and phase modulation characteristics and they are not uniform at each gray value of SLM (Tiwari et al., 2020). Hence, it modulates state of polarization with change in gray levels of SLM. The speckle pattern further propagates towards the charged coupled device (CCD) plane. The 45° linearly polarized light reflected from the BS1 and folded by mirror M1 is focused at the ground glass plate GG2 using MO2. The focal spot at GG2 is placed at an off-axis in order to generate a reference Stokes wave with uniform amplitude profile and a linear phase structure as described in Eq. (5.11). The

speckle coming out of the GG2 propagates towards the CCD plane. Both the ground glasses are placed at distance z=280mm from the CCD plane in order to make a lensless Fourier transform geometry for the Stokes waves as described in Eqs. (5.12) and (5.13). The random fields coming from two independent diffusers are combined by BS2 and coherently add to generate the resultant speckle for the orthogonal polarization components as described in Eq. (5.6). The light further passes through a QWP, which is rotated at an angle θ with x direction and filtered by a LP. The transmission axis of the LP is placed in the x direction and the resultant field is captured by a monochrome CCD camera. The camera has a 14-bit dynamic range with a resolution of 2750X2200 pixels and a pixel pitch of 4.54 micron (Prosilica GX2750). Both ground glasses are static during the recording of the intensity distribution of the resultant speckle field. The intensity is recorded for four different orientation angles of the QWP as described in the previous section and four intensity correlation holograms are digitally obtained from the experimentally recorded speckle patterns.

5.4   Results and Discussion

We have applied this technique for different cases of objects and demonstrated 3D imaging as distribution of the spatial structure of the GSPs. In our first case, we consider a digital Fourier transform hologram (DFTH) of two longitudinally separated objects by a distance 50mm as shown in Fig. 5.3. And this DFTH is used as an object displayed at the SLM plane. Resultant speckle patterns for this case are shown in Fig. 5.4 for the four different orientations of the QWP.
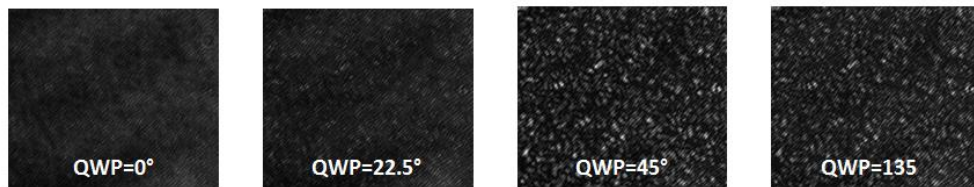
Fig. 5.4. Raw intensity speckle images recorded in CCD.

The recorded intensity patterns are random which do not have any visual information. Spatially averaged two-point intensity correlation functions are digitally evaluated from the recorded speckle patterns that correspond to each of the QWP rotation, which are equivalent to $\Gamma(\Delta r, \theta)$ with $\Delta r = r_2 - r_1$. Fourier analysis operation and appropriate combinations of processed spectra of the intensity correlation holograms provide GSPs.

To evaluate the quality of reconstruction, we introduce parameters like visibility, reconstruction efficiency and peak signal to noise ratio (PSNR). The visibility is defined as the extent to which the reconstruction is distinguishable from the background noise. It is given by the ratio of the average intensity level of object, to the background intensity level (Tripathi et al., 2012)

$$V_{obj} = \frac{I_{O_{avg}}}{I_{B_{avg}}}$$

(5.17)

where, V_{obj} is the visibility of the object, $I_{O_{avg}}$ is the average intensity of the object and $I_{B_{avg}}$ is the average intensity of the background. Reconstruction efficiency η is another parameter used to measure the quality of reconstruction (Tripathi et al., 2012). It is given as the ratio of the object signal to the total power and calculated as

$$\eta = \frac{I_{O_{avg}}}{I_{O_{avg}} + I_{B_{avg}}}$$

(5.18)

PSNR is also one of the parameters to analyze the quality of reconstruction. PSNR is defined as the ratio of the maximum possible power of a signal to the power of corrupting noise that affects the quality (Huynh-Thu and Ghanbari, 2008). PSNR in logarithmic decibel (dB) is calculated as

$$PSNR = 10\log_{10}\frac{MAX_\mathbf{o}{}^2}{MSE}$$

<div align="right">(5.19)</div>

where, $MAX_\mathbf{0}$ is the maximum possible pixel value of the object and MSE is the cumulative squared error between the compressed and the original image.

Results of the GSPs at the plane z= 280mm are shown in Figs. 5.5(a) – 5.5(d). These results can be used to digitally propagate the GSPs to different planes and results at plane z+Δz =330mm are shown in Figs. 5.5(e) – 5.5(h). Phase structure of the reconstructed object $S_0(\Delta\mathbf{r})$ is shown in Fig. 5.5(i). From the experimental results, it is clear that light field impinging the ground glass GG1 is predominantly linear. The calculated visibility (V_{obj}), reconstruction efficiency (η) and the PSNR values for the images are shown in Fig. 5.5.
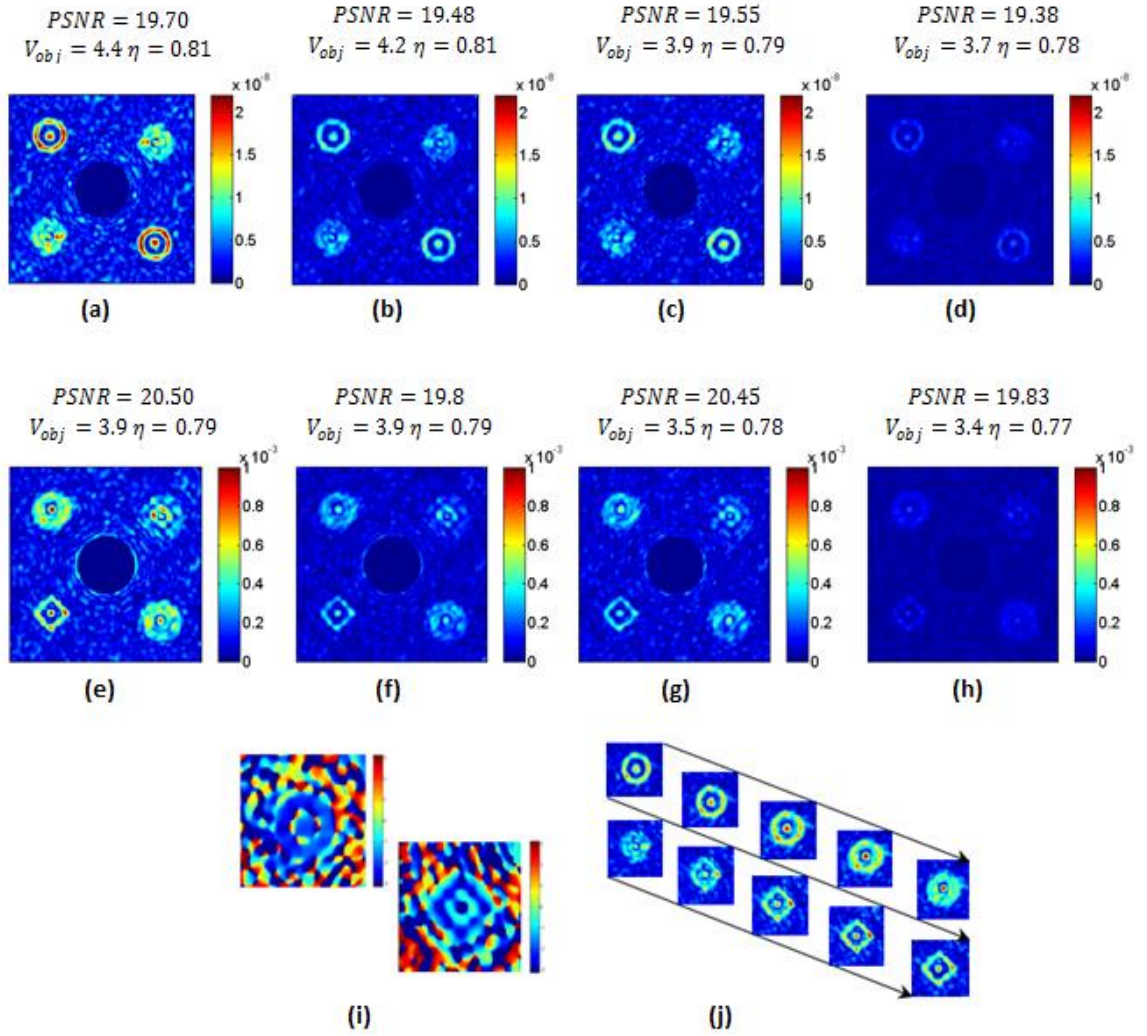
Fig. 5.5. Imaging of a 3D object through a scattering media. Figs. 5(a)-5(h) are the elements of GSPs and their amplitude distribution (a) $S_0(\Delta r)$, (b) $S_1(\Delta r)$, (c) $S_2(\Delta r)$, and (d) $S_3(\Delta r)$ at z=280mm plane and (e) $S_0(\Delta r)$, (f) $S_1(\Delta r)$, (g) $S_2(\Delta r)$, and (h) $S_3(\Delta r)$ at z=330mm plane. (i) Shows the reconstructed phase of the two objects. (j) 3D representative diagram showing focusing of the two objects with depth separation of Δz=50mm.
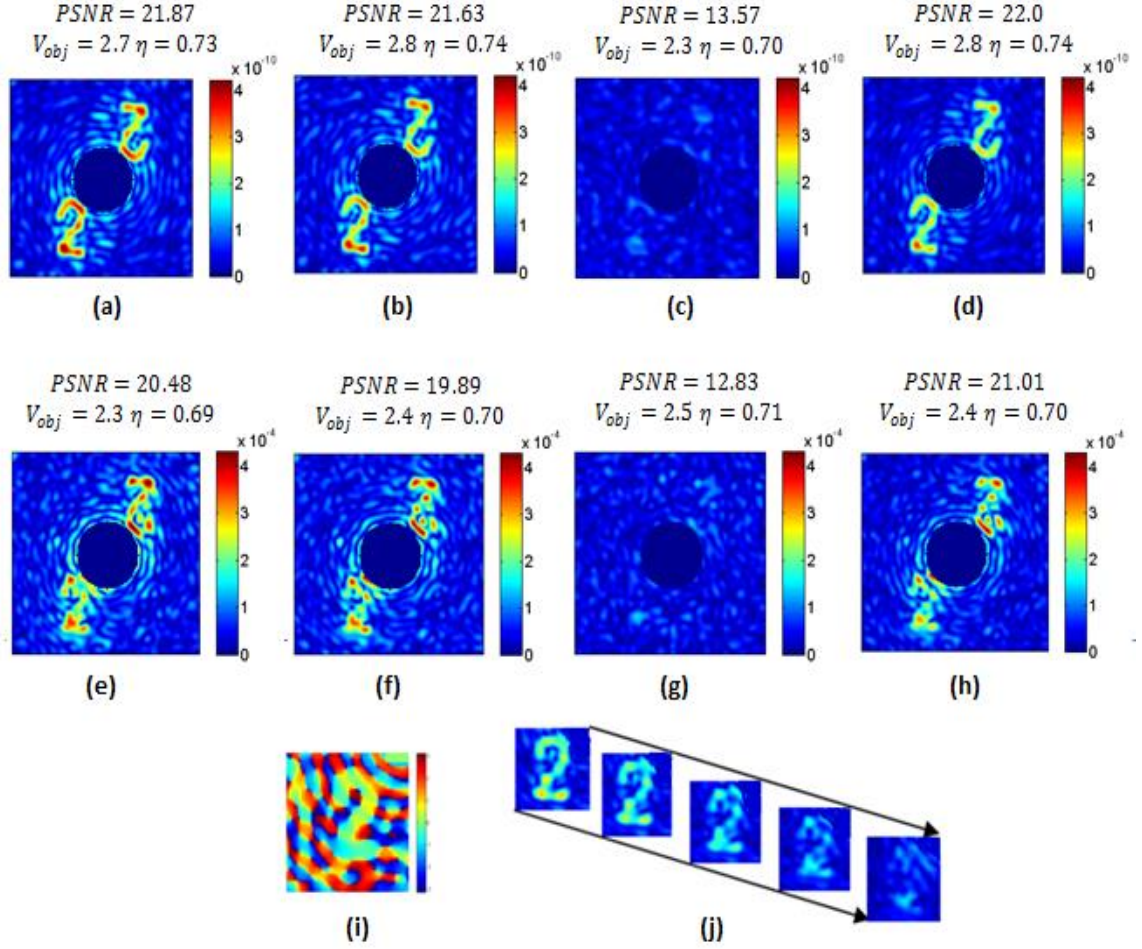
Fig. 5.6. Imaging of an object through a scattering media. Figs. 6(a)-6(h) are the elements of GSPs and their amplitude distribution (a) $S_0(\Delta r)$, (b) $S_1(\Delta r)$, (c) $S_2(\Delta r)$, and (d) $S_3(\Delta r)$ at z=280mm plane and (e) $S_0(\Delta r)$, (f) $S_1(\Delta r)$, (g) $S_2(\Delta r)$, and (h) $S_3(\Delta r)$ at z=310mm plane (i) Shows the reconstructed phase of the object. (j) 3D representative diagram showing focusing of the object with different depth separations.

Reconstruction of another polarization hologram $s(\hat{r})$ was carried out and results are shown in Figs. 5.6(a)- 5.6(h). In this case, we consider an object '2' encoded into the Fourier transforming hologram. Figures 5.6(a)- 5.6(d) represent the corresponding GSPs of an object at z=280mm plane. Whereas Figs. 5.6(e) – 5.6(h) show the propagated GSPs at different depth z+Δz =310mm, calculated by using numerical beam propagation technique based on angular spectrum method. Figures 5.6(a) – 5.6(d) show that the

object displayed on the ground glass GG1 has a predominantly elliptical polarization. A phase structure of the reconstructed object $S_0(\Delta \boldsymbol{r})$ is shown in Fig. 5.6(i) as distribution of phase of the GSPs. The calculated visibility (V_{obj}), reconstruction efficiency (η) and the PSNR values for the images are shown in Fig. 5.6.

In summary, we have experimentally demonstrated the imaging through scattering media by employing the Stokes holography with the Hanbury Brown-Twiss approach. The object information is encoded into the hologram and hidden behind the scattering media is successfully recovered from the polarization speckles by using a Lensless Fourier transform geometry for the Stokes waves and making use of the intensity correlation. This is possible by recovering the 3D-GSPs of the randomly polarized light fields. The demonstrated technique is well efficient in retrieving the information by reconstructing objects at their actual positions and provides a 3D complex field imaging facility. This technique can be used to retrieve anisotropic features of the objects lying behind the scattering media. Reconstruction results are quantitatively estimated by determining visibility, reconstruction efficiency and PSNR.

CHAPTER 6
COMBINING COMPRESSED SENSING WITH INTENSITY CORRELATION FOR IMAGING

6.1 Introduction

Holography reconstructs the object in non-invasive and label free environment. We are in the era of digital imaging, in which images are recorded by digital cameras and reconstructed in computer using digital algorithms. On axis and off axis position of a reference wave with respect to object can be utilized to make different types of holograms. Depending on experimental geometry of recorded hologram, several numerical techniques have been developed to efficiently reconstruct the hologram, some of these are Fresnel transformation, Convolution approach and Fourier reconstruction etc. (Schnars et al., 2002). Among many available digital holographic geometries, the Fourier hologram attracts significant attention. It is highlighted that a Fourier transform hologram (FTH) produces high resolution images in wave front reconstruction images. Fourier transform plays a pivotal role in the variety of imaging modalities ranging from homogeneous to inhomogeneous media. FTH is a non-iterative imaging technique which is widely used in the field of biology and material science (Kreis, 2006; Stroke, 1965). In FTH, the reference wave is chosen to be a point source placed in the object plane. When monochromatic coherent light source illuminates the object plane, object wave and the reference wave create interference pattern which forms the hologram in the far field plane (Fourier plane). Desired object image is then recovered by taking inverse Fourier transform (IFT) in a single step deterministic computation (Shapiro, 2005; Fienup, 1987). Utilization of a single Fourier transform operation to the recorded FTH provides the object information and hence make this geometry more appealing and computationally less expensive. For instance, FT hologram can be used to preserve and encode the object information as a distribution of the complex coherence function of the random field and technique is

referred to as correlation holography. In recent years, our group has developed several new modalities of the correlation holography for imaging of the scalar and vectorial objects from the randomly scattered light.

In order to fulfill sampling requirements or control the random light grain size in 3D, one must carefully limit the spatial extent of the FTH at the random scattering medium. However, restriction in the size of FTH causes a poor signal to noise ratio and distorted reconstruction. To overcome this limitation, it is always desired to use efficient schemes that can be used to reconstruct the full signal faithfully from a set of sparse measurements. In this chapter, we present a new approach to retrieve the complete signal even with the availability of limited size FTH. This becomes possible by combing correlation holography with compressed sensing (CS). Compressed sensing (also known as compressive sensing, compressive sampling, or sparse sampling) is a popular sparse signal processing technique for efficiently acquiring and reconstructing a signal, from few measurements, through optimization (Candes et al., 2006; Candes and Wakin, 2008). CS has emerged as a new framework for signal acquisition and sensor design. The basic principle behind the CS theory is, the sparsity of a signal can be exploited to recover it from far fewer samples than required by the Shannon-Nyquist sampling theorem, by finding solution to the underdetermined liner systems. CS enables a potentially large reduction in the sampling and computation costs for sensing signals that have a sparse or compressible representation. An early breakthrough in signal processing was the Nyquist – Shannon sampling theorem. It states that if the signal's highest frequency is less than half of the sampling rate, then the signal can be reconstructed perfectly. The main idea is that with prior knowledge about constraints on the signal's frequencies, fewer samples are needed to reconstruct the signal. It has been demonstrated that given knowledge about a signal's sparsity, the signal may be reconstructed even with fewer samples than the sampling theorem required (Candes and Wakin, 2008; Donoho, 2006; Candes and Romberg, 2007; Candes et al., 2006). The fundamental idea behind CS: rather than first sampling at a high rate and then compressing the sampled data, we would like to find ways to directly sense the data in a compressed form i.e., at a lower sampling rate. CS has been utilized in a variety of applications to solve missing data problem.

The proposed chapter highlights the potential of compressed sensing in the imaging through a random scattering medium. This method can reduce the noise level in recovered signal and super-resolved images can be obtained using the CS-based technique compared to the usual FT. The demonstrated technique is well efficient in retrieving the information by reconstructing objects from limited sized FTH. Quantitative analysis has been carried out to compare the quality of reconstruction using inverse Fourier transform (IFT) and CS techniques. The finding highlights that the CS reconstruction is better than that of IFT reconstruction.

6.2 Principle

6.2.1 Fourier transform holography

Recoding of hologram for intensity correlation holography is much similar to that in convention holography. In our work, we have adopted Fourier transform geometry to synthetically generate the hologram, object and point source reference wave are in the front focal plane of lens and the detector is located in back focal plane of the lens as shown in fig. (6.1).

Let us consider an off- axis object expressed by a local field distribution $E(x_0, y_0)$ propagates to the Fourier plane by virtue of the Fourier transform lens. The complex amplitude to be recorded at the hologram plane becomes the Fourier spectrum of the object field

$$E(\hat{r}) = E(\hat{x}, \hat{y}) = \iint E(x_0, y_0) \exp[-i\frac{2\pi}{\lambda f}(\hat{x}x_0 + \hat{y}y_0)]d\hat{x}d\hat{y}$$

(6.1)
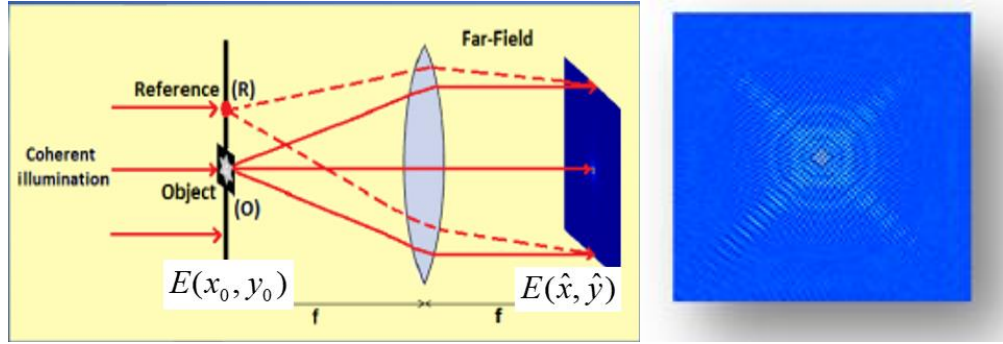
Fig. 6.1. Formation of Fourier hologram.

In synthesizing the hologram numerically, we remove autocorrelation term which become the source of an unwanted autocorrelation image.

The hologram is illuminated by a monochromatic beam through the scattered/ground glass plane and generates a speckle field. A schematic representation of the generation of speckle field is shown in Fig. (6.2). The scattered field $E_O(r)$ on the Fourier transform plane for fixed time t, is given by:

$$E_O(r) = \int E_O(\hat{r}) \exp(i\phi(\hat{r})) \exp[-i\frac{2\pi r \cdot \hat{r}}{\lambda f}] d\hat{r}$$

(6.2)

Here, $E_O(\hat{r})$ is the field incident on the ground glass and $\hat{r}$ is position vector on the ground glass plane, $\phi(\hat{r})$ a random phase introduced by the ground glass, λ the wavelength of the light, f the focal length of the Fourier transforming lens. Suffix O stands for 'object' speckle and this is used to distinguish from the reference speckle which will be defined later.
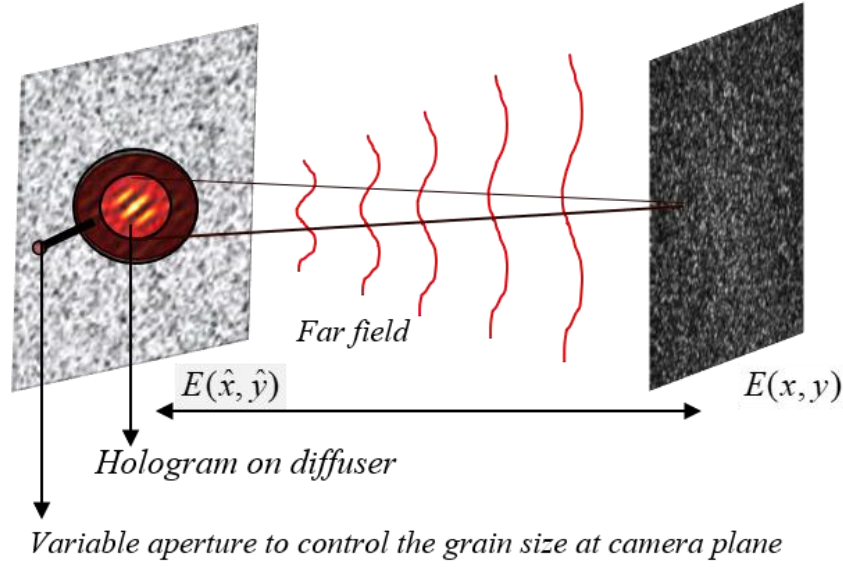
Fig. 6.2. Geometry of reconstruction of hologram in intensity correlation holography

The correlation of the randomly scattered field is evaluated under the assumption of stationarity and ergodicity in space and is given by (Takeda, 2013)

$$W_O(\Delta r) = \left\langle E_O^*(r_1) E_O(r_2) \right\rangle_s = \int E_O^*(r_1) E_O(r_1 + \Delta r) dr_1$$
$$= \int |E_O(\hat{r})|^2 \exp\left[-i\frac{2\pi}{\lambda f} \Delta r \cdot \hat{r} \right] d\hat{r}$$

$$(6.3)$$

Here $W_O(\Delta r)$ represents two-point correlation, $\Delta \boldsymbol{r} = \boldsymbol{r}_2 - \boldsymbol{r}_1$ and $\left\langle \cdot\cdot \right\rangle_s$ represents spatial averaging and the relation $\int \exp\left[-i\frac{2\pi}{\lambda f}(\hat{\boldsymbol{r}}_2 - \hat{\boldsymbol{r}}_1)\cdot \boldsymbol{r}_1 \right] dr_1 = \delta(\hat{\boldsymbol{r}}_2 - \hat{\boldsymbol{r}}_1)$ is used in Eq. (6.3). For a random field obeying Gaussian statistic, there exist a relation between the fourth order correlation and second order correlation, and this is given as

$$\Gamma(\Delta r) = \langle \Delta I(r)\, \Delta I(r + \Delta r) \rangle \propto |W_O(\Delta r)|^2 \tag{6.4}$$

where $\Delta I(\boldsymbol{r}) = I(\boldsymbol{r}) - \langle I(\boldsymbol{r}) \rangle$ is an intensity fluctuation with respect to its mean value. Equation (6.4) emphasize that cross-covariance of the intensity is composed of

contributions of modulus square of second order correlation and phase information. However, this lost phase of the complex coherence function can be retrieved by using a known reference complex coherence function with the help of off- axis holography. To apply this, we generate a reference speckle pattern and spatial coherence of this field is given as

$$W_R(\Delta r) = \int circ(\frac{\hat{r} - \hat{r}_g}{a}) \exp[-i\frac{2\pi}{\lambda f}\Delta r \cdot \hat{r}]d\hat{r}$$

(6.5)

Here $\hat{r} = \hat{r}_g$ represents lateral shift of the reference beam of radius 'a' on the ground glass plane. Let us consider coherent addition of the object and reference speckles, the intensity at the Fourier plane is given as

$$I(r) = |E(r)|^2 = |E_O(r) + E_R(r)|^2$$

(6.6)

where $E_R(r)$ is the speckle due to the reference source. Since the resultant intensity is a speckle hologram, the mutual coherence function corresponding to it should have contributions arising from $|E_O(r)|^2$, $|E_R(r)|^2$ and the mixed terms. The coherence function of the resultant speckle field is

$$W(\Delta r) = \langle E^*(r_1)E(r_1 + \Delta r)\rangle$$
$$= \langle [E_O(r_1)E_R(r_1)] * [E_O(r_1 + \Delta r)E_R(r_1 + \Delta r)]\rangle$$

(6.7)

Since the scatterers used to realize the object- and reference beams are different, we are justified in taking the contribution from the mixed term zero, i.e., $\langle E_O^*(r_1)E_R(r_1 + \Delta r)\rangle = 0$. Therefore, the resultant mutual coherence function for the resultant intensity is

$$W(\Delta r) = W_O(\Delta r) + W_R(\Delta r)$$

(6.8)

The fourth order intensity correlation of the resultant speckle field is given as

$$\langle \Delta I(r)\Delta I(r+\Delta r)\rangle = \left|W(\Delta r)\right|^2$$

$$= \left|W_O(\Delta r)\right|^2 + \left|W_R(\Delta r)\right|^2 + W_O^*(\Delta r)W_R(\Delta r) + W_O(\Delta r)W_R^*(\Delta r) \tag{6.9}$$

$$D_{h;ij}O = \begin{cases} O_{i+1,j} - O_{i,j} & if \quad i < n \\ 0 & if \quad i = n \end{cases}$$

Here $W_O^*(\Delta r)$ and $W_R^*(\Delta r)$ denote complex conjugate of the coherence functions of the random scattered fields engineered by object and reference source respectively. Interference fringes exist in the cross-covariance of the intensity of the resultant speckle. This interference fringe results due to superposition of the complex coherence of the object and reference speckle fields. The off-axis geometry for superposition of the two speckle fields is important for experimental implementation of the proposed idea. This geometry modulates fringes of the intensity correlation with properly selected carrier frequency in such a way that Fourier spectrum of the 'object' coherence field gets separated from the central background or dc. The complex coherence of the object speckle field is retrieved using the Fourier transform.

6.2.2 Compressive sensing framework

The application of CS in this framework assists to reconstruct the signal from the incomplete information (Donoho, 2006). The information available in blocked FTH is less than the usual FTH. It has been shown that the measurements of signal can be from the space domain or from frequency domain (Candes and Romberg, 2005). In the FTH, the captured hologram is in the Fourier domain and hence measurements are the available frequency components of the FTH. The blocked FTH can be represented as

$$I_W = WI$$

where I denotes FTH of an unknown object O of size $n \times n$, and I_W is filtered Fourier hologram of O. I_W is of the same size of I but lacks frequency components those are filtered out (zero frequencies) and has only M measurements. W is the window that mimics the filter and removes the frequency components (lower or higher). W takes the N values from I and gives M measurements, $(M < N)$.

In our investigation, we have modelled the beam stop by choosing W as low pass filter. Computing inverse Fourier transform of I_W, makes it ill-posed or under determined problem (Akshay et al., 2018). As I_W is the filtered FTH with blocked frequencies, by assigning missing frequencies with any random values while keeping the measured (observed)frequencies unchanged, there are an infinite number of solutions possible. It is impossible to find unique solution to this situation hence some iterative method is required for reconstruction. In order to recover the missing contents of FTH, CS requires some additional information (Candes and Wakin, 2008).

If the underlying signal is a 2D object image and the measurements are in frequency domain, an alternate recovery model is that the gradient of image is sparse (Rudin et al., 1992). Let $O_{i,j}$ denote pixel in the ith row and j^{th} column of an n x n object O, and define the gradient operators

$$D_{v;ij}O = \begin{cases} O_{i,j+1} - O_{i,j} & if \quad i < n \\ 0 & if \quad i = n \end{cases} \tag{6.10}$$

The total variation of O is sum of the magnitudes of these discrete gradients at every points

$$TV(O) = \sum_{ij} \sqrt{(D_{h;ij}O)^2 + (D_{v;ij}O)^2} = \sum_{ij} \left\| D_{ij}O \right\|_2 \tag{6.11}$$

By enforcing the sparsity constraint on the total variation (TV) of O, we recover O' by solving optimization problem based on sparse gradient of the object (Candes and Romberg, 2005).

$$O' = \min \left\| TV(O) \right\| \quad \text{subject to} \quad I_W = WI \tag{6.12}$$

where O' is required reconstructed object. It has been proved that, Eq. (6.12) will recover O' for piecewise constant O with sufficiently few edges (i.e., $D_{ij}O$ is non zero for few numbers of indices ij - gradient of object is sparse) (Candes and Romberg, 2005). Eq. (6.12) is the convex optimization problem in CS literature (Candes and Wakin, 2008; Candes et al., 2006). The optimization problem posed in Eq. (6.12) can be recasted as Second Order Cone Program (SOCP) as explained in Ref. [25] is given by

$$\min \sum_{ij} t_{ij} \quad \text{subject to} \quad \left\| D_{ij} O \right\|_2 \leq t_{ij} \quad , \qquad I_W = WI \tag{6.13}$$

where i; j = 1; ::::; n. SOCP can be solved efficiently with a generic log-barrier algorithm (Candes and Romberg, 2005). Logarithmic barrier function approximately formulates the inequality constrained of Eq. (6.13) as an equality constrained problem to which Newton's method with equality constraints can be applied (Boyd and Vandenberghe, 2004). The standard log-barrier method transforms the Eq. (6.13) into a series of linearly constrained programs given by

$$\min \sum_{ij} t_{ij} - \frac{1}{\tau^k} \sum_{ij} \log \left(-\left\| D_{ij} O \right\|_2 + t_{ij} \right) \text{ subject to} \qquad I_W = WI \tag{6.14}$$

where $\tau > 0$ is the log barrier parameter that sets the accuracy of approximation. Initially τ^{-1} is defined as N/TV (O') and at every log barrier iterations k, the value of τ is updated by factor μ (Candes and Romberg, 2005). Hence, $\tau^{k+1} = \mu \tau^k$ and $\tau^{k+1} > \tau^k$. Total number of log barrier iteration K is given by

$$K = \left\lceil \frac{\log N - \log \eta - \log \tau^{-1}}{\log \mu} \right\rceil \tag{6.15}$$

where N is number of elements of I. The log barrier algorithm terminates for duality gap $N/\tau^k < \eta$, and μ is the factor by which barrier constant τ is updated (Candes and Romberg, 2005). As number of iterations increases CS gives improved result than compared to the previous iterations. Number of log barrier iterations can be increased by selecting lowest possible values of μ (> 1) and η. Default values of μ and τ are 10 and 10^{-4} used in this analysis respectively. The flow chart of entire recovery process to obtain O' from I_W is shown in Fig. 6.3.
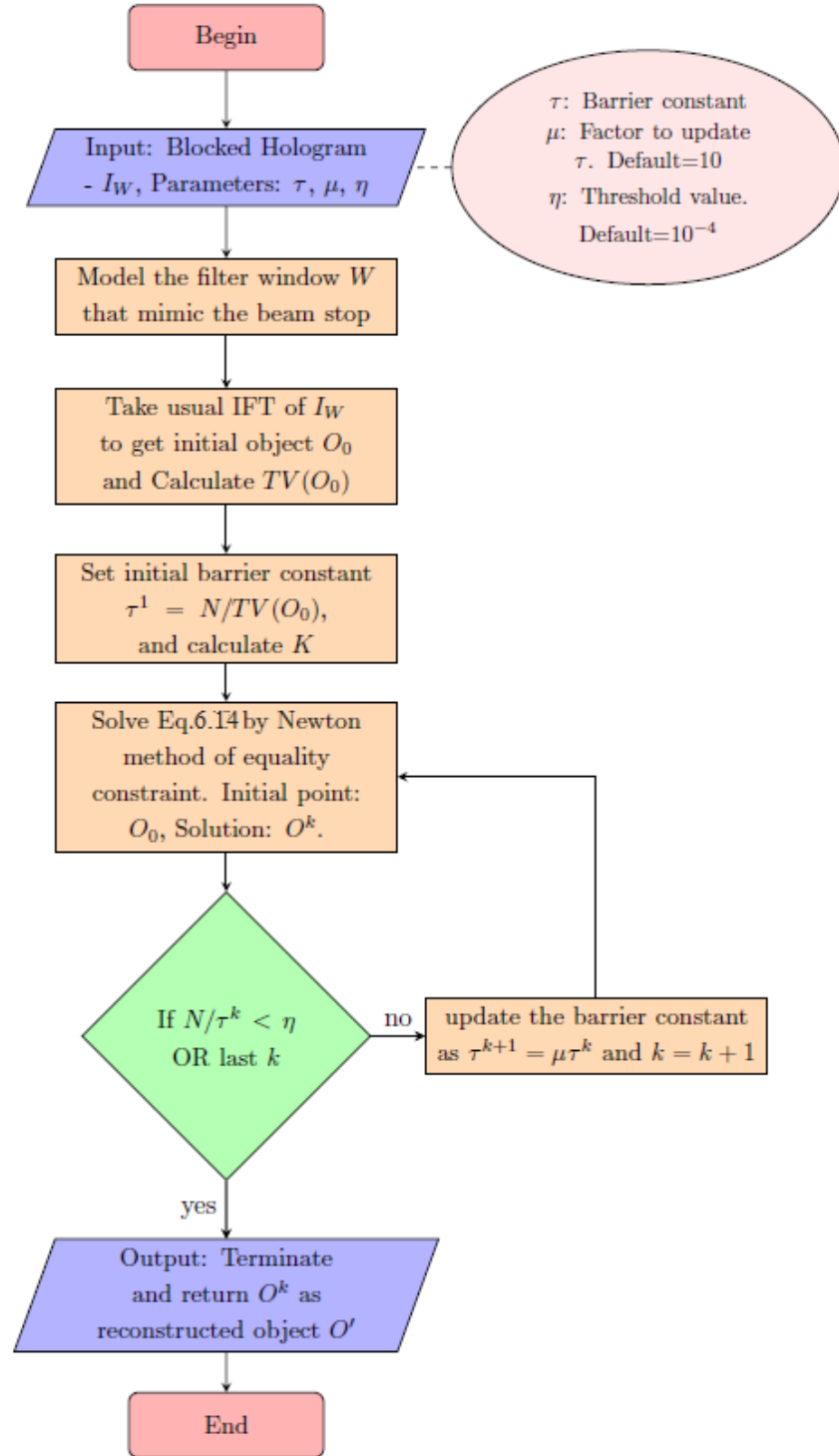
Fig. 6.3. Flow chart to reconstruct object O' from I_w (Picture source: Akshay et al., 2018)

6.3 Experiment Implementation

We developed an experimental strategy equipped with an off- axis holography technique to retrieve the complex coherence function of the speckle fields. The experimental geometry to retrieve the complex coherence function using off-axis holography technique is shown in Fig. 6.4.
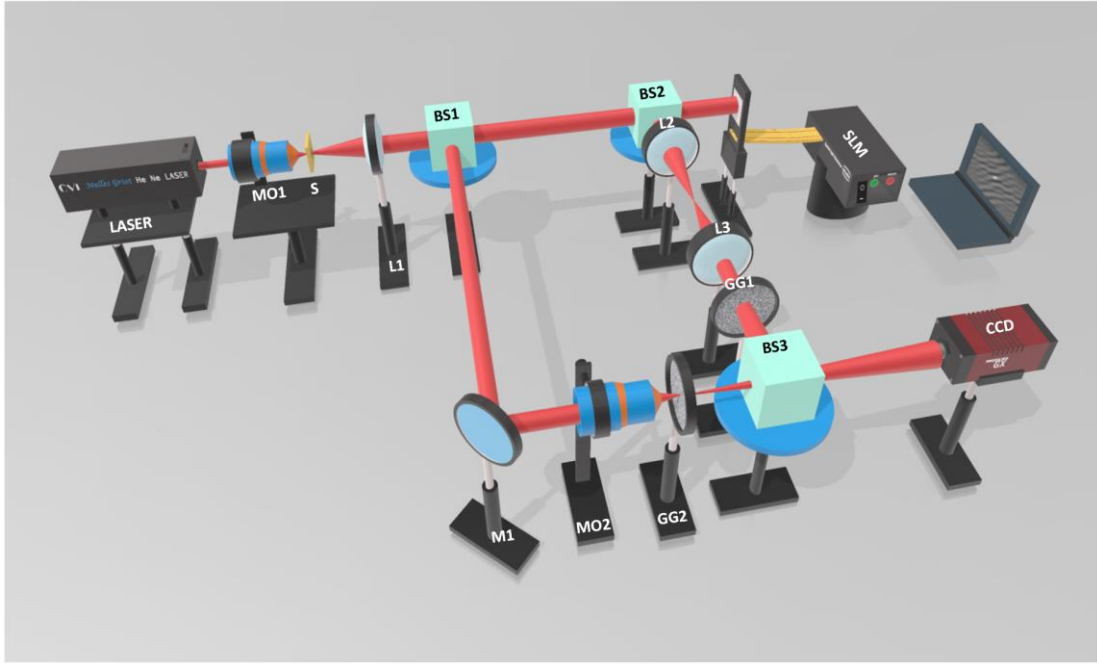
Fig. 6.4. Experimental set-up for the lensless Stokes holography. MO: microscope objective; S: pinhole; L: lens; BS: beam splitter; SLM: spatial light modulator; GG: ground glass; M: mirror; CCD: charge coupled device.

A linearly polarized beam from a He-Ne laser of wavelength 633nm (Melles Griot 25-LHP-928-230) is spatially filtered with microscope objective O1 (20X, NA=0. 40) and pinhole S (10µm) and subsequently collimated by lens L1(f=150mm). The collimated beam splits into two arms by a non-polarizing beam splitter BS1. The transmitted beam illuminates the spatial light modulator SLM (Holoeye LC-R 720, reflective type; pitch pixel=20µm) which carries hologram of an object (O) and this hologram is projected at the scattering plane by a 4f imaging system with unit magnification. The digital hologram displayed on the SLM is a computer-generated hologram (CGH) of off-axis objects and

numerically recorded in the Fourier geometry as shown in Fig. 6.1. Figure 6.1shows the formation of Fourier transform hologram encoding the object information.

Light coming from the SLM travels through the ground glass GG1 (DG20/120/MD, Thorlab, 3mm thickness) and gets randomly distorted and generates speckle pattern. The speckle pattern further propagates towards the charged coupled device (CCD) plane. The 45° linearly polarized light reflected from the BS1 and folded by mirror M1 is focused at the ground glass plate GG2 using MO2. The focal spot at GG2 is placed at an off-axis in order to generate a reference wave with uniform amplitude profile and a linear phase structure as described in Eq. (6.11). The speckle coming out of the GG2 propagates towards the CCD plane. Both the ground glasses are placed at distance z=280mm from the CCD plane in order to make a lensless Fourier transform geometry. The random fields coming from two independent diffusers are combined by BS2 and coherently add to generate the resultant speckle at camera plane. The camera has a 14-bit dynamic range with a resolution of 2750X2200 pixels and a pixel pitch of 4.54 micron (Prosilica GX2750). Both ground glasses are static during the recording of the intensity distribution of the resultant speckle field.

6.4   Result & Discussion

The resultant speckle field due to coherent super position of object and reference speckle is recorded by CCD camera and the resultant speckle field is shown in Fig. 6.5 The speckle grain size at camera plane can be controlled by varying aperture in the object arm of the interferometer.
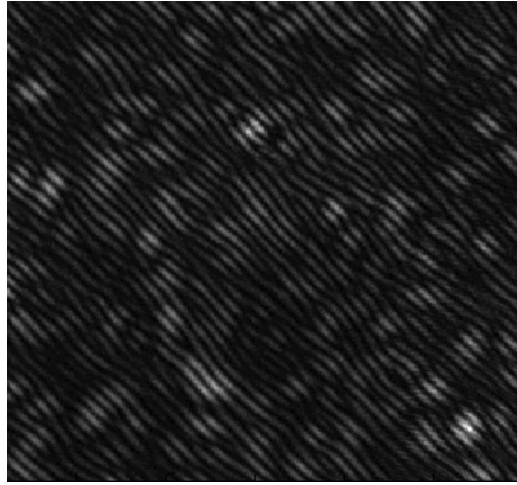
Fig. 6.5. Random speckle pattern captured by the CCD camera

The cross- covariance of the intensity distribution of the resultant speckle is obtained by spatial averaging under condition of spatial stationarity and ergodicity. The fourth-order intensity correlation of the speckle pattern results in interference fringes and is shown in Fig. 6.6. The interference fringe results due to superposition of the complex coherence of the object and reference speckle fields.
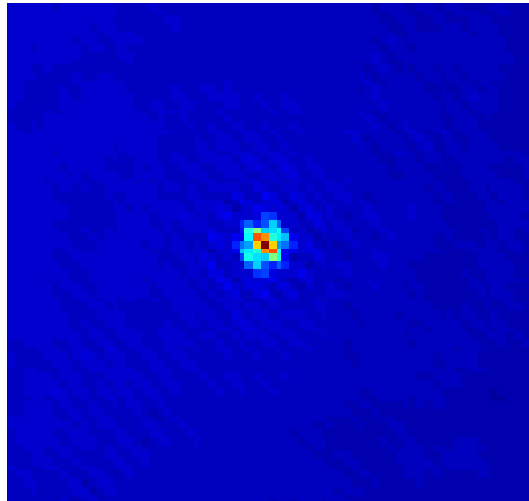
Fig. 6.6. Results of fourth order correlation showing interference fringes

The use of Fourier fringe analysis technique separates the spectra from dc part in the spatial frequency domain. High spatial carrier frequency due to linear phase of the

reference coherence function plays important role in separation of the frequency spectrum from the dc. Properly select one of the spectra and move it to center as shown in Fig. 6.7.
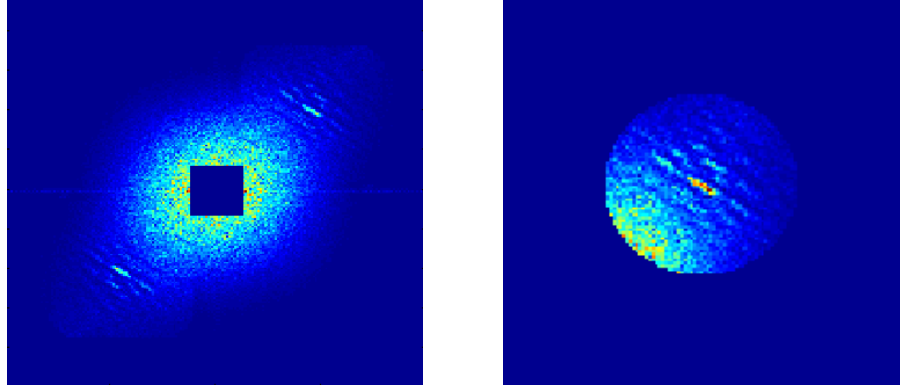
Fig. 6.7. Results of Fourier fringe analysis (left) and Centrally shifted frequency spectrum (right)

Inverse Fourier transform of properly selected centrally shifted frequency spectrum retrieves the complex coherence function of the speckle field as shown in Fig. 6.8.
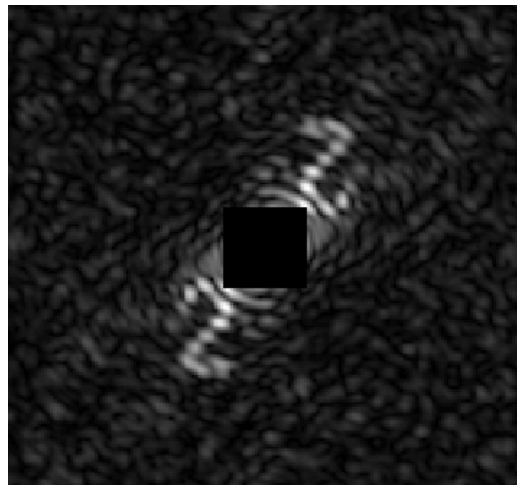
Fig. 6.8. Reconstruction with usual IFT

In Fig. 6.7, centrally shifted frequency spectrum is mixed with DC term that limits the spatial extent of the FTH at the random scattering medium and causing a distorted reconstruction of letter '2' with usual IFT. To avoid this problem, size of FTH is restricted using a low pass filter patch and resulted again poor reconstruction as shown in Fig. 6.9.
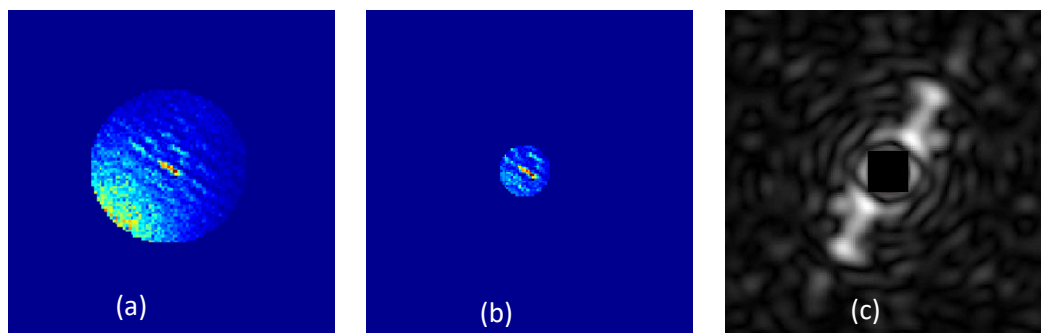
Fig. 6.9. (a). FTH, (b). FTH with low pass filter and (c). Reconstruction with usual IFT

To demonstrate the effectiveness of CS technique in the reconstruction, FTH with restricted size is then taken for post processing using CS based framework. Fig. 6.10 shows results obtained using CS based reconstructions. Much improvement is seen even with the 3rd iteration, it can be enhanced further with higher iterations.
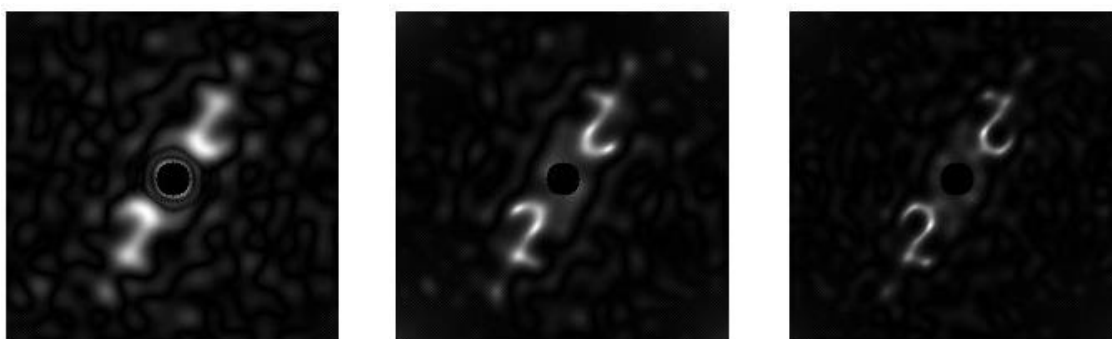
Fig. 6.10. CS based reconstruction with higher iteration

Some more results are presented to demonstrate the performance of CS technique for various objects as shown in Figs. 6.11 and 6.12. The results show the robustness of CS reconstruction technique for limited size FTH. It is evident from both the results that images are super resolved and noise is completely reduced when they are reconstructed using higher iterations.

Fig. 6.11. (a). IFT based reconstruction and (b). CS based reconstruction
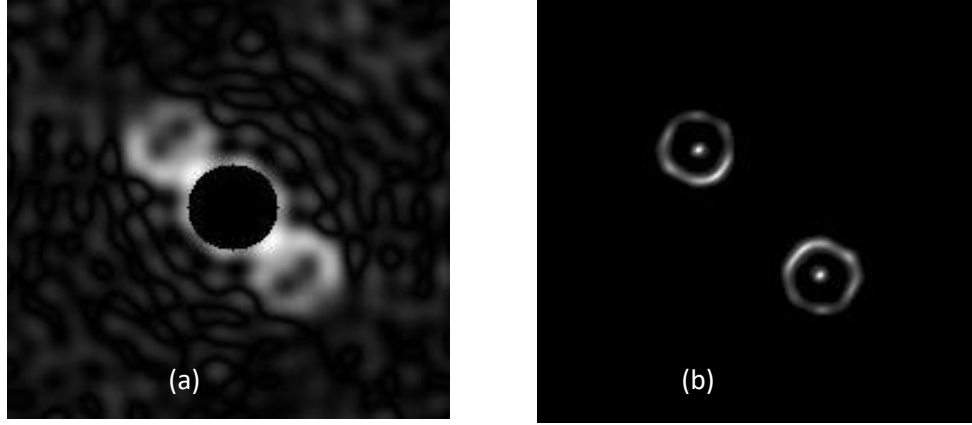
Fig. 6.12. (a). IFT based reconstruction and (b). CS based reconstruction

In summary, a detailed investigation is carried out for the reconstruction of limited size FTH using the inverse Fourier transform and a technique equipped with compressed sensing. Our work highlights significance of CS framework in the reconstruction of the object information for apertured FTH.

CHAPTER 7
CONCLUSION

The work successfully investigates the properties of randomly fluctuating field in scalar and vectorial domain using Hanbury Brown Twiss (HBT), both theoretically and experimentally. For analysis of laser speckle pattern and the effective utilization of their randomness, the statistical properties are investigated. Polarization sensitive studies can be effectively carried out using the investigations and development of such new experimental techniques that are capable of treating coherence and polarization together, in account. The laser speckle pattern of a spatially fluctuating random field can be synthesized and analyzed using this technique. Various polarization fluctuations and results are presented throughout the thesis. The polarization fluctuation in the random field is synthesized by introducing different vortex modes into orthogonal polarization components of the light prior to random scattering from a diffuser. Spatially varying polarization states are generated by introducing the helical modes, i.e., vortex, in one of the orthogonal polarization components of the incident light. This makes coupling between the spatial and polarization modes of the light.

The HBT interferometer based on two-point intensity correlation is combined with speckle holography to retrieve the complex information of a random field. The thesis presents the study of polarization and coherence of a random field, mainly in vectorial domain. A new experimental technique demonstrates the imaging through scattering media by employing the Stokes holography with the Hanbury Brown-Twiss approach. This approach is based on Lensless Fourier transform holography to recover object information i.e., Stokes parameters from a scattering medium. Furthermore, making use of the lensless Fourier transform holograms of the GSPs depth recovery of the object is done. This is implemented by digital propagation of the GSPs rather than mechanical

scanning of the detector. This is arguably the first such attempt to exploit the interference of GSPs to realize lensless Fourier transform hologram for the Stokes vector waves. The HBT type interferometer for 3D imaging of the polarized objects, is also a maiden attempt through this thesis.

Another major highlight of the thesis is the demonstration of compressed sensing in the imaging through a random scattering medium. This method can reduce the noise level in recovered signal and super-resolved images can be obtained using the CS-based technique compared to the usual FT. The demonstrated technique is well efficient in retrieving the information by reconstructing objects from limited sized FTH. The reconstruction is found to be very effective even in the cases of low sampling. A quantitative analysis has been carried out to compare the quality of reconstruction using inverse Fourier transform (IFT) and CS techniques. The CS reconstruction is conclusively better than IFT reconstruction.

REFERENCES

1. A. Al-Qasimi, M. Lahiri, D. Kuebel, D. F. V. James, and E. Wolf. (2010). The influence of the degree of cross-polarization on the Hanbury Brown-Twiss effect. *Opt. Express 18*, 17124-17129.

2. A. Kumar, J. Banerji, and R. P. Singh. (2012). Hanbury Brown-Twiss-type experiments with optical vortices and observation of modulated intensity correlation on scattering from rotating ground glass. *Phys. Rev. A 86, 013815*.

3. A. Perrin, R. Bücker, S. Manz, T. Betz, C. Koller, T. Plisson, T. Schumm, and J. Schmiedmayer. (2012). Hanbury Brown and Twiss correlations across the Bose-Einstein condensation threshold. *Nature Physics 8*, 195-198 .

4. Akhlaghi M I and Dogariu A. (2017). Single-shot coherent noise suppression by spatial interferometric heterodyning. *Opt. Lett. 42*, 2378-2381.

5. Archbold, E. Burch, J. and Ennos, A. (1970). Recording of in-plane surface displacement by double-exposure speckle photography. *Ennos, A Opt. Acta*, 17(12) 883–898.

6. Azzam, R. M. (2016). Stokes-vector and Mueller-matrix polarimetry [Invited]. *J. Opt. Soc. Am. A 33*, 1396-1408.

7. Bartelt H, Lohmann A W, Wirnitzer B. (1984). Phase and amplitude recovery from bispectra. *Appl. Opt. 23*, 3121-3129.

8. Baym, G. (n.d.). *The physics of Hanbury Brown-Twiss intensity interferometry: from stars to nuclear collisions.*

9. Bianchi, S. (2014). Vibration detection by observation of speckle patterns. *Appl. Opt.*, 53(5), 931–936.

10. Boyd S and Vandenberghe L. (2004). *Convex Optimization.* Cambridge university press.

11. Briers D., Duncan D. D., Hirst E. R., Kirkpatrick S. J., Larsson M., Steenbergen W., Stromberg T., and Thompson O. B.,. (2013). Laser speckle contrast imaging: theoretical and practical limitations. *J. Biomed. Opt*, 18(6), 066018 .

12. Bromberg, Y. L. (2010). Hanbury Brown and Twiss interferometry with interacting photons. *Nature Photon*, 4, 721-726.

13. Bruce G. D., O'Donnell L., Chen M., and Dholakia K. (2019). Overcoming the speckle correlation limit to achieve a fiber wavemeter with attometer resolution. *Opt. Lett.*, 44(6), 1367–1370.

14. Bruce G. D., O'Donnell L., Chen M., Facchin M., and Dholakia K. (2020). Femtometer resolved simultaneous measurement of multiple laser wavelengths in a speckle wavemeter. *Opt. Lett.*, 45(7), 1926–1929.

15. Burch J. and Tokarski J. (1968). Production of multiple beam fringes from photographic scatterers. *Opt. Acta* , 15(2), 101–111.

16. Candes E and Romberg J. (2005). l1-Magic: Recovery of Sparse Signals via Convex Programming. *URL: www.acm. caltech. edu/l1magic/downloads/l1magic. pdf. 4:14.*

17. Candes EJ and Wakin MB. (2008). An introduction to compressive sampling . *IEEE signal processing 25(2)*, 21-30.

18. Candes EJ, Romberg J, Tao T. (2006). Robust uncertainty principles: Exact signal reconstructionfrom highly incomplete frequency information. *IEEE Transactions on information theory 52(2)*, 489-509.

19. Cao, H. (2017). Perspective on speckle spectrometers. *J. Opt.*, 19(6), 060402.

20. Chakrabarti M., Jakobsen M. L., and Hanson S. G. (2015). Speckle-based spectrometer. *Opt. Lett.*, 40(14), 3264–3267.

21. D. Singh and R. K. Singh. (2018). Lensless Stokes holography with the Hanbury Brown-Twiss approach. *Opt. Express 26*, 10801-10812.

22. Dainty, J. C. (1984). *Laser Speckle and related Phenomena.* Springer.

23. Das B, Bisht N S, Vinu R V, Singh R K. (2017). Single Shot Digital Holographic Imaging through a Scattering Layer. *Appl. Opt. 56*, 4591-4597.

24. Davis, J. (2018). *Fourty years of progress in Long-Baseline optical interferometryy: 2005 Robert Ellery Lecturs.*

25. Erkmen, B. I & Shapiro J. H. (2010). Ghost imaging: from quantum to classical to computational. *Advanced in Optics and Photonics, 2 (4)*, 4-5-450.

26. F. Gori, M. Sanarsiero. R. Borghi, and E. Wolf. (2006). Effects of coherence on the degree of polarization in a Young interference pattern. *Opt. Lett.*, 31, 688-690.

27. Fienup, J. R. (1978). Reconstruction of an object from the modulus of its Fourier transform. *Opt. Lett. 3*, 27-29.

28. Freund I. and Berkovits R. (1990). Surface reflections and optical transport through random media: coherent backscattering, optical memory effect, frequency, and dynamical correlations. *Phys. Rev. B*, 41(1), 496–503.

29. G. S. Reddy, V. Kumar, Y. Miyamoto, and R. P. Singh. (2017). Scattering of Poincare beams: polarization speckles. *Opt. Express 25*, 19886-19893.

30. G. Wu and T. D. Visser. (2014). Hanbury Brown-Twiss effect with partially coherent electromagnetic beams. *Optics Letters 39(9)*, 2561-2564.

31. Goldstein, D. H. (2010). *Polarized light.* CRC Press.

32. Goodman, J. (2020). *Speckle Phenomena in Optics: Theory and Applications, Second Edition.*

33. Goodman, J. W. (1976). Some fundamental properties of speckle. *Opt. Soc. Am. 66*, 1145-1150.

34. Goodman, J. W. (2000). *Statistical optics.* Wiley.

35. Goodman, J. W. (2000). *Statistical Optics.* Wiley-Interscience.

36. Goodman, J. W. (2007). *Speckle Phenomena in Optics: Theory and Applications.* Roberts.

37. Goodman, J. W. (2007). *Speckle Phenomenon in Optics: Theory and Applications.* Roberts& Co.

38. Gori, F. M. Santarsiero, Borghi, R. and Piquero, G. (2000). Use of the van Cittert Zernike theorem for partially polarized sources. *Opt. Lett*, 25, 1291-1293.

39. Gupta R. K., Bruce G. D., Powis S. J., and Dholakia K. (2019). Deep learning enabled laser speckle wavemeter with a high dynamic range. *arXiv*, 1910.10702.

40. Hanson S. G., Jakobsen M. L., and Chakrabarti M. . (2015). Speckle-based wavemeter. *SPECKLE 2015: VI International Conference on Speckle Metrology* (p. vol. 9660 p. 96600U). International Society for Optics and Photonics.

41. H Roychowdhury and E Wolf. (2005). Young's interference experiment with light of any state of coherence and of polarization. *Opt. Commun*, 252, 268-274.

42. Hanbury Brown, R. and Twiss,R. Q. (1956). Correlation between photons in two coherent beams of light. *Nature*, 177, 27-29.

43. Hannonen A, Friberg A T, Setala T. (2016). Classical spectral ghost ellipsometry. *Opt. Lett. 41*, 4943.

44. Hannonen A, Friberg A T, Setala T. (2017). Classical ghost-imaging spectral ellipsometer. *J. Opt. Soc. Am. A 34*, 1360-1368.

45. Hassinen,T.Tervo,J. Setala,T. and. Friberg,A. T. (2011). Hanbury Brown-Twiss effect with electromagnetic waves. *Optics Express*, 19(16): 15188-15195.

46. Idell P S, Fienup J R, Goodman R S. (1987). Image synthesis from non-imaged laser-speckle patterns. *Opt. Lett. 12*, 858-860.

47. J. R. Kuhn, Z. Wu, and M. Poenie. (2001). Modulated polarization microscopy: a promising new approach to visualizing cytoskeleton dynamics in living cells. *Biophyc. J. 80*, 972.

48. J. Tervo, T. Setala, and A. T. Friberg. (2003). Degree of coherence for electromagnetic fields. *Opt. Express*, 11, 1137-1143 .

49. J. Tervo, T. Setälä, and A. T. Friberg. (2003). Degree of coherence for electromagnetic fields. *Opt. Express 11*, 1137-1143.

50. Katz, O. Heidmann, P. Fink, M. and Gigan, S. (2014). Non-invasive single-shot imaging through scattering layers and around corners via speckle correlations. *Nat. Photonics*, 8(10), 784–790 .

51. Kellock H, Setala T, Friberg A T, Shirai T. (2014). Polarimetry by classical ghost diffraction. *J. Opt. 16*, 915-918.

52. Kittel, C. (1976). *Introduction to Solid State Physics, 5th edn.* New York: Wiley.

53. Kittel, C. (1976). *Introduction to Solid State Physics, 5thEdn.* New York: Wiley.

54. Korotkova, O. (2006). Changes in the intensity fluctuations of a class of random electromagnetic beams on propagation. *J. Opt. A, Pure Appl. Opt. 8*, 30-37.

55. Kumar, A. Banerji, J. and Singh, R. P. (2012). Hanbury Brown-Twiss-type experiments with optical vortices and observation of modulated intensity correlation on scattering from rotating ground glass. *Phys. Rev. A*, 86, 013815.

56. L. B. Cohen, R. D. Keynes, and B. Hille. (1968). Light scattering and birefringence changes during nerve activity. *Nature 218*, 438.

57. Lapchuk A, Kryuchyn A, Petrov V, Yurlov V, Klymenko V. (2013). Optimal speckle suppression in laser projectors using a single two-dimensional Barker code diffractive optical element. *J. Opt. Soc. Am. A. 30*, 22-31.

58. Luis, A. (2007). Degree of coherence for vectorial electromagnetic fields as a distance between correlation matrices. *J. Opt. Soc. Am. A*, 24, 1063- 1068.

59. M. Shribak, and R. Oldenbourg. (2003). Techniques for fast and sensitive measurements of two-dimensional birefringence distributions. *Appl. Opt. 42*, 3009.

60. M. Takeda, W. W. (2014). Spatial statistical optics and spatial correlation holography; A review. *Opt. Review, 21*, 849-861.

61. M. Takeda, W. Wang, D. N. Naik, and R. K. Singh. (2014). Spatial statistical optics and spatial correlation holography: a review. *Opt. Rev. 21*, 849-861 .

62. M. Takeda, W. Wang, and S. G. Hanson. (2010). Polarization speckles and generalized Stokes vector wave: a review. *Proc. SPIE 7387*, 73870 V.

63. Mandel, L. a. (1995). *Optical Coherence and Quantum Optics.* Cambridge University.

64. Mandel, L., & Wolf, E. (1995). *Optical Coherence and Quantum Optics.*

65. Mazilu M., Mourka A., Vettenburg T., Wright E. M., and Dholakia K. (2012). Simultaneous determination of the constituent azimuthal and radial mode indices for light fields possessing orbital angular momentum. *Appl. Phys. Lett.*, 100(23), 231115.

66. Mazilu M., Vettenburg T., Di Falco A., and Dholakia K. (2014). Random super-prism wavelength meter. *Opt. Lett.*, 39(1), 96–99.

67. Mehta D S, Naik D N, Singh R K, Takeda M. (2012). Laser speckle reduction by multimode optical fiber bundle with combined temporal, spatial, and angular diversity . *Appl. Opt. 51*, 1894-1904.

68. Mehta D. S. and Srivastava V. (2012). Quantitative phase imaging of human red blood cells using phase shifting white light interference microscopy with color fringe analysis. *Applied Physics Letters*, 101 (20) 203701.

69. Metzger N. K., Spesyvtsev R., Bruce G. D., Miller B., Maker G. T., Malcolm G., Mazilu M., and Dholakia K. (2017). Harnessing speckle for a sub-femtometer resolved broadband wavemeter and laser stabilization, . *Nat. Commun.*, 8(1), 15610.

70. Mourka A., Mazilu M., Wright E., and Dholakia K. (2013). Modal characterization using principal component analysis: application to bessel, higher-order gaussian beams and their superposition. *Sci. Rep.*, 3(1), 1422.

71. O. Korotkova, and E. Wolf. (2005). Generalized Stokes parameters of random electromagnetic beams. *Opt. Lett.*, 30, 198-200.

72. O'Donnell L., Dholakia K., and Bruce G. D. (2020). High speed determination of laser wavelength using Poincaré descriptors of speckle. *Opt. Commun.*, 459, 124906.

73. Padgett M. J. & Boyd R W. (2017). An introduction to ghost imaging: Quantum ad classica. *Philosphical transactions of the Royal Society of London A: Mathematical Physical and Engineering Sciences , 375*, 2099.

74. R. K. Singh, D. N. (2013). Vectorial van Cittert-Zernike theorem based on spatial averaging: experimental demonstrations. *Opt. Lett. 38*, 4809-4812 .

75. R. K. Singh, D. N. (2014). Characterization of spatial polarization fluctuations in scattered field. *J. Opt. 16, 105010*, 1-12.

76. R. K. Singh, D. N. Naik, H. Itou, Y. Miyamoto, and M. Takeda. (2014). Characterization of spatial polarization fluctuations in scattered field. *J. Opt. 16*, 105010.

77. R. K. Singh, R. V.Vinu, and A. M. Sharma. (2014). Recovery of complex valued objects from two-point intensity correlation measurement. *Appl. Phys. Lett. 104, 111108*, 1-4.

78. R. V. Vinu and R. K. Singh. (2015). Experimental determination of generalized Stokes parameters. *Opt. Lett. 40*, 1227-1230.

79. Rakesh Kumar Singh, D. N. Naik, H. Itou, Y. Miyamoto, and M. Takeda. (2012). Stokes holography. *Opt. Lett.*, 37, 966-968.

80. Redding B. and Cao H. (2012). Using a multimode fiber as a high-resolution, low-loss spectrometer. *Opt. Lett.*, 37(16), 3384–3386.

81. Redding B., Liew S. F., Sarma R., and Cao H. (2013). Compact spectrometer based on a disordered photonic chip. *Nat. Photonics*, 7(9), 746–751.

82. Redding B., Popoff S. M., and Cao H. (2013). All-fiber spectrometer based on speckle pattern reconstruction. *Opt. Express*, 21(5), 6584–6600.

83. Rudin LI, Osher S, Fatemi E. (1992). Nonlinear total variation based noise removal algorithms. *Physics D: Non linear phenomena 60(1-4)*, 259-268.

84. R. Hanbury Brown, J. Davis, and L. R. Allen. (1974). The angular diameter of 32 stars. *In monthly notice of the Royal Astronomical Society*, 167, 121-136.

85. Robert Hanbury Brown and Richard Q Twiss. (1900- 1975). *" A test of a new type of stellar interferometer on Sirius" In: A source book in astronomy and astrophysics.*

86. S. Sahin, O. Korotkova, G. Zhang, and J. Pu. (2009). Free-space propagation of the spectral degree of cross-polarization of stochastic electromagnetic beams. *J. Opt. A, Pure Appl. Opt. 11*, 085703.

87. S. G. Reddy, S. Prabhakar, A. Kumar, J. Banerji, and R. P. Singh. (2014). High order optical vortices and formation of speckles. *Opt. Lett.39*, 4364-4367.

88. S. N. Volkov, D. F. V. James, T. Shirai, and E. Wolf. (2008). Intensity fluctuations and degree of cross-polarization of stochastic electromagnetic beams. *J. Opt. A, Pure Appl. Opt. 10*, 055001 .

89. Schmitt J M, Xiang S H, Yung K M. (1999). Speckle in optical coherence tomography. *J. Biomed. Opt. 4* , 95.

90. Schnars Ulf and Werner Juptner. (2005). *Digital holography.* Springer.

91. Schultheiss, V. H. Batz, S. and Peschel, U. (2016). Hanbury Brown and Twiss measurements in curved space. *Nature Photon*, 10, 106-111.

92. Shi D, Hu S, Wang Y. (2014). Polarimetric ghost imaging. *Opt. Lett. 39*, 1231-1234.

93. Shirai T, Kellock H,Setala T, Friberg A T. (2011). Visibility in ghost imaging with classical partially polarized electromagnetic beams. *Opt. Lett. 36*, 2880-2882.

94. Singh R K, Vinu R V, Sharma A M. (2014). *Appl. Phys. Let*, 104111108/1-4.

95. Singh R K, Vyas S, Miyamoto Y. (2017). Lensless Fourier transform holography for coherence waves. *J. Opt.* , 19115705.

96. Singh R. K., Vinu R. V. and Sharma A. (2014). Recovery of complex valued objects from two-point intensity correlation measurement. *Applied Physics letters*, 104, 111108.

97. Singh, R. K. (2017). Hybrid correlation holography with a single pixel detector. *Optics Letter 42*, 2515 .

98. Singh, R. K. Naik, D. N. Itou, H. Miyamoto, Y. and Takeda, M. (2011). Vectorial coherence holography. *Optics Express*, 19(12): 11558-11567.

99. Singh, R. K. Naik, D. N. Itou, H. Miyamoto, Y. and Takeda, M. (2012). Stokes holography. *Optics Letters*, 37(5): 966-968.

100. Singh, R. K. Vinu, R. V. and Sharma, A. M. (2014). Recovery of complex valued objects from two-point intensity correlation measurement. *Appl. Phys. Lett.*, 104, 111108/1-4.

101. Sirohi, R. S. (1933). *Speckle metrology.* New York: Marcel Dekker.

102. Soni, N. K. Vinu, R. V. and Singh, R. K. (2016). Polarization modulation for imaging behind the scattering medium. *Opt. Lett.*, 41(5), 906–909.

103. Sorrentini J, Zerrad M, Amra C. (2009). Statistical signatures of random media and their correlation to polarization properties. *Opt. Lett. 34*, 2429-2431.

104. T. Hassinen, J. T. (2011). Hanbury Brown-Twiss effect with electromagnetic waves. *Opt. Express* , 19, 15188-15195.

105. T. Hassinen, J. Tervo, T. Setala, and A. T. Friberg. (2011). Hanbury Brown-Twiss effect with electromagnetic waves. *Opt. Express 19*, 15188-15195.

106. T. Setälä, J. Tervo and A. T. Friberg. (2006). Stokes parameters and polarization contrast inYoung's interference experiment. *Opt. Letter*, 31, 2208-2210.

107. T. Setälä, J. Tervo, and A. T. Friberg. (2004). Complete electromagnetic coherence in the space-frequency domain. *Opt. Lett. 29*, 328-330.

108. T. Setala, T. Tervo, and A. T. Friberg. (2004). Complete electromagnetic coherence in the space-frequency domain. *Opt. Lett.*, 29, 328-330.

109. T. Shirai and E. Wolf. (2007). Correlations between intensity fluctuations in stochastic electromagnetic beams of any state of coherence and polarization. *Opt. Commun. 272*, 289-292.

110. T. Tani, M. Shribak, and R. Oldenbourg. (1996). A new view on polarization microscopy. *Nature 381*, 811.

111. Takeda M, Wang W, Hanson S G. (2010). Polarization speckles and generalized Stokes vector wave: a review [invited]. *Proceedings of SPIE, the International Society for Optical Engineering*, (pp. 73870V/1-7).

112. Takeda, M. (2013). Spatial stationarity of statistical optical fields for coherence holography and photon correlation holography. *Optics Letters*, 38(17): 3452-3455.

113. Takeda, M. Wang, W. Naik, D. N. and Singh, R. K. (2014). Spatial statistical optics and spatial correlation holography: A review. *Optical Review*, 21(6): 849-861.

114. Tervo J, Tervo S, Friberg A T. (2003). Degree of coherence for electromagnetic fields. *Opt. Ex 11*, 1137-1143.

115. Tran T T, Svensen O, Chen X, Akram M N. (2016). Speckle reduction in laser projection displays through angle and wavelength diversity. *Appl. Opt. 55*, 1267-1274.

116. Twiss, R. H. (1956). Correlation between photons in two coherent beams of light. *Nature 177*, 27-29.

117. Twiss, R. H. (1957). Interferometry of the intensity fluctuations in light, I: basic theory: the correlation between photons in coherent beams of radiation. *Proc. Roy. Soc. A 242*, (pp. 300-324). London.

118. U. C. Wiedemann and U. Heinz. (1997). Resonance contributions to Hanbury-Brown-Twiss correlation radii. *Phys. Rev. C 56*, 3265-3286.

119. V. H. Schultheiss, S. Batz, and U. Peschel. (2016). Hanbury Brown and Twiss measurements in curved space. *Nature Photon. 10*, 106-111.

120. Vinu R V and Singh R K. (2015). Synthesis of statistical properties of a randomly fluctuating polarized field. *Appl. Opt. 54*, 6491-6497.

121. Tiwari V., Gautam S. K., Naik D. N., Singh R. K., and Bisht N. S. (2020). Characterization of a spatial light modulator using polarization-sensitive digital holography. Applied Optics, Vol. 59, No. 7, 2024-2030.

122. Vorontsov M A and Kolosov V. (2005). Target-in-the-loop beam control: basic considerations for analysis and wave-front sensing. *J. Opt. Soc. Am. A 22*, 126-141.

123. Wang W., Yokozeki T., Ishijima R., Takeda M., and Hanson S. G. (2006). Optical vortex metrology based on the core structures of phase singularities in Laguerre-Gauss transform of a speckle pattern. *Opt. Express*, 14(22), 10195–10206.

124. Wiedemann, U. C. and Heinz, U. (1997). Resonance contributions to Hanbury-Brown-Twiss correlation radii. *Phys. Rev. C*, 56, 3265-3286.

125. Wolf, E. (2003). Unified theory of coherence and polarization of random electromagnetic beams. *Phys. Lett. A.*, 312, 263-267.

126. Wolf, E. (2007). *Introduction to the theory of coherence and Polarization of light.* Cambridge: Cambridge University Press.

127. Wolf, E. (2007). *Introduction to the Theory of Coherence and Polarization of Light.* Cambridge University.

128. Wolf, L. M. (1995). *Optical Coherence and Quantum Optics.* Cambridge University Press.

129. X. Yu, J. Hong, C. Liu, and M. K. Kim. (2014). Review of digital holographic microscopy for three-dimensional profiling and tracking: Review. *Opt. Eng 53*, 112306.

130. Y. Bromberg, Y. L. (2010). Hanbury Brown and Twiss interferometry with interacting photons. *Nature Photon. 4*, 721-726.

131. Y. Chen, F. Wang, J. Yu, L. Liu, and Y. Cai. (2016). Hanbury Brown-Twiss effect with electromagnetic waves hermite-Gaussian correlated Schell-model beam. *Opt. Express 24*, 15232-15250.

132. Y. Chen, F. Wang, L. Liu, C. Zhao, Y. Cai, and O. Korotkova. (2014). Generation and propagation of a partially coherent vector beam with special correlation functions. *Phys. Rev. A 89*, 013801.

133. Y. Xin, Y. Chen, Q. Zhao, and M. Zhou. (2008). Effect of cross-polarization of electromagnetic source on the degree of polarization of generated beam. *Opt. Commun. 281*, 1954-1957.

134. Zalevsky Z., Beiderman Y., Margalit I., Gingold S., Teicher M., Mico V., and Garcia J.,. (2009). Simultaneous remote extraction of multiple speech sources and heart beats from secondary speckles pattern. *Opt. Express*, 17(24), 21566–21580.

135. Zhao P and Gao W. (2015). Illumination Angle Three-Dimensional Model for Speckle Noise Suppression in Laser Projector. *J. Display Tech. 12*, 442-446.

LIST OF PUBLICATIONS BASED ON THE THESIS

PUBLISHED

1. **Singh, D** and Singh, R. K. (2018). Lensless Stokes holography with the Hanbury Brown-Twiss approach. *Opt. Express* 26, 10801-10812.

2. **Singh, D.** Chen, Z. Pu, J and Singh, R. K. (2018). Recovery of polarimetric parameters from non-imaged laserspeckle. *Journal of Optics* 20 (8), 085605.

3. Vetal, A P. **Singh, D**. Singh, R. K. and Mishra, D. (2018). Reconstruction od aperture Fourier Transform Hologram using compressed sensing. *Optics and Lasers in Engineering* 111, 227-235.

4. Chen, Z. **Singh, D.** Singh, R. K. and Pu, J (2020). Complex field measurement in a single pixel hybrid correlation holography. *Journal of Physics Communications* 4 (4), 045009.

CONFERENCE PAPERS

1. **Singh, D** and Singh R. K. (2016). Measuring polarization vector from the diffused light. International conference on Fibre Optics and Photonics, Tu5E. 4

2. **Singh, D**. Vetal, A. P. Singh R. K. and Mishra, D. (2017). Compressed sensing applications in imaging through random media. Student Conference on Optics and Photonics (SCOP), PRL Ahmedabad.

3. Vinu, R. V. **Singh, D**. Pu, J and Singh, R. K. (2018). Effect of speckle illumination on holographic recording and reconstruction. Biomedical imaging and Sensing Conference 10711, 107110Q.